Multiple valence-space and core-excited band terminations in Ho and Er isotopes

E. S. Paul,[1,*] J. Simpson,[2,†] M. A. Riley,[3,‡] J. S. Baron,[3] P. J. T. Hampson,[1] X. Wang,[3,§] A. Aguilar,[3,‖] D. E. Appelbe,[2] A. D. Ayangeakaa,[4,5] A. J. Boston,[1] H. C. Boston,[1] D. B. Campbell,[3,‖] M. P. Carpenter,[6] C. J. Chiara,[6,7,¶] R. M. Clark,[8,**] M. Cromaz,[8] I. G. Darby,[9,††] A. O. Evans,[1] P. Fallon,[8] U. Garg,[10] A. Görgen,[8,‡‡] D. J. Hartley,[11] C. R. Hoffman,[6] R. V. F. Janssens,[4,5] D. T. Joss,[2,§§] D. S. Judson,[1] F. G. Kondev,[6] K. Lagergren,[3] T. Lauritsen,[6] I. Y. Lee,[8] J. T. Matta,[10,‖‖] S. L. Miller,[3] M. Mustafa,[1] P. J. Nolan,[1] J. Ollier,[2] M. Petri,[8,¶¶] A. Pipidis,[3] D. C. Radford,[12] J. M. Rees,[1] J. P. Revill,[1,***] L. L. Riedinger,[9] J. F. Sharpey-Schafer,[13] C. M. Sullivan,[1] C. Teal,[3] J. Thomson,[1] P. J. Twin,[1] C. Unsworth,[1,†††] D. Ward,[8,**] S. Zhu,[6,**] J. Gellanki,[14,‡‡‡] and I. Ragnarsson[14]

[1]*Department of Physics, University of Liverpool, Liverpool L69 7ZE, United Kingdom*
[2]*STFC Daresbury Laboratory, Daresbury, Warrington WA4 4AD, United Kingdom*
[3]*Department of Physics, Florida State University, Tallahassee, Florida 32306, USA*
[4]*Department of Physics and Astronomy, University of North Carolina, Chapel Hill, North Carolina 27599, USA*
[5]*Triangle Universities Nuclear Laboratory, Duke University, Durham, North Carolina 27708, USA*
[6]*Physics Division, Argonne National Laboratory, Argonne, Illinois 60439, USA*
[7]*Department of Chemistry and Biochemistry, University of Maryland, College Park, Maryland 20742, USA*
[8]*Nuclear Science Division, Lawrence Berkeley National Laboratory, Berkeley, California 94720, USA*
[9]*Department of Physics and Astronomy, University of Tennessee, Knoxville, Tennessee 37996, USA*
[10]*Department of Physics, University of Notre Dame, Notre Dame, Indiana 46556, USA*
[11]*Department of Physics, U.S. Naval Academy, Annapolis, Maryland 21402, USA*
[12]*Physics Division, Oak Ridge National Laboratory, Oak Ridge, Tennessee 37830, USA*
[13]*Department of Physics, University of Zululand, P/B X1001, KwaDlangezwa, 3886, South Africa*
[14]*Division of Mathematical Physics, LTH, Lund University, P.O. Box 118, SE-221 00 Lund, Sweden*

(Received 9 December 2025; accepted 15 May 2026; published 30 June 2026)

High-spin structures of holmium ($Z = 67$) and erbium ($Z = 68$) isotopes are presented near mass 160, a region where collective and single-particle modes of excitation compete in the generation of angular momentum at the highest experimentally attainable spins in atomic nuclei. The level schemes of the ^{156,157,158}Ho isotopes have been significantly extended, reaching spins in the $40\hbar$ to $55\hbar$ range, through multiple experiments utilizing the Gammasphere spectrometer. In particular, several new noncollective band-terminating states are reported for these nuclei. The nature of these states, including both valence-space terminations and core-excited oblate-configurations, is discussed in terms of proton particle-hole (p-h) excitations across the semimagic $Z = 64$ shell closure. Cranked-Nilsson–Strutinsky (CNS) calculations have been used to interpret the nature of these noncollective states. The corresponding terminating states in $^{154–159}$Er are also included, providing a systematic

[*]Contact author: esp@ns.ph.liv.ac.uk
[†]Contact author: john.simpson@stfc.ac.uk
[‡]Contact author: mriley@admin.fsu.edu
[§]Present address: Department of Physics, California Polytechnic State University, San Luis Obispo, California 93407, USA.
[‖]Present address: Lawrence Livermore National Laboratory, 7000 East Ave., Livermore, California 94550-9234, USA.
[¶]Present address: U.S. Army Combat Capabilities Development Command Army Research Laboratory, Adelphi, Maryland 20783, USA.
[**]Deceased.
[††]Present address: United Kingdom National Nuclear Laboratory, Birchwood Park, Warrington, WA3 6AE, United Kingdom.
[‡‡]Present address: Department of Physics, University of Oslo, N-0316 Oslo, Norway.
[§§]Present address: Department of Physics, University of Liverpool, Liverpool L69 7ZE, United Kingdom.
[‖‖]Present address: Physics Division, Oak Ridge National Laboratory, Oak Ridge, Tennessee 37830, USA.
[¶¶]Present address: School of Physics, Engineering and Technology, University of York, Heslington, York YO10 5DD, United Kingdom.
[***]Present address: Applied Nuclear Physics Ltd, 41A Main Street, Cockermouth CA13 9JS, United Kingdom.
[†††]Present address: STFC Daresbury Laboratory, Daresbury, Warrington WA4 4AD, United Kingdom.
[‡‡‡]Present Address: Department of Physics and Electronics, Hansraj College, University of Delhi 110007, India.

Published by the American Physical Society under the terms of the Creative Commons Attribution 4.0 International license. Further distribution of this work must maintain attribution to the author(s) and the published article's title, journal citation, and DOI.

description of band termination in this mass region. In addition, three weak rotational structures have been assigned to ^{157}Ho at the highest spins. These collective bands are proposed to be based on a triaxial strongly deformed nuclear shape, involving neutron p-h excitations across the $N = 82$ shell gap.

DOI: 10.1103/393p-ghvk

I. INTRODUCTION

The study of high-spin states in atomic nuclei elucidates the competing mechanisms generating angular momentum in such finite mesoscopic systems. Both collective and single-particle degrees of freedom contribute to the building of angular momentum and the manifestation of different intrinsic shapes [1]. In this regard, results are presented here for so-called band-terminating states in the region around ^{158}Er, the nucleus that serves as the original textbook example of this phenomenon in heavy rare-earth nuclei (see Refs. [1,2] and references therein). This paper presents new high-spin experimental results for the ^{156,157,158}Ho isotopes at high spin, including the establishment of new terminating states. The results are interpreted through comparison with theoretical calculations based on the cranked Nilsson-Strutinsky (CNS) formalism [3]. The relevant physical phenomena are summarized below.

A. Band termination

Band termination occurs when the nucleus evolves, with increasing spin, from collective rotational behavior to specific noncollective states. In the standard case, this evolution is from a prolate to an oblate shape. In these noncollective levels, the angular momentum is generated totally by single-particle, aligned configurations. The terminating spin $I_{\max}$ can be calculated by summing the spins of the maximally aligned protons and neutrons within a single-particle configuration. Effectively, all valence nucleons outside quantum shell closures align their angular momenta to provide these relatively pure states, which are now experimentally accessible with current-day highly sensitive gamma-ray spectrometers. Such valence-space terminations, approaching $50\hbar$, are well established in ^{156,157,158,159}Er [2,4–6] and neighboring Ho nuclei such as ^{155,157}Ho [7,8].

B. Higher-spin excitations

Progressing to spins higher than those achievable by valence-space terminations requires particle-hole (p-h) excitations across major shell closures. In the ^{157,158}Er isotopes, several weak, high-energy transitions (1.5–2.5 MeV) feeding the established band-termination states reflect the larger energy needed for these particle-hole excitations [2,9,10]. Secondary core-excited termination was previously established in both ^{155}Ho and ^{156}Er at $4\hbar$ above the valence-space terminations, and was interpreted as 1p-1h proton excitations across the $Z = 64$ shell gap [7]. Guided by simple expectations of available single-particle configurations, and backed by CNS calculations, several new band-termination states have been established in ^{156,157}Ho, involving both valence-space and core-excited terminations. Furthermore, higher-order proton p-h excitations (e.g., 2p-2h, 3p-3h, etc.) can form collective structures with $I_{\max}$ values beyond $50\hbar$, which can bypass the favored valence-space terminations at $\approx 45\hbar$. Evidence for such structures is presented here for the ^{156,157}Ho isotopes.

C. Triaxial structure and structural competition

High moment-of-inertia sequences have been observed in ^{157}Ho. These are interpreted as triaxial strongly deformed (TSD) structures, analogous to those observed in ^{157,158}Er [11,12]. The existence of these TSD bands, which require both proton p-h excitations across the $Z = 64$ shell gap in addition to neutron p-h excitations across the $N = 82$ shell closure, highlights the intense competition between collective and single-particle modes in the $A \approx 160$ mass region, demonstrating the rich structural evolution under extreme angular momentum.

II. EXPERIMENTAL DETAILS AND ANALYSIS

This work reports on results obtained from three separate experiments using the γ-ray spectrometer Gammasphere [13,14]. The experiments were performed at the Argonne National Laboratory (ANL) and Lawrence Berkeley National Laboratory (LBNL) using average beam intensities of 2 to 3 particle nanoamperes.

A. Gammasphere at ANL

High-spin structures in ^{155,156,157,158}Ho were studied at ANL using Gammasphere equipped with 101 Compton-suppressed HPGe detectors [13,14]. A ^{37}Cl beam of energy 180 MeV was used to bombard two stacked thin self-supporting foils of ^{124}Sn, of combined thickness 1.1 mg/cm^2. This reaction produced holmium isotopes through the ^{124}Sn(^{37}Cl, xn)$^{161-x}$Ho reaction. A total of 10^{10} events was collected, where each one contained at least five Compton-suppressed γ rays. Approximately 10^{11} quadruple-coincident γ-ray events (γ^4) were unfolded from the raw data for analysis. The results for ^{155}Ho have previously been published in Ref. [7].

High-spin states in ^{159}Er were obtained from another experiment at ANL. This nucleus was populated via the ^{116}Cd(^{48}Ca, $5n$) reaction using a 215-MeV ^{48}Ca beam and studied with Gammasphere with 101 detectors. The target comprised two self-supporting ^{116}Cd foils with a total thickness of 1.1 mg/cm^2. A total of 1.9×10^9 events was accumulated, where each one contained at least seven Compton-suppressed γ rays. These data have been published in Ref. [6] but, in the present work, a minor correction is made

to the excitation energy of the state $6\hbar$ below the valence-space terminating level.

B. Gammasphere at LBNL

High-spin structures in ^{158}Ho were also studied at LBNL using the ^{114}Cd(^{48}Ca, $p3n$) reaction at a beam energy of 215 MeV and Gammasphere with 102 detectors, in the same configuration as at ANL. The target consisted of two stacked, thin, self-supporting ^{114}Cd foils of 1.1 mg/cm^2 combined thickness. A total of 1.2×10^9 events was accumulated, where each one contained at least seven coincident Compton-suppressed γ rays.

C. Off-line analysis

The data from each experiment were studied separately off-line through high-fold coincidence analysis techniques by generating γ^3 (cube) and γ^4 (hypercube) events for analysis with the Radware software package [15,16]. Level schemes were constructed based on γ-ray coincidence relationships and relative intensities. The ordering of transitions based on relative intensities is particularly useful at the highest spins, where the level energies no longer follow simple $I(I+1)$ quantum-rotor behavior in the band-termination region. In the present work, the built-in background subtraction [17] in Radware was modified to incorporate the background-subtraction technique of Ref. [18]. Spectra were generated by using double γ^2 and triple γ^3 coincidences created from combinations of single gates and/or lists of transitions in a gate-list [15] to improve statistics. Self-coincidences are excluded.

To determine γ-ray multipolarities, angle-specific spectra were analyzed to obtain angular-intensity ratios based on the method of directional correlations from oriented states [19,20]. For ^{156}Ho [21], the detectors used for the angular-intensity ratios were grouped into two sets, consisting of several rings in which the spectra are added together. One set contained detectors in rings around $\theta = 35^\circ$ or 145° with respect to the beam direction, and the other consisted of detectors around $\theta = 90^\circ$. Simultaneous triple (γ^3) coincidence requirements were applied to the data and the remaining γ rays projected into the angle-specific spectra. Angular-intensity ratios, R, of a transition were then calculated as

$$R = \frac{I_\gamma(\theta = 35^\circ \text{ or } 145^\circ)}{I_\gamma(\theta = 90^\circ)}. \quad (1)$$

The R values were normalized to 1.0 for known stretched-quadrupole ($E2$) transitions, and this then gives a value of $\approx$0.65 for pure stretched dipoles.

III. EXPERIMENTAL RESULTS

In the following sections, the experimental results are presented successively for the ^{156,157,158}Ho ($Z = 67$) isotopes and then for ^{159}Er ($Z = 68$). The results focus on the high-spin behavior of these nuclei. Detailed properties of the γ-ray transitions assigned to each isotope are presented in the Appendixes. These include level and transition energies, relative intensities, angular-intensity ratios, and spin-parity assignments.

A. High-spin states in ^{156}Ho

The initial analysis of the data for the doubly odd ^{156}Ho nucleus, including angular-distribution and angular-correlation measurements, can be found in Ref. [21]; the present work expands upon these results. Partial level schemes of ^{156}Ho are presented in Figs. 1 and 2. The bands in ^{156}Ho have not been connected to the 4^- ground state [23], so an additional energy y is indicated in Fig. 1, as defined in Ref. [24]. The level scheme generally confirms and updates the previously published work of Ref. [22]. The band labeling is adopted from Ref. [24] where eight rotational structures were identified.

Figure 1 displays the strongly populated, negative-parity band 1, together with another high-intensity positive-parity sideband (band 2). In addition, sequences of irregular levels are labeled as band 9. Figure 2 shows band 1 together with two other negative-parity sidebands (bands 3 and 5). New levels and transitions are labeled in red, while candidate noncollective oblate states are highlighted in blue.

Relative spin-parity (I^π) values have been measured for many transitions from the angular-correlation measurements. However, since the absolute values are not known, all I^π quantum numbers are shown in parentheses.

Several other (lower-spin) bands [22] observed in ^{156}Ho will be addressed in a forthcoming publication to complete the analysis of this nucleus from the present data.

1. Bands 1 and 2

Bands 1 and 2 (see Fig. 1) represent strongly coupled (interleaved signature-partner) bands, which were previously observed by Cullen *et al.* [22]. Band 1 represents the yrast structure at low spin and was established up to $I^\pi = (36^-)$ and (35^-) in the even-spin and odd-spin sequences, respectively [22]. The present work confirms this and extends the even-spin branch (band 1a) to (44^-) and the odd-spin one (band 1b) to (39^-). Representative spectra for bands 1a and 1b are shown in Figs. 3(a) and 3(b), respectively; all spectra shown in this work have been binned at 1 keV per channel. Figure 3 clearly shows the extensions of both the even and odd-spin signature-partners of band 1, and that the even-spin partner, band 1a, becomes more dominant at the highest spins.

Band 2 was previously established up to (36^+) and (37^+) in the even and odd-spin sequences [22]. This band is now extended in the even-spin branch (band 2a) to (46^+) and the odd-spin one (band 2b) to (39^+). An additional 1115-keV transition, assumed to be of stretched $E2$ character, is also observed to feed the (35^+) state.

2. Band 9

Band 9 is a sequence newly identified in this work. It comprises irregular structures, typical in a noncollective regime, and feeds into band 2 from spin 38 to 30. Representative spectra to highlight these new transitions in band 9 are in Fig. 4(a), for even spin, and Fig. 4(b) for odd spin. It can be seen that there is a particularly low-lying (41^+) state in band 9b, which is strongly yrast at this spin. Many high-energy transitions ($\approx$1–2 MeV) have been established feeding this especially low-lying state, as evident in the inset of Fig. 4(b).

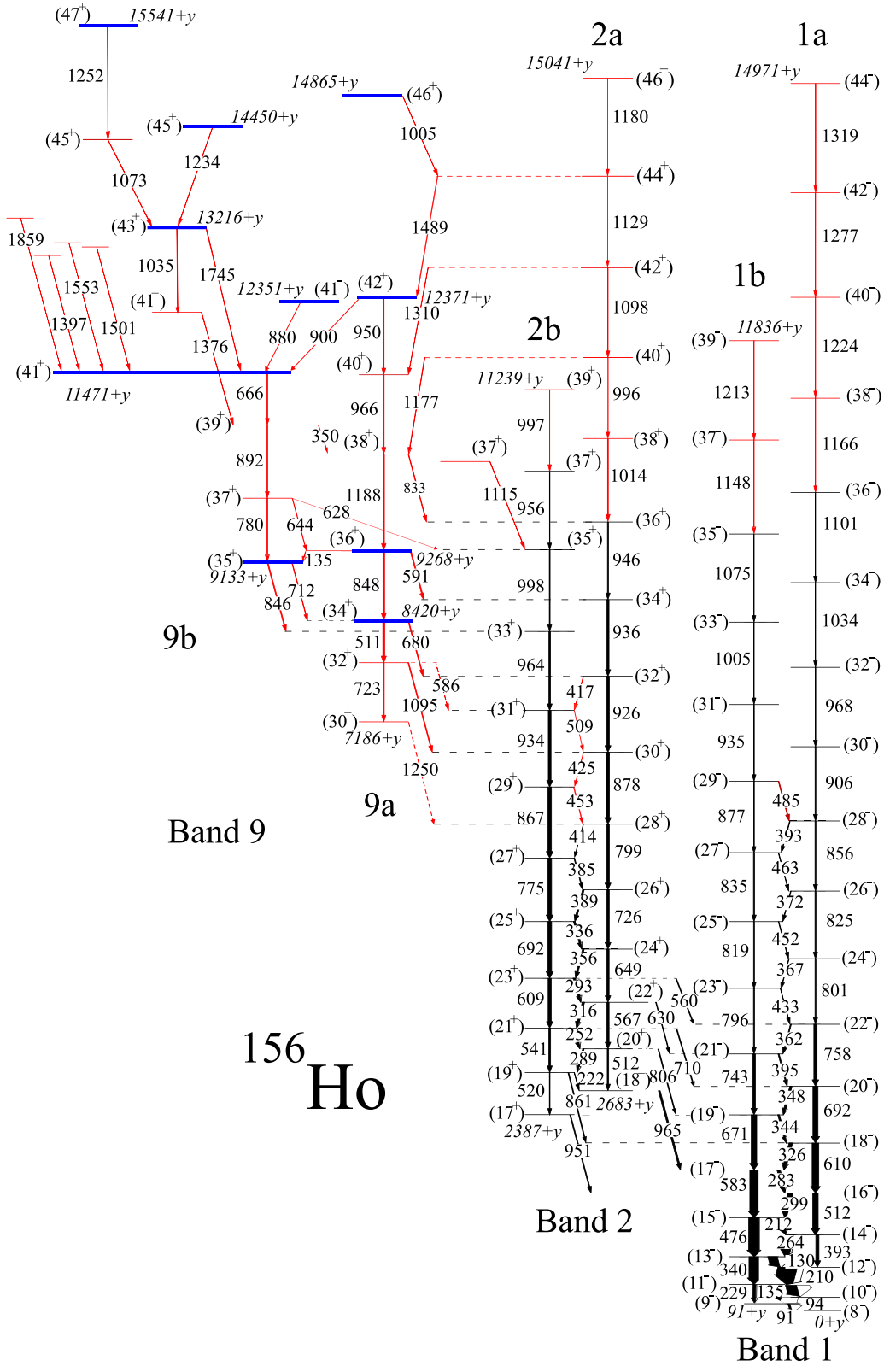


FIG. 1. Partial level scheme for ^{156}Ho with bands 1, 2, and 9. These bands in ^{156}Ho have not been connected to the 4^- ground state, so an additional energy y is indicated. New states and γ-ray transitions, extending the work of Ref. [22], are in red. Blue states indicate candidate oblate $\gamma = 60^\circ$ states, see Sec. IV and Table I. Arrow widths are proportional to intensity for transitions of intensity >5%. The white portion in an arrow represents the internal-conversion fraction.

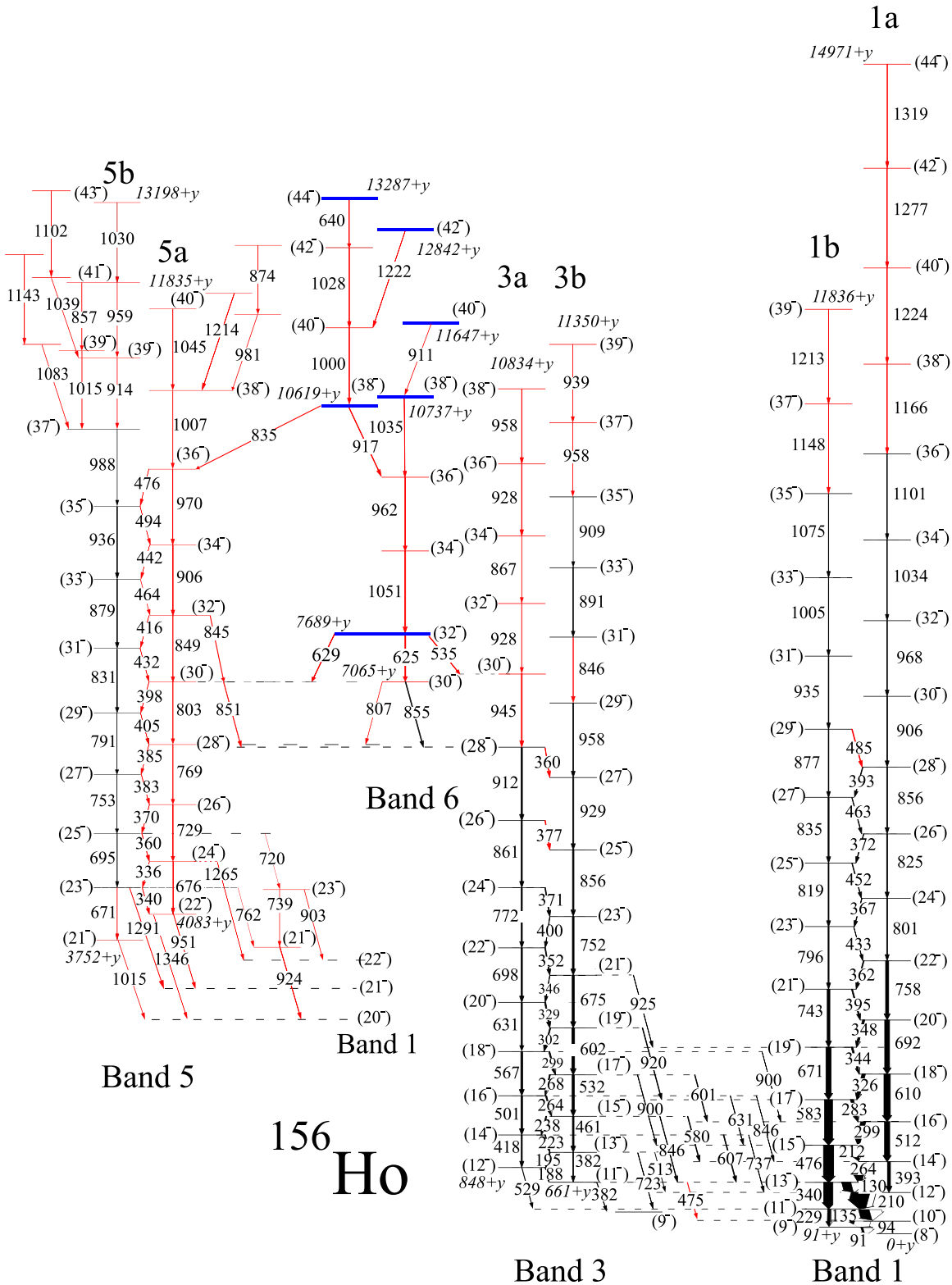


FIG. 2. Partial level scheme for ^{156}Ho with the negative-parity bands 1, 3, 5, and 6 in ^{156}Ho. These bands in ^{156}Ho have not been connected to the 4^- ground state, so an additional energy y is indicated. New states and γ-ray transitions, extending the work of Ref. [22], are in red. Blue states indicate candidate oblate $\gamma = 60^\circ$ states, see Sec. IV and Table. I. Arrow widths are proportional to intensity, for transitions of intensity >5%. The white portion in an arrow represents the internal-conversion fraction.

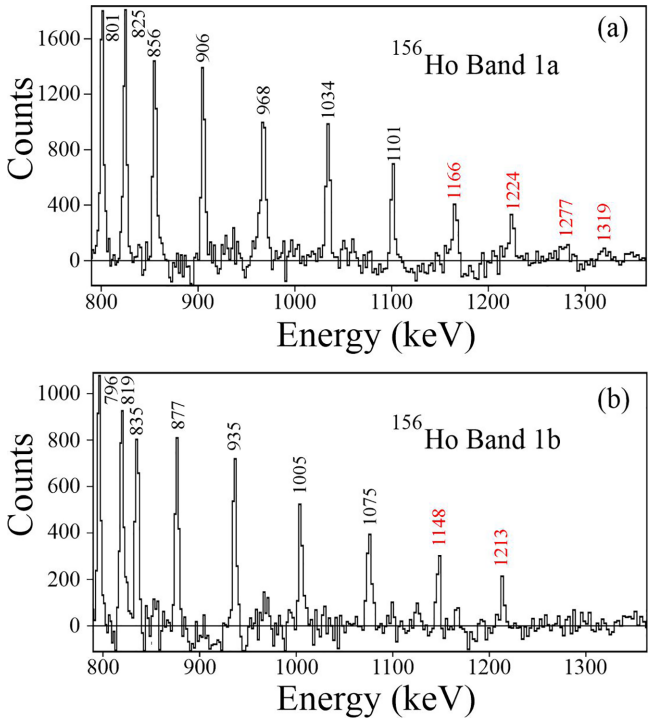


FIG. 3. Triple-gated γ^4 coincidence spectra representative of (a) band 1a, and (b) band 1b in ^{156}Ho, respectively. The band 1(a) spectrum in panel (a) was generated using gate-lists with the requirement $l1$-$l1$-$l2$; list $l1$ contains in-band transitions from 512 (16^-) → (14^-) to 968 keV (32^-) → (30^-), while list $l2$ contains those from 1034 (34^-) → (32^-) to 1277 keV (42^-) → (40^-). The band 1b spectrum in panel (b) was generated with the requirement $l1$-$l1$-$l2$; list $l1$ contains in-band transitions from the 671 (19^-) → (17^-) to 935 keV (31^- → 29^-) and list $l2$ contains those from 1005 (33^-) → (31^-) to 1213 keV (39^-) → (37^-). Newly identified transitions are indicated in red.

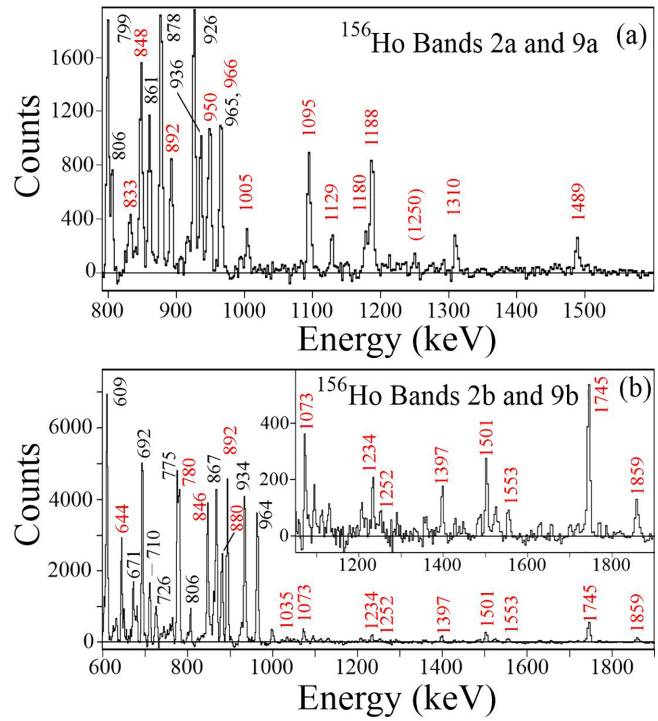


FIG. 4. High-energy part of triple-gated γ^4 coincidence spectra for (a) bands 2a and 9a, and (b) bands 2b and 9b in ^{156}Ho, respectively. The spectrum in panel (a) was generated with the requirement $l1$-$l1$-$l1$; list $l1$ includes in-band transitions from 649 (24^+ → 22^+) to 878 keV (30^+ → 28^+) in band 2a, and those from 1095 (32^+ → 30^+) to 966 keV (40^+ → 38^+) in band 9a. The spectrum in panel (b) was generated with the requirement $l2$-$l2$-666 keV (41^+ → 39^+); list $l2$ includes in-band transitions from 692 (25^+ → 23^+) to 964 keV (33^+ → 31^+) in band 2b, the 846 (35^+ → 33^+) to 892 keV (39^+ → 37^+) ones in band 9b, and the 965 keV (18^+ → 17^-) transition. Newly identified transitions are indicated in red.

3. Bands 3, 5, and 6

Band 3 represents another strongly coupled band with interleaved signature partners. It was originally established in Ref. [22] and assigned as a positive-parity structure based on a $\nu i_{13/2} \otimes \pi g_{7/2}$ configuration. However, in the current work, this band is reassigned to a negative-parity structure and its spin increased by $1\hbar$. Band 3 has numerous weak-linking transitions into band 1. Previously, many stretched and nonstretched $E1$ transitions were proposed for these links. Instead, these transitions are reassigned to be $\Delta I = 1$ ($M1/E2$) and $\Delta I = 2$ ($E2$) transitions. Our crucial high-fold angular-correlation measurement 0.67(5) for the 607-keV γ ray, linking bands 3 and 1, implies $\Delta I = 1$ character ($M1/E2$) for this transition ($14^- \rightarrow 13^-$). This precludes either a $\Delta I = 2$ (stretched $E2$) or a $\Delta I = 0$ (nonstretched $E1$) character for this transition. Hence, it establishes the new relative spin-parity between bands 1 and 3, confirming that they both appear to be negative-parity sequences.

Band 6 feeding into band 3 at the (28^-) level is a newly identified irregular structure. The angular-correlation measurements for band 3, band 6, and the connecting 855-keV transition are consistent with the assignments up to (36^-) in band 6. Representative spectra for bands 3 and 6 are provided in Fig. 5. The new transitions in Fig. 5(b) at 846, 958, and 938 keV extend band 3b to (39^-).

Band 6 also decays to a new, strongly coupled structure, band 5. The transitions in band 5b from 695 ($25^- \rightarrow 23^-$) to 988 keV ($37^- \rightarrow 35^-$) were observed previously by Cullen *et al.* [22] and this sequence was assigned as a decoupled band. No spin-parity assignments were made in Ref. [22]. In this work, band 5b is extended and established to be the odd-spin partner of a strongly coupled structure. The even-spin partner, band 5a, is observed from (22^-) to (40^-). The spin-parity assignments in band 5 are based on the high-fold angular-correlation measurements of the γ rays linking bands 5 and band 1, and are consistent with the decay of band 6 into both bands 3 and 5. A crucial high-fold angular-correlation measurement 0.59(4) for the 951-keV γ ray linking bands 5 and 1 implies stretched-dipole character ($M1/E2$) for this transition ($22^- \rightarrow 21^-$). Figures 6(a) and 6(b) display transitions in the odd- (5b) and even-spin (5a) branches of this sequence. The interleaving nature of this strongly coupled structure is evident in these spectra. At spin values near $40\hbar$, both branches of band 5 are fed by a series of high-energy

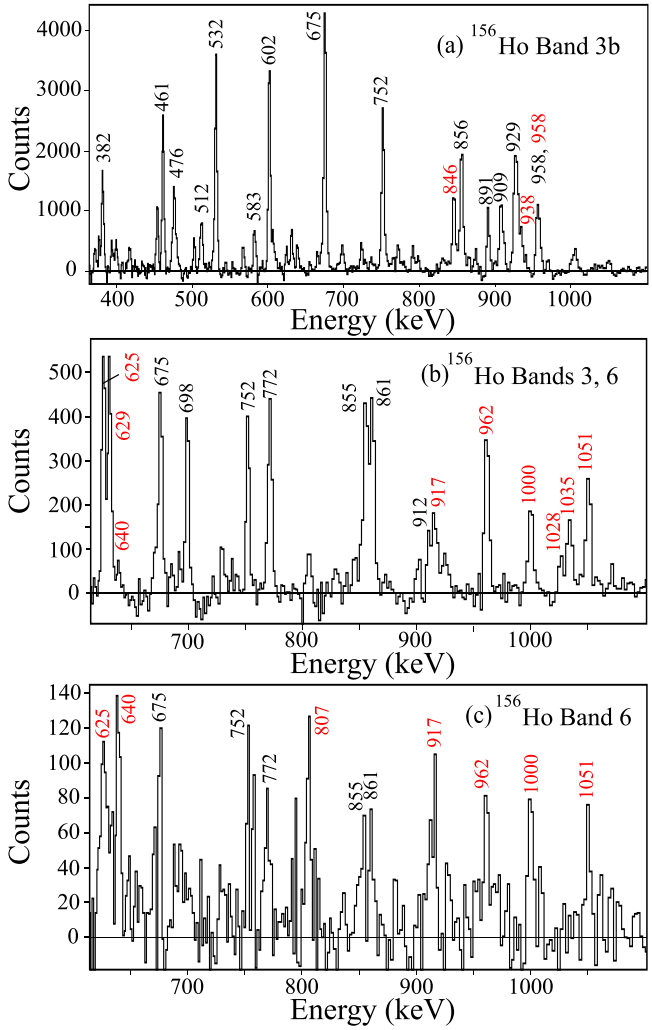


FIG. 5. Representative triple-gated γ^4 coincidence spectra for bands 3 and 6 in ^{156}Ho. The spectrum in panel (a) was generated with the requirement $I1$-$I2$-$I2$; the list $I1$ includes in-band transitions from 382 ($13^- \rightarrow 11^-$) to 752 keV ($23^- \rightarrow 21^-$) while list $I2$ includes in-band transitions from 856 ($25^- \rightarrow 23^-$) to 891 keV ($33^- \rightarrow 31^-$) in band 3b. The spectrum in panel (b) was generated with the requirement $I3$-$I3$-912 keV ($28^- \rightarrow 26^-$) in band 3a; list $I3$ includes transitions in band 6 from 625 ($32^- \rightarrow 30^-$) to 1000 keV ($40^- \rightarrow 38^-$). The spectrum in panel (c) highlights the highest-spin transitions in band 6 up to the 640-keV one ($44^- \rightarrow 42^-$); this spectrum has the gating requirement $I4$-$I4$-1028 keV ($42^- \rightarrow 40^-$), where list $I4$ includes the 625-, 1051-, 962-, 917-, and 1000-keV transitions in band 6. Newly identified transitions are indicated in red.

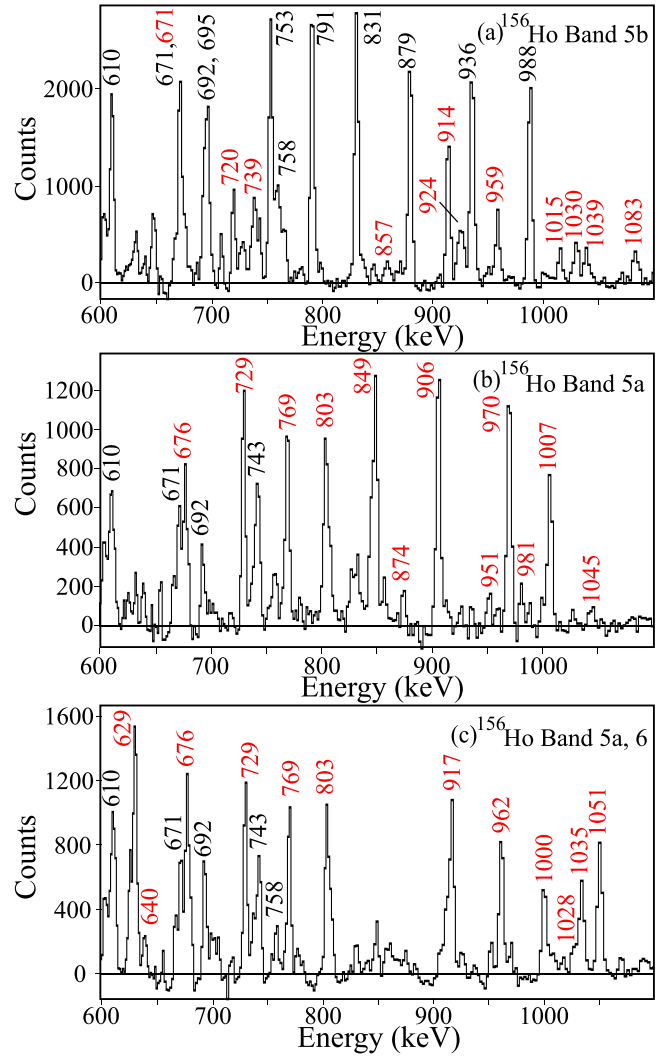


FIG. 6. Representative triple-gated γ^4 coincidence spectra for bands 5 and 6 in ^{156}Ho. The spectrum in panel (a) was generated with the requirement $I1$-$I1$-$I2$; the list $I1$ includes in-band transitions from 695 ($25^- \rightarrow 23^-$) to 879 keV ($33^- \rightarrow 31^-$) while list $I2$ includes in-band transitions from 936 ($35^- \rightarrow 33^-$) to 959 keV ($41^- \rightarrow 39^-$) in band 5b. The spectrum in panel (b) was generated with the requirement $I1$-$I1$-$I2$; list $I1$ includes in-band transitions from 676 keV ($24^- \rightarrow 22^-$) to 803 keV ($30^- \rightarrow 28^-$) while list $I2$ includes in-band transitions from 849 ($32^- \rightarrow 30^-$) to 1007 keV ($38^- \rightarrow 36^-$) in band 5a. The spectrum in panel (c) was generated with the requirement $I1$-$I1$-$I1$; list $I1$ includes in-band transitions from 729 ($26^- \rightarrow 24^-$) to 803 keV ($30^- \rightarrow 28^-$) in band 5a and from 629 ($32^- \rightarrow 30^-$) to 962 keV ($36^- \rightarrow 34^-$) in band 6. Newly identified transitions are in red.

transitions, indicating a change of character, see Sec. IV. At spin 28^- and 30^-, band 5a is fed by decays from band 6. Figure 6(c) shows transitions in bands 5 and 6. This spectrum is similar to Fig. 5(c), indicating a similar decay strength from band 6 to both bands 5 and 3.

B. High-spin states in ^{157}Ho

The present work has significantly extended the level scheme of ^{157}Ho toward higher spin ($40\hbar$–$55\hbar$) in comparison with the previous work of Radford *et al.* [8]. Preliminary analysis of this work can be found in Ref. [25]. A partial level scheme for the highest-spin states in ^{157}Ho is presented in Fig. 7, where the labeling of the bands is adopted from Ref. [8]. Candidate oblate $\gamma = 60^\circ$ levels are highlighted in blue. This work concentrates on new states at high spin in bands 2, 4, and 7. No reliable angular-correlation measurements could be obtained for the high-spin transitions;

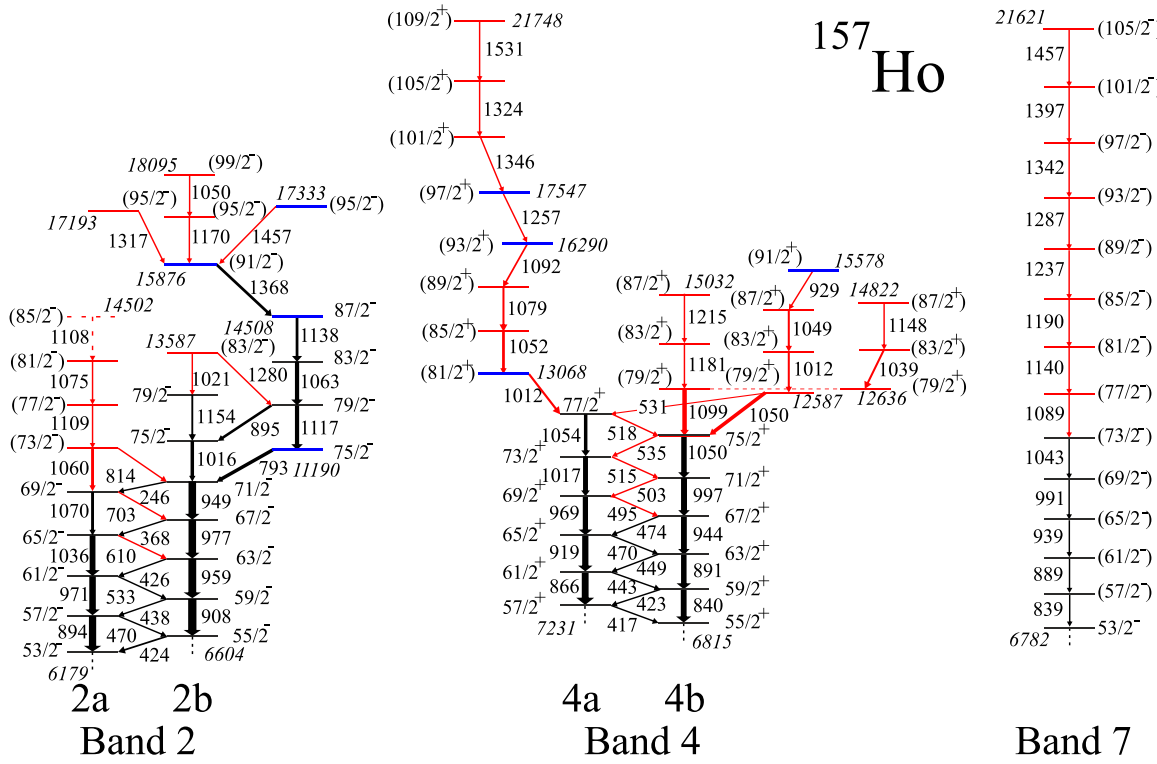


FIG. 7. High-spin region of the levels in bands 2, 4, and 7 in ^{157}Ho. The excitation and transition energies for known states, in black, are taken from Ref. [8]. New states and γ-ray transitions are in red. Blue states indicate candidate oblate $\gamma = 60^\circ$ states, see Sec. IV and Table I.

hence, the highest spin-parity assignments are given in parentheses.

1. Band 2

Band 2 is a negative-parity structure that defines the yrast levels in ^{157}Ho in the $15\hbar$–$30\hbar$ spin range, where it appears as a strongly coupled band with minimal signature splitting. Band 2a was previously observed up to $69/2^-$, while band 2b was extended to $79/2^-$ in addition to other states up to $87/2^-$ and $(91/2^-)$ [8]. Gascon *et al.* [26] using a backed target Doppler-shift attenuation method (DSAM) analysis found for band 2b above $71/2^-$ that "states with a low collectivity feed the band at higher spin, consistent with the interpretation of the irregular sequence starting at spin $75/2^-$ in terms of band termination." Band 2a has now been extended up to $(81/2^-)$, tentatively $(85/2^-)$, and band 2b up to $(99/2^-)$, see Fig. 7. A representative coincidence spectrum for band 2 is shown in Fig. 8(a). The irregular nature of band 2 at high spin is evident.

2. Band 4

Positive-parity band 4 is another strongly coupled sequence. Band 4a was previously observed up to $77/2^+$ [8] and has now been extended to $(109/2^+)$. Band 4b was known up to $75/2^+$ and has now been delineated up to $(91/2^+)$. A representative coincidence spectrum for band 4 is presented in Fig. 8(b). This spectrum specifically displays the extension of the signature $\alpha = -1/2$ branch, band 4a, and its transition from a regular collective band to noncollective behavior.

3. Band 7

Band 7 is a decoupled structure that was previously observed up to the 1043-keV $(73/2^- \rightarrow 69/2^-)$ transition [8], but has now been greatly extended to $(105/2^-)$ with the inclusion of a further eight transitions. A triple-gated γ^4 coincidence spectrum for band 7 is shown in Fig. 8(c). The regular spacing of the transitions is indicative of collective rotational behavior extending to very high spin.

4. Collective high-spin bands

Three further decoupled rotational structures have been tentatively assigned to ^{157}Ho. Their γ ray-energy spacings imply high dynamic moments of inertia. Representative spectra for these sequences, labeled TSD1, TSD2, and TSD3, in order of relative intensity, are displayed in Fig. 9 and are thought to be examples of triaxial strongly deformed (TSD) structures. The bands are too weak to generate meaningful quadruple coincidence spectra. Instead, triple coincidence ones were generated with double-gating conditions. Overall, this work agrees with the spectra presented in Ref. [25]. TSD1 was also reported in Ref. [27]; however, the high-energy transitions are updated in this work. The γ-ray energies are listed in Appendix B. All three bands are of very low intensity, even lower than that of the TSD bands in ^{157,158}Er, which have estimated intensities of the order of 10^{-4} of the strongest yrast transition [11]. The spectra exhibit coincidence relationships with the low-spin yrast transitions in both ^{156}Ho and ^{157}Ho. However, the relative intensity compared with

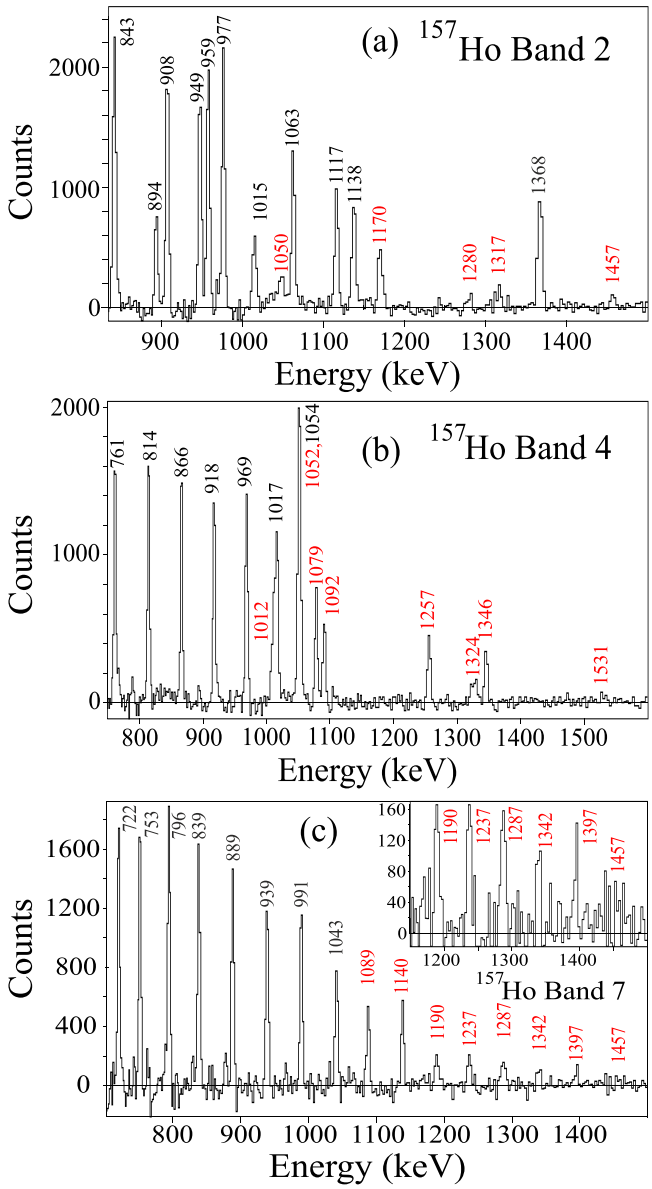


FIG. 8. High-energy part of triple-gated γ^4 coincidence spectra representative of (a) band 2, (b) band 4, and (c) band 7 in ^{157}Ho, respectively. The spectrum in panel (a) was generated with the requirement $l1$-$l1$-$l2$; list $l1$ includes in-band transitions from 591 ($43/2^- \rightarrow 39/2^-$) to 949 keV ($71/2^- \rightarrow 67/2^-$) in band 2b while $l2$ includes the 1117 ($79/2^- \rightarrow 75/2^-$), 1063 ($83/2^- \rightarrow 79/2^-$), 1138 ($87/2^- \rightarrow 83/2^-$), and 1170 keV ($95/2^- \rightarrow 91/2^-$) transitions. The spectrum in panel (b) was generated with the requirement on $l1$-$l1$-$l2$; list $l1$ includes in-band transitions in band 4a from 703 ($49/2^+ \rightarrow 45/2^+$) to 1054 keV ($77/2^+ \rightarrow 73/2^+$) while $l2$ includes the 1012 ($81/2^+ \rightarrow 77/2^+$), 1079 ($89/2^+ \rightarrow 85/2^+$), and 1092 keV ($93/2^+ \rightarrow 89/2^+$) transitions. The spectrum in panel (c) was generated with the requirement $l3$-$l3$-$l3$; list l includes in-band transitions from 650 ($37/2^- \rightarrow 33/2^-$) to 1397 keV ($101/2^- \rightarrow 97/2^-$). Newly identified transitions are labeled in red.

the total projection of all data shows a relative increase in ^{157}Ho by a factor of 2 to 3 compared with ^{156}Ho when in coincidence with the gating conditions used in Fig. 9 for

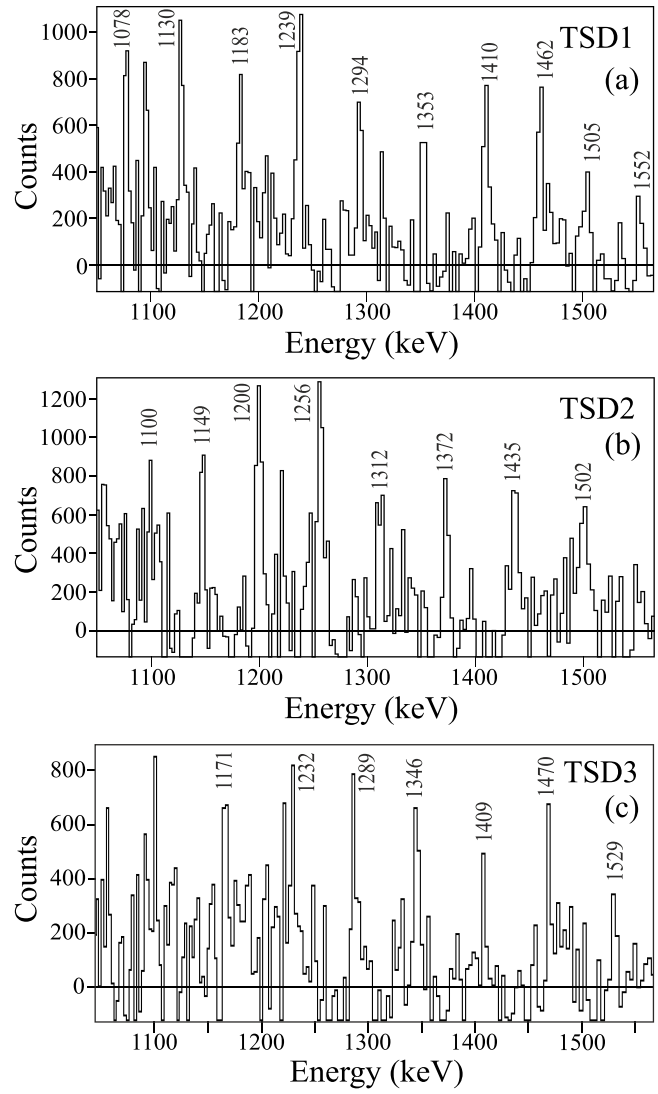


FIG. 9. Double-gated γ^3 spectra for the three TSD structures tentatively assigned to ^{157}Ho. The spectrum in panel (a) was generated with the requirement l-l; the list l contains transitions from 1183 to 1462 keV. The spectrum in panel (b) was generated with the requirement l-l; the list l contains transitions from 1149 to 1435 keV. The spectrum in panel (c) was generated with the requirement l-l; the list l contains transitions from 1171 to 1409 keV.

all bands. Therefore, all three bands are tentatively assigned to ^{157}Ho.

C. High-spin states in ^{158}Ho

The high-spin level structure of doubly odd ^{158}Ho has been extended. This nucleus was populated in the ^{114}Cd(^{48}Ca, $p3n$) ^{158}Ho and ^{124}Sn(^{37}Cl, $3n$) ^{158}Ho reactions. The level scheme and spectra presented here are taken from the ^{114}Cd(^{48}Ca, $p3n$) ^{158}Ho dataset since the statistics are higher. Both datasets produce consistent results, however.

Band 1 forms a strongly coupled structure in ^{158}Ho and is yrast. The high-spin level scheme is displayed in Fig. 10. The spin and parity assignments are taken from those reported in

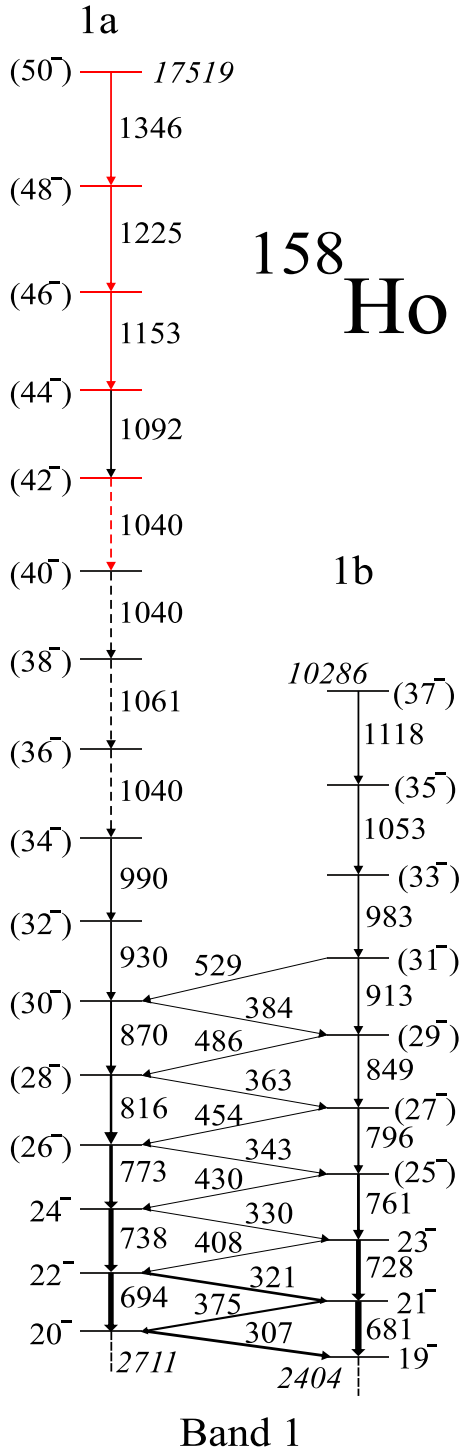


FIG. 10. Level scheme for band 1 in ^{158}Ho; 1a even spin, 1b odd. The excitation energy is based on the accepted values in Ref. [28], which is based on Ref. [29]. All energies shown are from this work and in agreement with those in Ref. [28]. The spin-parity of states above 23^- and 24^-, established in Ref. [29], are tentative. New states and γ-ray transitions are in red.

Refs. [29,30] and accepted in Ref. [28]. The sequence of in-band transitions up to the 23^- and 24^- levels is in agreement with Ref. [29]. Above these states, transitions up to the first 1040-keV γ ray in the even-spin branch and the 1118-keV one

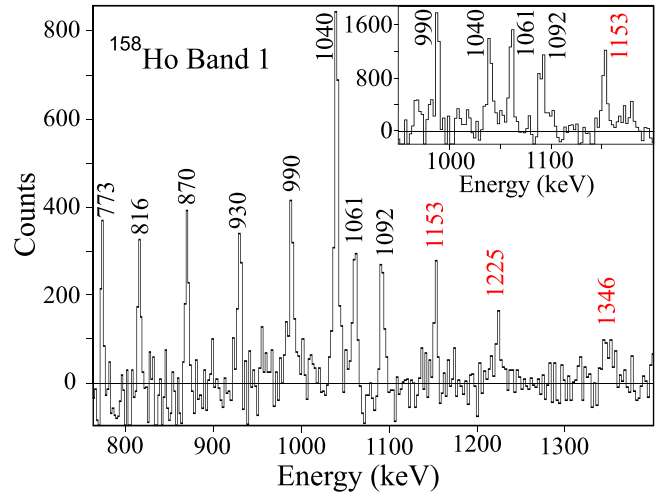


FIG. 11. High-energy part of a triple-gated γ^4 coincidence spectrum for the even-spin ($\alpha = 0$) component of band 1 in ^{158}Ho. The spectrum was generated with the requirement l-l-1040-keV; list l includes in-band transitions from 738 ($24^- \rightarrow 22^-$) to 1225 keV ($48^- \rightarrow 46^-$), excluding the 1040-keV triplet. The inset is a double-gated γ^3 coincidence spectrum with the requirement 1040-1040-keV. Newly identified transitions are in red.

in the odd-spin branch were reported in Ref. [31], although the spins are 2 units lower than the accepted values [28,29], also adopted in this work. The states above 23^- and 24^- are labeled in parentheses. The linking transitions between the even and odd-spin branches are confirmed. The even-spin branch above 24^- is extended to (50^-). The new in-band transitions are assumed to be of stretched-$E2$ character. The exact ordering of the 1061-keV γ ray and the 1040-keV triplet is uncertain and is indicated by dashed lines in Fig. 10. New transitions and states are in red. The 1053-keV ($35^- \rightarrow 33^-$) and 1118-keV ($37^- \rightarrow 35^-$) transitions reported in Refs. [28,29] could not be confirmed but are included for completeness. A representative spectrum for high-energy transitions in band 1a is given in Fig. 11. The continuation to high spin in the even-spin branch is similar to that observed in band 1a in ^{156}Ho. The inset in Fig. 11 is a double coincidence at 1040-keV demonstrating that this is a triplet.

D. High-spin states in ^{159}Er

A comprehensive level scheme for ^{159}Er has been published in Ref. [6] from the same dataset as reported here. This work presents a minor correction to this scheme in the terminating branch of the yrast positive-parity states. The new level structure is given in Fig. 12, where collective states from $I^\pi = 77/2^+$ together with a terminating sequence from $89/2^+$ are shown. The high-spin states above $(77/2^-)$ in the negative-parity band 2 are also displayed. The change is the re-ordering of the 1154- and 1342-keV transitions so that the former directly feeds the 14 117-keV state. This redefines the energy of the lower $89/2^+$ state at 15 271 keV. Evidence for this change is presented in the spectra of Fig. 13. In Fig. 13(b), the intensity of the 1153- and 1154-keV doublet

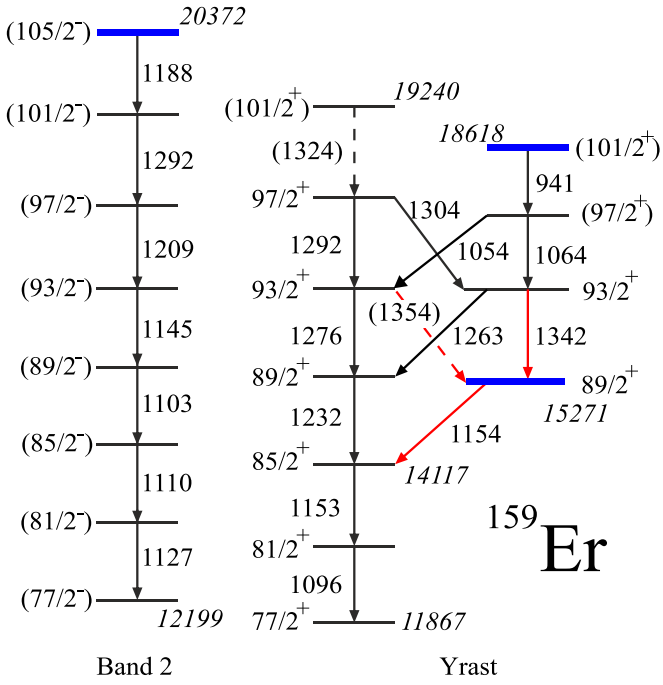


FIG. 12. The high-spin states in ^{159}Er [6] from $77/2^+$ in the yrast positive-parity structure and $(77/2^-)$ in the negative-parity, band 2. The order of the 1154- and 1342-keV transitions (red) is changed compared with Ref. [6]. The states in blue are predicted oblate $\gamma = 60^\circ$ configurations, see Sec. IV and Table II.

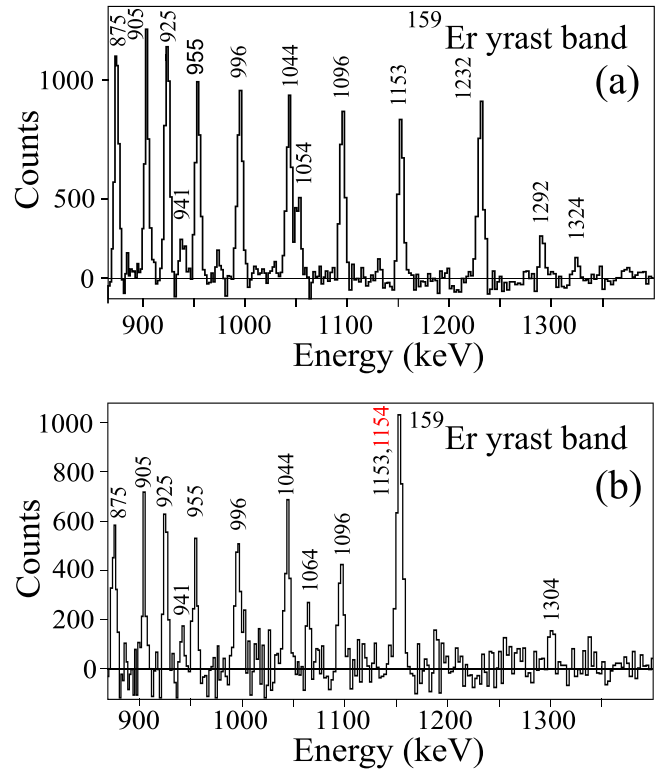


FIG. 13. High-energy part of triple-gated γ^4 coincidence spectra for the $\alpha = +1/2$ yrast band of ^{159}Er. The spectrum in panel (a) was generated with the requirement l-l-1276 keV, while the spectrum in panel (b) was generated with the requirement l-l-1342 keV. The list l for both spectra includes the in-band transitions from 626 ($33/2^+ \rightarrow 29/2^+$) to 1096 keV ($81/2^+ \rightarrow 77/2^+$).

confirms the revised ordering of the transitions in the terminating branch.

IV. BAND TERMINATION

Band termination demonstrates one of the different ways in which angular momentum is manifested in a finite mesoscopic system. In the region of nuclei discussed here with particles outside a ^{146}Gd core, low-energy and -spin prolate nuclear states that generate their angular momentum from collective motion can evolve into oblate noncollective ones at high spin. At this point, the angular momentum is simply given by the sum of the individual j_x values of all the valence particles outside closed quantum shells. To illustrate this transition, together with the evolution of nuclear shapes to ultrahigh spin, potential-energy surface (PES) calculations, see, e.g., Ref. [3], are presented in Fig. 14 for the $(\pi, \alpha) = (-, +1/2)$ configuration in ^{157}Ho at various values of spin-parity, i.e., $I^\pi = 21/2^-$, $61/2^-$, $101/2^-$, and $141/2^-$. The surfaces are shown in terms of polar (ε_2, γ) Hill–Wheeler coordinates, see, e.g., Ref. [32]. It can be clearly seen that local minima appear, corresponding to several different shapes and deformations, in ^{157}Ho over this range of angular momenta. For instance, prolate ($\gamma = 0^\circ$), oblate ($\gamma = 60^\circ$), and triaxial ($\gamma \approx \pm 30^\circ$) minima are evident at different values of the quadrupole deformation ε_2. Hence, the energy surface is sufficiently soft, with respect to deformation, that competing nuclear shapes can be realized and stabilized by the occupation of specific nucleonic configurations. At the highest spins, both highly deformed triaxial ($\gamma \approx 25^\circ$) and oblate ($\gamma = 60^\circ$) shapes are predicted, in addition to a superdeformed prolate one ($\varepsilon_2 \approx 0.65$, $\gamma \approx 0^\circ$).

A. Valence-space termination

In terms of the transition from the collective to noncollective band-termination regime, special energetically favored states have been well established at spin $\approx 45\hbar$ in heavy rare-earth nuclei around ^{158}Er, see, i.e., Ref. [2] and references therein. These states can generally be classified by the number of high-j $h_{11/2}$ protons, and $i_{13/2}$ neutrons in their configurations, denoted as $[p;n]$. For Ho/Er, there are 3/4 protons outside the $Z = 64$ semimagic shell and so configurations with $p = 3$ and $p = 4$ are expected. For the neutron numbers of the nuclei discussed here, $n = 1$ to $n = 3$ is anticipated, with the other neutrons beyond $N = 82$ being distributed in $h_{9/2}/f_{7/2}$ orbitals.

An especially noteworthy type of termination occurs for states associated with maximally aligned single-particle configurations involving all valence particles outside the $Z = 64$ and $N = 82$ cores. The terminating spin can be readily determined by simply adding up all the valence-particle spins to achieve the maximum achievable value I_{max} for these so-called valence-space configurations.

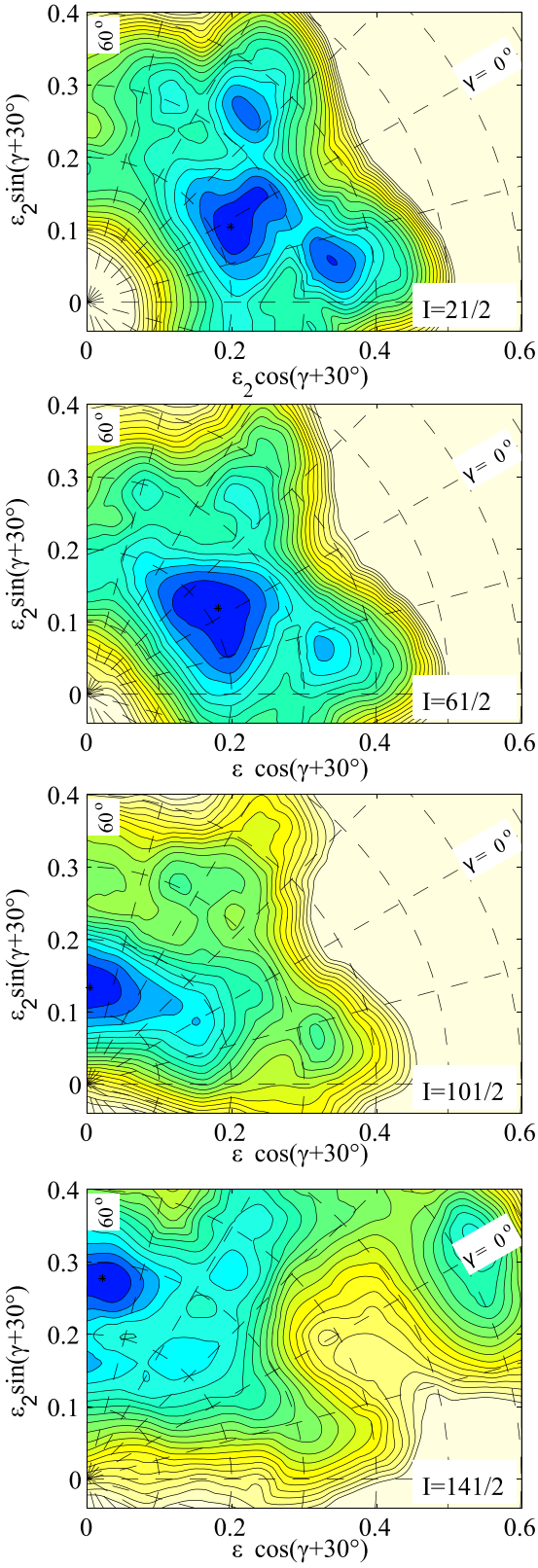


FIG. 14. PES surfaces for the $(\pi, \alpha) = (-, +1/2)$ configuration in ^{157}Ho, calculated at various spins. The energy contours are separated by 0.25 MeV.

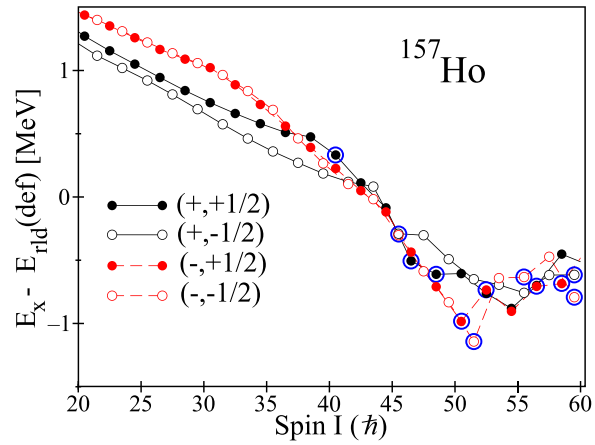


FIG. 15. Calculated CNS excitation energies relative to a deformed rotating-liquid-drop reference, plotted as a function of spin, for the yrast states in ^{157}Ho, for the four possible combinations of parity and signature. Terminating oblate configurations are encircled in blue. It can be seen that the collective yrast line for spins less than $45\hbar$ is replaced by a noncollective yrast line for higher spins.

B. Core-excited termination

Higher-spin states can be reached by forming particle-hole (p-h) excitations across the $Z = 64$ shell gap, which effectively increases the number of particles and holes outside the core. Simple one-particle–one-hole (1p-1h) excitations typically add $4\hbar$ to $5\hbar$ before terminating into additional core-excited noncollective configurations. The lowest-energy 1p-1h excitation occurs by promoting a proton from the topmost $d_{5/2}/g_{7/2}$ pseudospin partner orbital below $Z = 64$. The proton hole preferentially contributes 5/2 units of spin in this excitation ($d_{5/2}$), although 7/2 is also possible ($g_{7/2}$), but with a higher energy cost. Both high-j $h_{11/2}$ and low-j $s_{1/2}/d_{3/2}$ orbitals are available above the $Z = 64$ gap for occupation by the excited proton. In particular, the promotion to the $s_{1/2}/d_{3/2}$ orbital is a positive-parity 1p-1h excitation, maintaining the parity of the high-spin states, while adding an extra $4\hbar$. However, promotion to the $h_{11/2}$ orbital is a negative-parity 1p-1h excitation, which contributes $5\hbar$ for $Z = 67$ Ho, but only $4\hbar$ for $Z = 68$ Er.

Further particle-hole excitations, i.e., 2p-2h across $Z = 64$, bring in even more, but limited, angular momentum to the system. Indeed, Cranked-Nilsson–Strutinsky (CNS) calculations, presented in Fig. 15, indicate that the theoretical yrast line in ^{157}Ho is dominated by many noncollective terminating states in the spin range $45\hbar$–$60\hbar$.

C. Terminating configurations

The single-particle configurations of potential terminating states can be seen in theoretical tilted Fermi-surface diagrams [33]. Such plots are displayed in Fig. 16 for terminating configurations in ^{157}Ho. These diagrams provide the calculated single-particle energies, e_j, for an oblate shape ($\gamma = 60^\circ$), with the x axis labeling the m_j projections of the

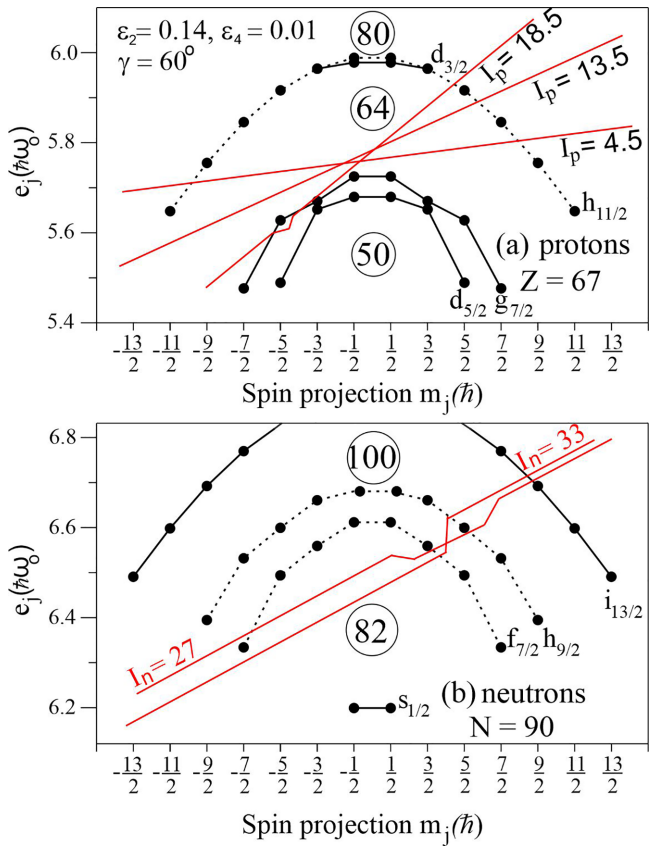


FIG. 16. Calculated single-particle energies at an oblate shape ($\gamma = 60°$), with the x axis labeling the m_j projections of the single-particle angular momentum j onto the nuclear symmetry axis. The tilted Fermi-surfaces (red) indicate potential terminating proton and neutron configurations in ^{157}Ho. It is convenient to refer to the different states as belonging to one specific j shell but, in practice, the subshells that can be referred to as pseudospin partners are strongly mixed and should rather be referred to as "dg" ($d_{5/2}/g_{7/2}$), "sd" ($s_{1/2}/d_{3/2}$), and "fh" ($f_{7/2}/h_{9/2}$), respectively.

single-particle angular momentum j onto the nuclear symmetry axis. The energy scale is given in terms of the oscillator quantum $\hbar\omega_0$, which is typically of the order of 8 MeV.

In Fig. 16(a), tilted Fermi surfaces are drawn for the proton configurations $(h_{11/2})^3$ and $(dg)^{-1}(h_{11/2})^4$. For the former configuration, the maximum spin available is $13.5\hbar$ (i.e., $I^\pi = 27/2^-$) and is achieved by the maximally aligned coupling of the $m_j = 11/2$, 9/2, and 7/2 substates. However, an antialigned coupling of the $m_j = 11/2$, 9/2, and $-11/2$ substates can yield a spin of $4.5\hbar$ ($I^\pi = 9/2^-$) instead. For the core-excited $(dg)^{-1}(h_{11/2})^4$ configuration, the maximum spin is $18.5\hbar$ ($I^\pi = 37/2^+$), with the extra $5\hbar$ coming from the fourth $h_{11/2}$ state ($m_j = 5/2$) and the $g_{7/2}$ hole ($m_j = -5/2$).

Figure 16(b) shows two competing neutron configurations, namely, the maximally aligned $(f_{7/2}/h_{9/2})^5(i_{13/2})^3$ configuration ($I^\pi = 33^-$) and the antialigned $(f_{7/2}/h_{9/2})^5(i_{13/2})^3$ one involving an $m_j = -7/2$ $f_{7/2}$ orbital ($I^\pi = 27^-$). These two neutron configurations provide noncollective oblate states that differ by $6\hbar$. Many examples of such states are now known in holmium and erbium nuclei, including the present results, and are subsequently discussed in Sec. VII A.

To investigate in detail the noncollective-terminating structures, calculations based on the CNS formalism, see, e.g., Ref. [3], have been performed for ^{156,157,158}Ho. The CNS model [34–36] is based on a modified anisotropic harmonic-oscillator Hamiltonian [37] that is cranked around one principal axis. The latest, configuration-constrained version, is able to fix the number of holes in $\pi d_{5/2}/g_{7/2}$ orbitals and particles in $s_{1/2}/d_{3/2}$ states, relative to $Z = 64$. This distinction, which is only possible at small deformations and for positive or close to zero γ values, works well for the description of high-spin states in $Z = 64$–72 isotopes [3].

A summary of various configurations in holmium and erbium isotopes corresponding to plausible single-particle terminating states are given in Tables I and II, respectively. The maximum spin available for each configuration $I_{\max}$ is given along with its parity. Valence-space and core-excited configurations in are also given. The notation is adopted from Ref. [3]. Note that specific configurations in the simple $[p, n]$ notation can yield more than one $I_{\max}$ value; this arises from any odd protons and neutrons within the subset of unlabeled states. Coupling of these odd particle parity and signature quantum numbers (π, α) can lead to doublets or even quadruplets for some configurations, as is evident in the tables. Detailed properties of these candidate terminating states are derived from CNS calculations, performed as a function of spin, in terms of the relative energies of the states and their quadrupole (ε_2, γ) deformation.

V. BAND TERMINATION IN HOLMIUM

In this section, the experimental results for the ^{156,157,158}Ho isotopes are presented in terms of alignment, i_x, and energies relative to an average deformed rotating-liquid-drop reference, $E - E_{\rm rld}$ [3,35]. The methods for defining the reference, as introduced in Ref. [35], have been employed here, making it possible to compare experiment and theory on an absolute scale. The alignment [40] is effectively the single-particle contribution to the nuclear angular momentum and is obtained by removing the underlying collective motion. Often this is done using a variable moment-of-inertia (VMI) reference, which is empirically found to be a quadratic function of rotational frequency for low-spin states [41]. The alignments of the bands are plotted in Fig. 17, with such a VMI reference and Harris parameters [41] $\mathcal{J}_0 = 32.1$ MeV$^{-1}\hbar^2$ and $\mathcal{J}_1 = 34$ MeV$^{-3}\hbar^4$. These parameters were chosen to result in a constant alignment for the $\pi h_{11/2} \otimes \nu(i_{13/2})^2$ configuration in ^{157}Ho [42,43].

The alignment, plotted as a function of rotational frequency, is particularly useful to determine the underlying single-particle configurations of the bands at low to medium spins through the observation or nonobservation of alignment gains (i.e., band crossings). The yrast bands in ^{158}Er and ^{159}Er are included in the alignment plots of Fig. 17 to indicate the expected frequency of the first and second $i_{13/2}$ neutron and first $h_{11/2}$ proton band crossings. At higher spin values in the terminating region, a distinction between single-particle and collective contributions is not

TABLE I. A summary of maximally aligned valence-space and core-excited configurations expected in holmium ($Z = 67$) isotopes for various combinations of proton and neutron states. The states are labeled in the shorthand notation $[p, n]$, where p is the number of $h_{11/2}$ protons and n is the number of $i_{13/2}$ neutrons. Particle-hole excitations into the (sd) orbital are also explicitly labeled. Corresponding experimental candidate states are shown bold and underlined. The experimental states for ^{155}Ho are taken from Ref. [7].

Protons	valence	1p–1h	1p–1h	2p–2h	2p–2h
	$\pi(h)^3_{13.5}$	$\pi(dg)^{-1}_{2.5,3.5}(h)^3_{13.5}(sd)^1_{1.5}$	$\pi(dg)^{-1}_{2.5,3.5}(h)^4_{16}$	$\pi(dg)^{-2}_{6}(h)^4_{16}(sd)^1_{1.5}$	$\pi(dg)^{-2}_{6}(h)^5_{17.5}$
	13.5^-	$17.5^-, 18.5^-$	$18.5^+, 19.5^+$	23.5^+	23.5^-
Neutrons			$^{155}_{67}$Ho, $N = 88$		
$\nu(fh)^5_{15.5,16.5}(i)^1_{6.5}$	[3;1]	[3(sd);1]	[4;1]	[4(sd);1]	[5;1]
$22^-, 23^-$	**35.5**$^+$, **36.5**$^+$	$39.5^+, 40.5^+, 40.5^+, 41.5^+$	40.5^-, **41.5**$^-$, $41.5^-, 42.5^-$	$45.5^-, 46.5^-$	$45.5^+, 46.5^+$
$\nu(fh)^4_{14}(i)^2_{12}$	[3;2]	[3(sd);2]	[4;2]	[4(sd);2]	[5;2]
26^+	**39.5**$^-$	**43.5**$^-$, 44.5^-	**44.5**$^+$, 45.5^+	49.5^+	49.5^-
			$^{156}_{67}$Ho, $N = 89$		
$\nu(fh)^6_{18}(i)^1_{6.5}$	[3;1]	[3(sd); 1]	[4;1]	[4(sd); 1]	[5;1]
24.5^+	**38**$^-$	**42**$^-$, 43^-	**43**$^+$, 44^+	48^+	48^-
$\nu(fh)^5_{15.5,16.5}(i)^2_{12}$	[3;2]	[3(sd); 2]	[4;2]	[4(sd); 2]	[5;2]
$27.5^-, 28.5^-$	**41**$^+$, **42**$^+$	**45**$^+$, **46**$^+$, 46^+, **47**$^+$	$46^-, 47^-, 47^-, 48^-$	$51^-, 52^-$	$51^+, 52^+$
$\nu(fh)^4_{14}(i)^3_{16.5}$	[3;3]	[3(sd); 3]	[4;3]	[4(sd); 3]	[5;3]
30.5^+	**44**$^-$	$48^-, 49^-$	$49^+, 50^+$	54^+	54^-
			$^{157}_{67}$Ho, $N = 90$		
$\nu(fh)^6_{18}(i)^2_{12}$	[3;2]	[3(sd); 2]	[4;2]	[4(sd); 2]	[5;2]
30^+	**43.5**$^-$	**47.5**$^-$, 48.5^-	**48.5**$^+$, 49.5^+	53.5^+	53.5^-
$\nu(fh)^5_{15.5,16.5}(i)^3_{16.5}$	[3;3]	[3(sd); 3]	[4;3]	[4(sd); 3]	[5;3]
$32^-, 33^-$	**45.5**$^+$, **46.5**$^+$	$49.5^+, 50.5^+, 50.5^+, 51.5^+$	$50.5^-, 51.5^-, 51.5^-, 52.5^-$	$55.5^-, 56.5^-$	$55.5^+, 56.5^+$
			$^{158}_{67}$Ho, $N = 91$		
$\nu(fh)^7_{18.5,19.5}(i)^2_{12}$	[3;2]	[3(sd); 2]	[4;2]	[4(sd); 2]	[5;2]
$30.5^-, 31.5^-$	$44^+, 45^+$	$48^+, 49^+, 49^+, 50^+$	$49^-, 50^-, 50^-, 51^-$	$54^-, 55^-$	$54^+, 55^+$
$\nu(fh)^6_{18}(i)^3_{16.5}$	[3;3]	[3(sd); 3]	[4;3]	[4(sd); 3]	[5;3]
34.5^+	48^-	$52^-, 53^-$	$53^+, 54^+$	58^+	58^-

possible. Indeed, in the CNS model, the total spin is obtained as the sum of all single-particle contributions with no attempt to divide further between collective and single-particle components.

Figure 18 displays the experimental energies, relative to a deformed rotating liquid-drop reference, plotted as a function of spin for the Ho isotopes.

A. Doubly odd ^{156}Ho

Band 1 in ^{156}Ho represents the low-spin yrast band and is based on the $\pi h_{11/2} \otimes \nu i_{13/2}$ configuration [22]. It has an initial alignment i_x of $\approx 6\hbar$ consistent with this single-particle assignment, see Fig. 17(a). Band 1 undergoes an alignment gain Δi_x of $\approx 6\hbar$ at $\omega \approx 0.40$ MeV/$\hbar$, which can be attributed to the rotational alignment (backbend) of the second and third $\nu i_{13/2}$ quasineutrons. Band 3 exhibits properties similar to band 1, in terms of signature splitting, or energy staggering, and measured $B(M1)/B(E2)$ ratios of reduced transition probabilities [21]. It is, therefore, also assigned to another $\pi h_{11/2} \otimes \nu i_{13/2}$ configuration. One scenario has the $i_{13/2}$ neutron simply moved to the unfavored-signature state. An alternative interpretation is that one of the bands involves a neutron 2p-2h excitation across $N = 82$, i.e., a paired $([505]11/2^-)^2$ excitation. This is in line with suggested configurations in ^{154}Dy [44] and ^{156}Dy [3].

Band 2, which starts at $I^\pi = (17^+)$, has been assigned a four-quasiparticle structure based on a $\pi h_{11/2} \otimes \nu h_{9/2}(i_{13/2})^2$ configuration [22]. This configuration uses the highest-spin single-particle states and is expected to be favored in energy. The high alignment of band 2 ($\approx 12\hbar$), see Fig. 17(a), is consistent with its four-quasiparticle structure. At $\omega \approx 0.46$ MeV/$\hbar$, this band exhibits an alignment gain that can be attributed to the rotational alignment of the second and third $\pi h_{11/2}$ quasiprotons. It has been suggested in Ref. [36] that such an alignment can also be understood as a change in the number of $h_{11/2}$ protons present in the configuration. The new CNS calculations, presented here, also support this scenario. In Fig. 19, a comparison of the experimental band 2 [Fig. 19(a)] with predicted [7;2] and [5;2] configurations [Fig. 19(b)] is shown. Around spin 32, these configurations cross such that the [5;2] one becomes yrast at higher spins. The steady downslope implies that this configuration is approaching termination which occurs at $I_{\max} = 52$ (see Table I). A similar situation occurs in ^{158}Ho (see Sec. V C), where the [5;3] configuration crosses the [7;3] one and becomes yrast at high spin.

Band 5, which starts at $I^\pi = (21^-)$, is interpreted as another four-quasiparticle structure in ^{156}Ho, in which the odd proton occupies a positive-parity state; it is thus assigned to the $\pi(dg) \otimes \nu(fh)(i_{13/2})^2$ configuration. It has a gain in alignment of $\approx 7\hbar$ from $\omega \approx 0.35$ to $\omega \approx 0.45$ MeV/$\hbar$,

TABLE II. A summary of maximally aligned valence-space and core-excited configurations predicted for erbium ($Z = 68$) isotopes for various combinations of proton and neutron states. The states are labeled in the shorthand notation $[p, n]$, where p is the number of $h_{11/2}$ protons and n is the number of $i_{13/2}$ neutrons. Particle-hole excitations into the (sd) orbital are also explicitly labeled. Corresponding experimental candidate states are bold and underlined and are taken from Refs. [38] (^{154}Er), [39] (^{155}Er), [4,7] (^{156}Er), [9,10] (^{157}Er), [2] (^{158}Er), and [6] (^{159}Er), respectively.

Protons	valence	1p–1h	1p–1h
	$\pi(h)^4_{16}$	$\pi(dg)^{-1}_{2.5,3.5}(h)^4_{16}(sd)^1_{1.5}$	$\pi(dg)^{-1}_{2.5,3.5}(h)^5_{17.5}$
	16^+	$20^+, 21^+$	$20^-, 21^-$
Neutrons		$^{154}_{68}$Er, $N = 86$	
$\nu(fh)^3_{10.5,11.5}(i)^1_{6.5}$	[4;1]	[4(sd); 1]	[5;1]
$17^-, 18^-$	**33**$^-$, 34^-	$37^-, 38^-, 38^-, 39^-$	$37^+, 38^+, 38^+, 39^+$
$\nu(fh)^2_8(i)^2_{12}$	[4;2]	[4(sd); 2]	[5;2]
20^+	**36**$^+$	$40^+, 41^+$	$40^-, 41^-$
		$^{155}_{68}$Er, $N = 87$	
$\nu(fh)^4_{14}(i)^1_{6.5}$	[4;1]	[4(sd); 1]	[5;1]
20.5^+	**36.5**$^+$	$40.5^+, 41.5^+$	$40.5^-, 41.5^-$
$\nu(fh)^3_{10.5,11.5}(i)^2_{12}$	[4;2]	[4(sd); 2]	[5;2]
$22.5^-, 23.5^-$	**38.5**$^-$, **39.5**$^-$	$42.5^-, 43.5^-, 43.5^-, 44.5^-$	$42.5^+, 43/2^+, 43.5^+, 44.5^+$
		$^{156}_{68}$Er, $N = 88$	
$\nu(fh)^5_{15.5,16.5}(i)^1_{6.5}$	[4;1]	[4(sd); 1]	[5;1]
$22^-, 23^-$	**38**$^-$, 39^-	$42^-, 43^-, 43^-, 44^-$	$42^+, 43^+, 43^+, 44^+$
$\nu(fh)^4_{14}(i)^2_{12}$	[4;2]	[4(sd); 2]	[5;2]
26^+	**42**$^+$	**46**$^+$, 47^+	$46^-, 47^-$
		$^{157}_{68}$Er, $N = 89$	
$\nu(fh)^6_{18}(i)^1_{6.5}$	[4;1]	[4(sd); 1]	[5;1]
24.5^+	**40.5**$^+$	$44.5^+, 45.5^+$	$44.5^-, 45.5^-$
$\nu(fh)^5_{15.5,16.5}(i)^2_{12}$	[4;2]	[4(sd); 2]	[5;2]
$27.5^-, 28.5^-$	**43.5**$^-$, **44.5**$^-$	$47.5^-, 48.5^-, 48.5^-, 49.5^-$	$47.5^+, 48.5^+, 48.5^+, 49.5^+$
$\nu(fh)^4_{14}(i)^3_{16.5}$	[4;3]	[4(sd); 3]	[5;3]
30.5^+	**46.5**$^+$	$50.5^+, 51.5^+$	$50.5^-, 51.5^-$
		$^{158}_{68}$Er, $N = 90$	
$\nu(fh)^6_{18}(i)^2_{12}$	[4;2]	[4(sd); 2]	[5;2]
30^+	**46**$^+$	$50^+, 51^+$	$50^-, 51^-$
$\nu(fh)^5_{15.5,16.5}(i)^3_{16.5}$	[4;3]	[4(sd); 3]	[5;3]
$32^-, 33^-$	**48**$^-$, **49**$^-$	$52^-, 53^-, 53^-, 54^-$	$52^+, 53^+, 53^+, 54^+$
		$^{159}_{68}$Er, $N = 91$	
$\nu(fh)^7_{18.5,19.5}(i)^2_{12}$	[4;2]	[4(sd); 2]	[5;2]
$30.5^-, 31.5^-$	$46.5^-, 47.5^-$	$50.5^-, 51.5^-, 51.5^-, 52.5^-$	$50.5^+, 51.5^+, 51.5^+, 52.5^+$
$\nu(fh)^6_{18}(i)^3_{16.5}$	[4;3]	[4(sd); 3]	[5;3]
34.5^+	**50.5**$^+$	$54.5^+, 55.5^+$	$54.5^-, 55.5^-$
$\nu(fh)^5_{15.5,16.5}(i)^4_{20}$	[4;4]	[4(sd); 4]	[5;4]
$35.5^-, 36.5^-$	51.5^-, **52.5**$^-$	$55.5^-, 56.5^-, 56.5^-, 57.5^-$	$55.5^+, 56.5^+, 56.5^+, 57.5^+$

consistent with the first $(\pi h_{11/2})^2$ alignment. Bands 3 and 5 both show further gains in alignment at their highest spins at $\omega \approx 0.50$ MeV/$\hbar$. These gains appear to be an indication of a change to a noncollective regime.

1. Positive-parity terminating states

Band 9 is newly identified in this work. It has an irregular structure that is linked to band 2, but not band 1. This suggests that band 9 has the same parity as band 2.

To understand the positive-parity nature, experimental and theoretical energies, relative to a deformed rotating-liquid-drop reference, $E - E_{\rm rld}$, are plotted for all ^{156}Ho bands in Fig. 20. Specifically, positive-parity states are in Figs. 20(a) and 20(c). Band 9 rapidly becomes yrast above spin $\approx 35\hbar$, as can be seen in Fig. 18(a), and has low-lying states at $I^\pi = (41^+)$ and (42^+). The yrast (41^+) level is particularly favored in energy and is found to be directly fed by several high-energy γ rays of energies 1397, 1501, 1553, and 1859 keV, see Fig. 1. The (42^+) state also feeds the (41^+) one via a 900-keV dipole transition. These states are interpreted as signature partners of a maximally aligned noncollective configuration, where the nuclear spin is wholly generated by the ten valence particles outside the spherical ^{146}Gd core. The 41^+ and 42^+ favored states represent the terminating $I_{\rm max}$ states of the $[p; n] = [3; 2]$ valence-space configuration. These are listed

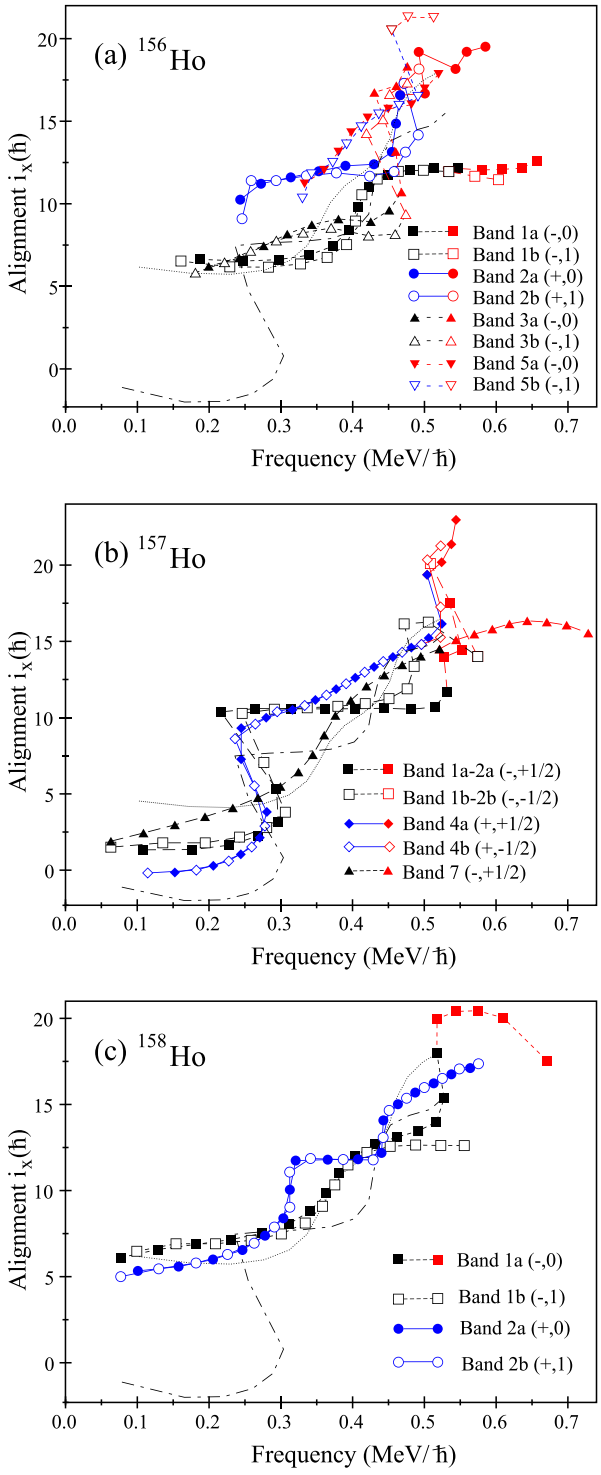


FIG. 17. Experimental alignments i_x as a function of the rotational frequency for bands in $^{156-158}$Ho. Bands are labeled as in the level schemes and by (parity, signature). New states are denoted by red symbols and lines. (a) Bands 1, 2, 3, and 5 in ^{156}Ho. (b) Bands 2, 4, and 7 in ^{157}Ho. The noncollective states are not included. (c) Bands 1 and 2 in ^{158}Ho. The data for band 2 are taken from Refs. [28,29]. The dot-dashed and dotted black lines are the yrast bands in ^{158}Er and ^{159}Er, respectively. These are plotted to show the expected position of the first and second $(\nu i_{13/2})^2$ neutron and first $(\pi h_{11/2})^2$ proton band crossings.

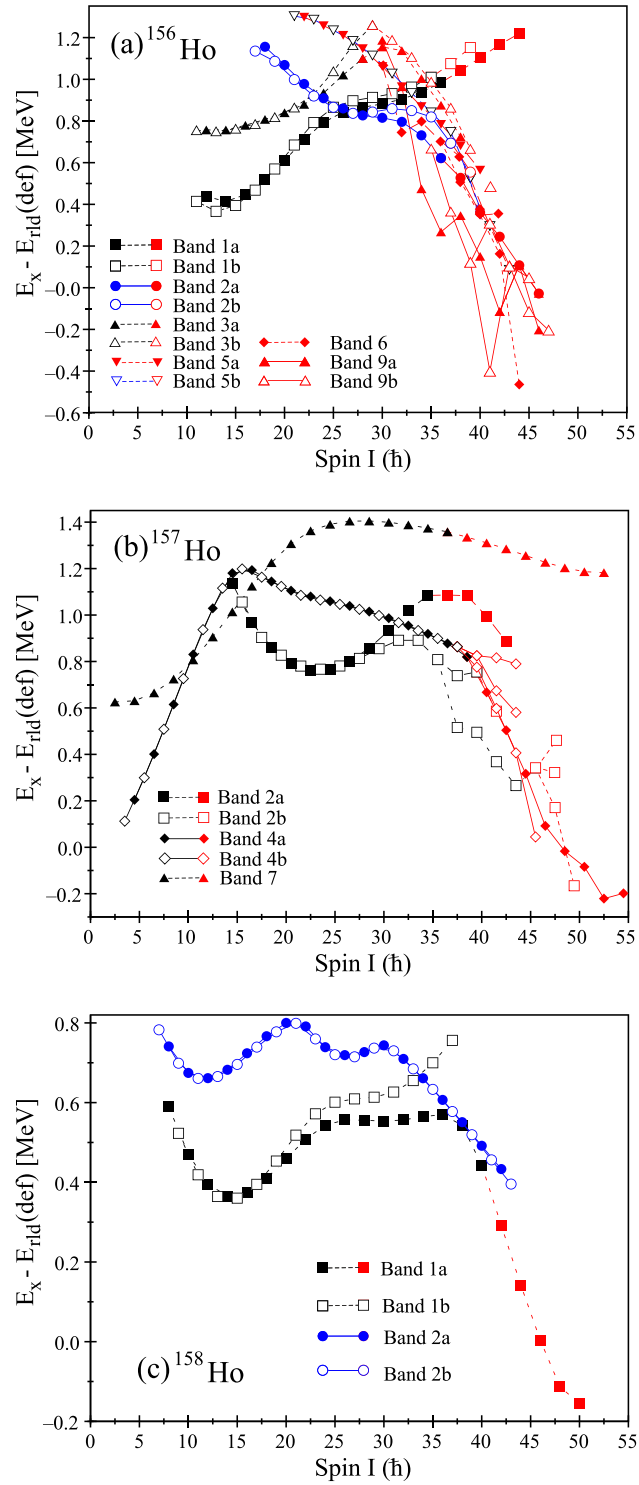


FIG. 18. Experimental excitation energy, relative to a deformed rotating-liquid-drop reference $E - E_{\rm rld}$, plotted as a function of spin I for bands in ^{156,157,158}Ho. New states are denoted by red symbols and lines. (a) Bands 1, 2, 3, 5, 6, and 9, in ^{156}Ho. (b) Bands 2, 4, and 7 in ^{157}Ho. (c) Bands 1 and 2 in ^{158}Ho. The data for band 2 are taken from Refs. [28,29]. The convention for labeling in the alignment, i_x (Fig. 17), and $E - E_{\rm rld}$, this figure, is as follows: Parity: solid lines denote positive parity, dashed ones for negative parity. Signature (α): Filled symbols denote $\alpha = 0$ (and $\alpha = +1/2$ for odd-A nuclei); open symbols denote $\alpha = 1$ (and $\alpha = -1/2$ for odd-A nuclei).

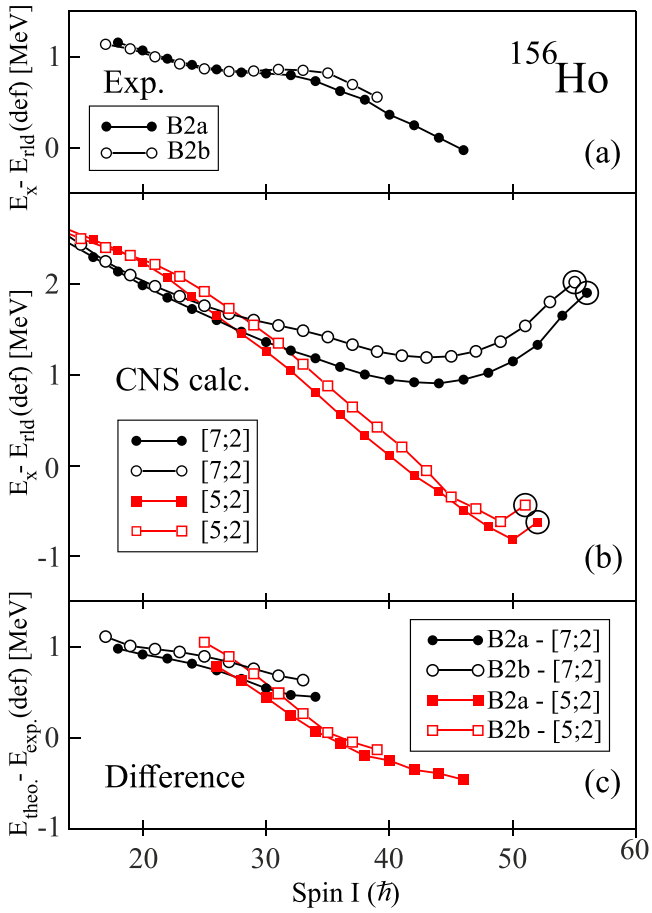


FIG. 19. (a) Energies, relative to a rotating liquid-drop reference, for band 2 in ^{156}Ho (the signature partners are labeled B2a and B2b). (b) CNS calculations for [7;2] and [5;2] configurations. (c) Energy differences between experiment and theory. Encircled states correspond to I_{max} oblate states.

as firm assignments in the summary table of configurations, Table III.

These clearly identified states, which are associated with relatively pure single-particle configurations, provide a theoretical way to assign spin and parity to the highest-spin states. This is particularly important for ^{156}Ho, where all spins and parities have been labeled as tentative, since the connection of all of the bands to the $I^\pi = 4^-$ ground state has not been rigorously established [24]. Nevertheless, theoretical confirmation together with the γ-ray angular-distribution analysis give confidence in the spin-parity assignment for the majority of levels observed. In addition, the 41^+ and 42^+ states correspond to the well-established terminating states in ^{158}Er at 48^- and 49^- [2,45], with the least favored proton and neutron removed, see Tables I and II.

Band 9 continues above the low-lying (41^+) valence-space terminating state via several high-energy (>1 MeV) transitions, which are assumed to be of stretched $E2$ character, and reaches a tentative spin of (47^+). The (41^+) terminating state also appears to be directly fed by high-energy transitions (1397, 1501, 1553, and 1859 keV), in a similar manner to that previously observed in ^{157,158}Er [2,9]; it costs a lot of energy to progress beyond these particularly favored, fully aligned states. Band 9a, including the low-lying (42^+) state, is also fed by several high-energy transitions from the highest levels of band 2a.

The $I^\pi = (43^+)$ state directly feeds the (41^+) level via the 1745-keV transition, and also decays to the 39^+ state of band 9b via consecutive γ rays of energies 1035 and 1376 keV. This state could correspond to the I_{max} value expected for the [4;1] configuration, see Table I, which involves the promotion of a proton, across the $Z = 64$ shell gap, into the fourth $h_{11/2}$ orbital. This 1p-1h excitation effectively increases the valence space to 12 particles or holes, enabling the higher I_{max} value. In this case, a proton is promoted from the positive-parity $d_{5/2}/g_{7/2}$ orbital into the negative-parity $h_{11/2}$ orbital, i.e., corresponds to a negative-parity 1p-1h excitation.

Alternatively, the proton may be promoted to the positive-parity $s_{1/2}/d_{3/2}$ orbital instead, i.e., a positive-parity 1p-1h excitation. Indeed, I_{max} states at 45^+, 46^+, 46^+, and 47^+ are expected for a 1p-1h positive-parity excitation of the [3;2] configuration given the available couplings of the odd proton and neutron. This quadruplet of states is labeled $[3(sd);2]$ in shorthand notation to emphasize that the excitation is into the $s_{1/2}/d_{3/2}$ orbital. The detailed single-particle configurations of these states are given in Table I. Specifically, the 45^+ and 46^+ levels represent 1p-1h proton excitations from the $m_j = -5/2\, d_{5/2}/g_{7/2}$ orbital into the $m_j = +3/2\, s_{1/2}/d_{3/2}$ one. Additional states with 46^+ and 47^+ at higher energy can be formed by promoting from the $m_j = -7/2$ orbital instead, i.e., corresponding to the opposite signature. Candidate states at (45^+), (46^+), and (47^+) for these terminating configurations are indeed observed in band 9, see Fig. 1.

At higher spin, the CNS calculations of Fig. 20(b) predict a series of low-lying (yrast) terminating states for $I^\pi = 48^+$–54^+. These represent the 1p-1h [4;3] excitation in addition to the 2p-2h $[4(sd);3]$ excitation, as listed in Table I.

2. Negative-parity terminating states

Figure 20(b) provides the experimental energies of the negative-parity states in bands 1, 3, 5, and 6 in ^{156}Ho, relative to a deformed rotating liquid-drop reference, plotted as a function of spin. Theoretical CNS calculations are displayed in Fig. 20(d) for negative-parity configurations. Possible experimental and theoretical oblate $\gamma = 60^\circ$ states are encircled.

For negative-parity configurations, valence-space terminations can be achieved in configurations with an odd number of $\nu i_{13/2}$ neutrons, namely, [3;1] and [3;3] states. The former configuration can accommodate $38\hbar$ of spin, while the latter can achieve $44\hbar$. The newly identified band 6 shows two relatively low-lying $I^\pi = (38^-)$ states. Theory predicts noncollective oblate 38^- states at similar energies for both the [3;1] and [3;3] configurations [see Figs. 20(b) and 20(d)]. For the [3;1] configuration, 38^- represents the maximum spin (I_{max}) that can be achieved, while it would correspond to an ($I_{max} - 6$) state of the [3;3] one.

Below spin $38\hbar$, theory suggests that the [3;1] configuration provides an appropriate description of the band, while above this the [3;3] configuration becomes lower in energy.

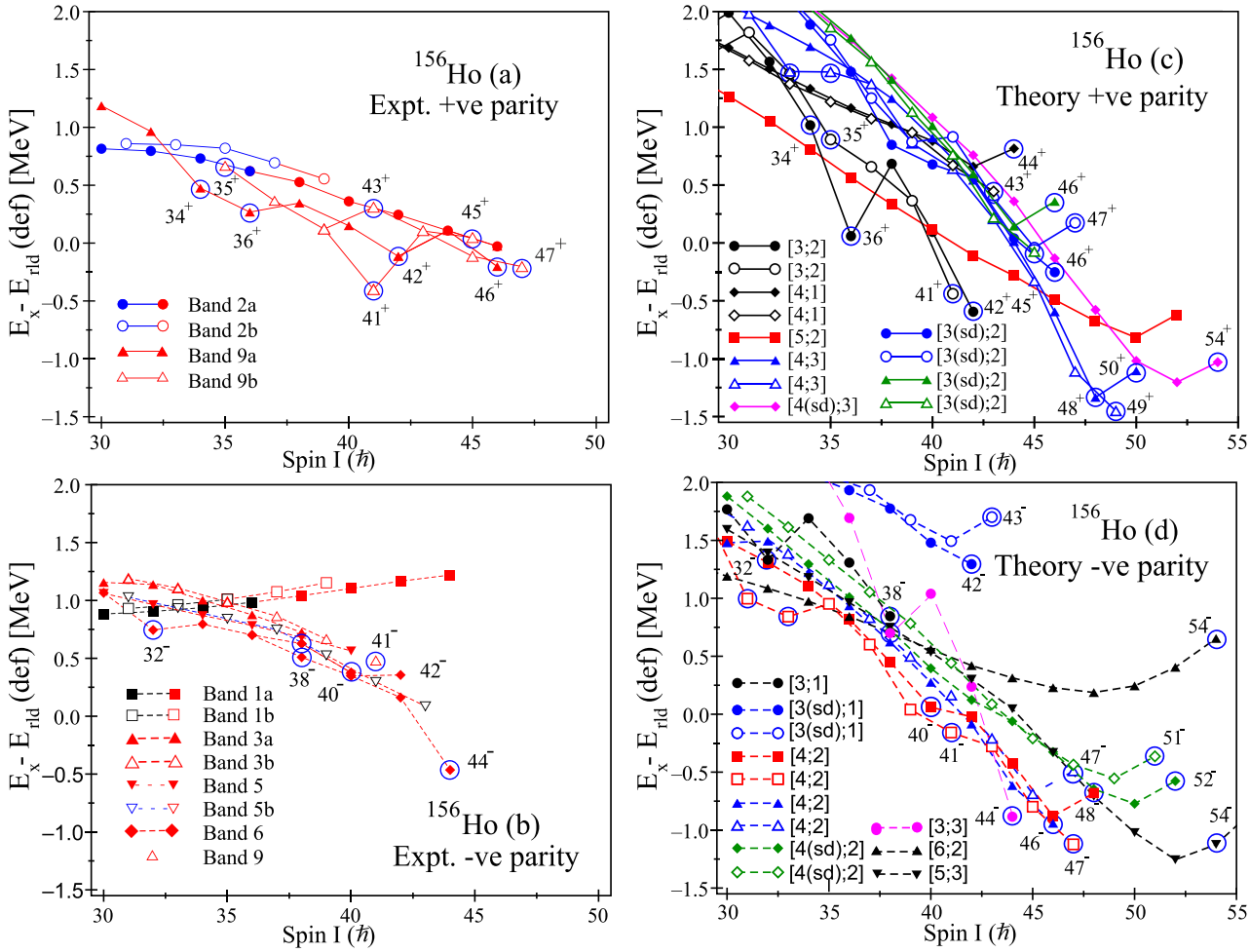


FIG. 20. Experimental and calculated excitation energies in ^{156}Ho, relative to a deformed rotating-liquid-drop reference, plotted as a function of spin. (a) Positive-parity experimental states, (b) negative-parity experimental ones, (c) low-lying positive parity calculated configurations, and (d) low-lying negative-parity ones. Blue circles indicate oblate ($\gamma = 60^\circ$) configurations. In the experimental plots such states are encircled where a possible corresponding oblate state is identified in theory. In the theory plots, states are labeled by their I^π values at high spin or where a candidate experimental state is suggested. The calculated configurations are defined in Table I.

This is reflected in the experimental $E - E_{\rm rld}$ plot of Fig. 20(b) with a sudden change in slope at spin $38\hbar$. Band 6 continues by three transitions up to $I^\pi = (44^-)$, where the [3;3] configuration should terminate. A second (42^-) level is seen decaying via a 1222-keV transition. This could represent the 1p-1h (sd) excitation of the [3;1] configuration, namely, [3(sd); 1] (see Table I). The (32^-) state of band 6 would then correspond to the $(I_{\rm max} - 6)$ oblate state of the [3;1] configuration. It decays to several closely lying (30^-) states (see Fig. 2). This is similar to the bandhead of band 9b, which also corresponds to a predicted $(I_{\rm max} - 6)$ oblate state of the [3;2] configuration.

Negative-parity states can also be formed by the [4;2] configuration. Here, the negative parity is achieved by a 1p-1h proton excitation into the fourth $\pi h_{11/2}$ orbital. This represents a core-excited configuration and is expected to terminate at $I^\pi = 46^-$ and 47^- [see Table I and Fig. 20(d)]. The CNS calculations imply that this configuration should exhibit favored $(I_{\rm max} - 6)$ states at 40^- and 41^-. There is indeed a candidate oblate state at (40^-) at the top of band 6, which decays via a 911-keV transition, and would represent an oblate to oblate transition.

Furthermore, a γ-ray of relatively low energy, 880 keV, feeds the favored (41^+) state of band 9b, see Fig. 1. It is unlikely that the feeding state has spin $42\hbar$, or $43\hbar$, since this would make the level particularly favored in energy, and hence not consistent with the overall agreement with theory. Therefore, a $41\hbar$ spin is more likely. There are no expected low-lying, positive-parity states at this spin, other than the lower-lying (41^+) state. Hence, a spin-parity assignment of (41^-) is proposed for the level and it can then be attributed to the $(I_{\rm max} - 6)$ state of the [4;2] configuration, as discussed above. Similar to the (40^-) decay, the 880-keV γ-ray would represent an oblate-to-oblate transition, but in this case of non-stretched $E1$ character. It is interesting to note that there are no odd-spin levels corresponding to negative-parity band 6 for the proposed 41^- to decay into by a stretched $E2$ transition. This is because the band 6 configurations below spin $40\hbar$ have an odd number of $h_{11/2}$ protons and $i_{13/2}$ neutrons but an even

TABLE III. A summary of oblate, $\gamma = 60^\circ$, states assigned to ^{156}Ho. The energies are given relative to the lowest level of band 1a, which lies at an unknown energy y above the ground state of this doubly odd nucleus. The configuration for states listed in bold face are more certain, the others are based on the comparisons with calculations, see text for details.

I^π	Energy (keV)	Config.	Spin	Band
32$^-$	7689	[3;1]	$I_{max} - 6$	6
34$^+$	8420	[3;2]	$I_{max} - 8$	9a
35$^+$	9133	[3;2]	$I_{max} - 6$	9b
36$^+$	9268	[3;2]	$I_{max} - 6$	9a
38$^-$	10 619	[3;3]	$I_{max} - 6$	6
38$^-$	10 737	[3;1]	I_{max}	6
40$^-$	11 647	[4;2]	$I_{max} - 6$	6
41$^+$	11 471	[3;2]	I_{max}	9b
41$^-$	12 351	[4;2]	$I_{max} - 6$	9b
42$^+$	12 371	[3;2]	I_{max}	9a
42$^-$	12 842	[3(sd); 1]	I_{max}	6
43$^+$	13 216	[4;1]	I_{max}	9b
44$^-$	13 287	[3;3]	I_{max}	6
45$^+$	14 450	[3(sd); 2]	I_{max}	9b
46$^+$	14 865	[3(sd); 2]	I_{max}	9a
47$^+$	15 541	[3(sd); 2]	I_{max}	9b

number of $f_{7/2}/h_{9/2}$ neutrons. The only way to achieve odd spin, or signature $\alpha = 1$, is to invoke the unfavored signatures of either the $h_{11/2}$ proton or the $i_{13/2}$ neutron, which is energetically expensive for these low-Ω orbitals.

Table III summarizes all of the candidate noncollective oblate states assigned to doubly odd ^{156}Ho, listing their energies, spins, parities, and shorthand configuration labels. Their full single-particle configurations are listed in Table I. States that are strongly supported by theory, or those where angular-correlation data are available, are indicated in bold face in the table. The configurations of the other states are based on comparisons with the CNS calculations.

B. ^{157}Ho

The bands in ^{157}Ho have been extended to significantly higher spins than previously observed [8], see Fig. 7, which shows states above spin $\approx 26\hbar$. Band 7 represents a decoupled collective structure built on the $\pi h_{9/2}[541]1/2^-$ orbital [8]. Bands 2 and 4 are based on strongly coupled $\pi h_{11/2}$ and $\pi g_{7/2}$ orbitals, respectively, and hence exhibit interleaved $E2$ ($\Delta I = 2$) signature sequences connected by $M1/E2$ dipole transitions. Experimental alignment i_x and $E - E_{rld}$ plots are shown in Figs. 17 and 18, respectively, for the relevant bands.

1. Positive-parity high-spin states

Band 4 in ^{157}Ho delineates all the positive-parity high-spin states uncovered in this nucleus. Excitation energies, relative to a deformed rotating liquid-drop reference, are presented in Fig. 21(a) as a function of spin, together with the CNS calculations in Fig. 21(c). Up to spin $77/2^+$, band 4 behaves as a regular, signature-degenerate sequence which can be attributed to the [6;2] structure. Above this spin, decreasing energies can be associated with the more-favored [4;2] configuration which terminates with $I_{max} = 97/2^+, 99/2^+$. Indeed, band 4a is traced up to a possible oblate terminating state for the [4;2] configuration at $(97/2^+)$. Its signature partner, band 4b, also progresses to higher spin; the 1099-1181-1215-keV sequence appears to be the smooth continuation of the [6;2] configuration, while the parallel 1050-1012-1049-929-keV branch appears to represent the [4;2] configuration.

The CNS calculations of Fig. 21(c) also demonstrate that the [3;3] valence-space configuration, a less regular structure, produces specific yrast, or near-yrast, oblate states at spin $81/2^+$, $91/2^+$, and $93/2^+$, that can compete with, or even perturb, the more collective [4;2] states at these spins. Indeed, evidence is seen for this with the $(93/2^+)$ level of band 4a and the $(91/2^+)$ level of band 4b lower than expected in Fig. 21. These spins represent the I_{max} values for the two signatures of the [3;3] configuration, see Table I. For band 4a, the positive-parity state at $(93/2^+)$ corresponds to the oblate 49^- states in ^{158}Er [2], while the $(91/2^+)$ level of band 4b corresponds to the 48^- oblate state. The $81/2^+$ state of band 4a could correspond to the $(I_{max} - 6)$ state of the [3;3] configuration, related to the 43^- oblate state in ^{158}Er.

Finally, band 4a is seen to continue to even higher spin via the 1346-1324-1531-keV sequence of transitions extending to a tentative spin of $(109/2^+)$. CNS calculations suggest that these states are associated with the [5;3] configuration, which ends up at $I^\pi_{max} = 113/2^+$, just $2\hbar$ higher than observed experimentally.

2. Negative-parity high-spin states

Band 2 in ^{157}Ho represents the complementary negative-parity states to the positive-parity sequence of band 4. Excitation energies, relative to a deformed rotating liquid-drop, are provided in Fig. 21(b) for negative-parity states in ^{157}Ho, as a function of spin, while CNS calculations are in Fig. 21(d). For negative parity, the CNS calculations suggest that the signature-degenerate [6;3] configuration is crossed by the [4;3] one around spin 47.5 (i.e., 95/2). Again, a valence-space configuration, [3;2], competes and provides a yrast fully aligned state at $87/2^-$, which could be assigned to the $I^\pi = 87/2^-$ state in band 2b. This $I^\pi = 87/2^-$ oblate state is related to the favored 46^+ level in ^{158}Er by the removal of an $h_{11/2}$ proton. In addition, the $75/2^-$ represents the $(I_{max} - 6)$ state of the [3;2] configuration, see Table IV.

The $87/2^-$ state of band 2b is fed by a high-energy 1368-keV transition from a presumed $(91/2^-)$ level. A possible interpretation is that it represents the $(I_{max} - 6)$ oblate state of the [4;3] configuration, which terminates at $I^\pi = 103/2^-$, see Table I. This $(91/2^-)$ level is then fed by three transitions (1170, 1317, 1457 keV) from presumed $I^\pi = (95/2^-)$ states; the 1170-keV transition has a further 1050-keV γ ray above it. The CNS calculations, see Fig. 21(d), indicate that configurations of the type [4;3] become yrast above spin 95/2, where the observed $(99/2^-)$ state at 18 095 keV would be one transition short of termination in the [4;3] configuration. This is another example of a configuration that can produce a quadruplet of states through the combination of odd protons and neutrons. The third, highest-energy, $(95/2^-)$

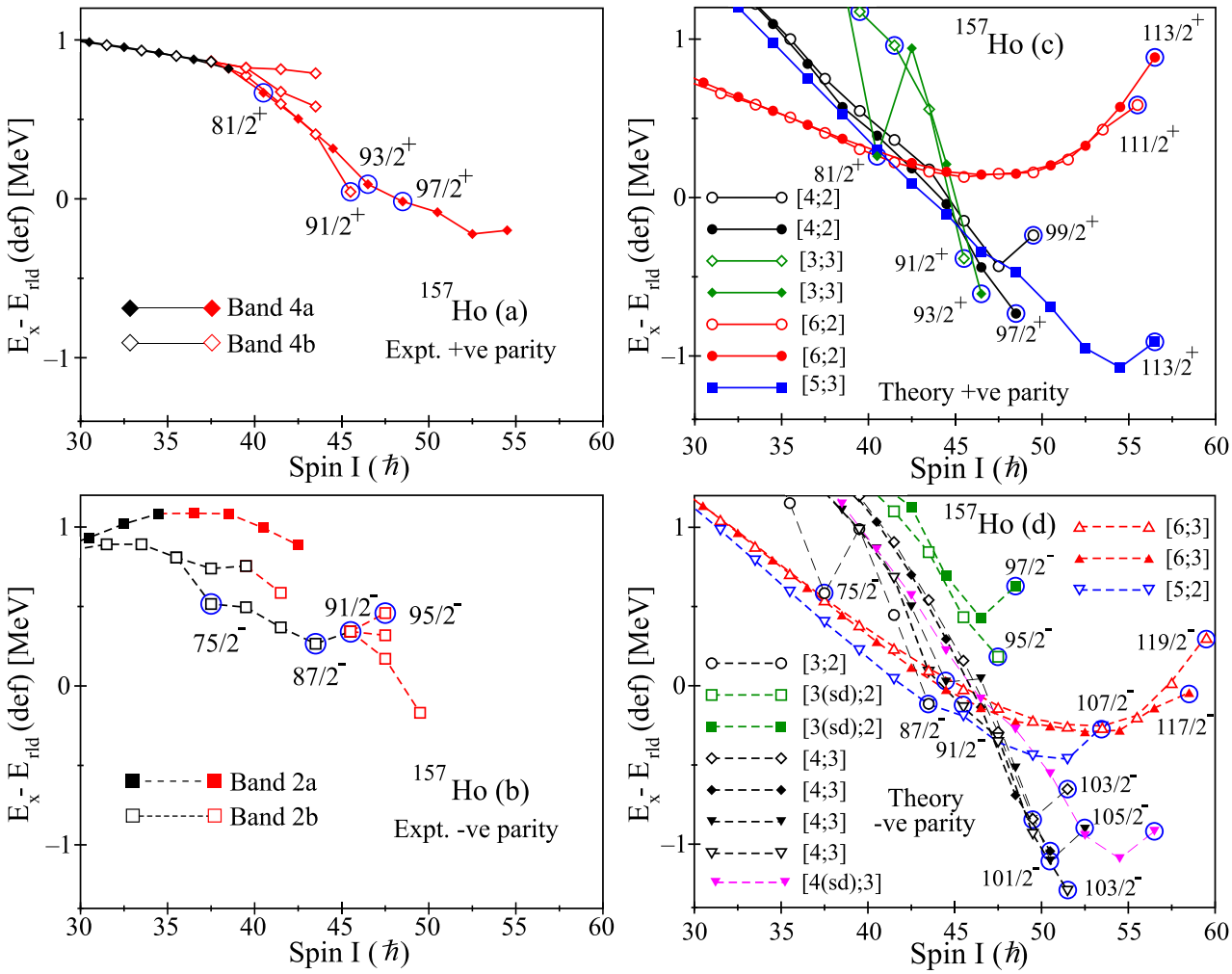


FIG. 21. Experimental and calculated excitation energies in ^{157}Ho, relative to a deformed rotating liquid-drop reference, as a function of spin. (a) Band 4, (b) band 2, (c) calculated low-lying positive-parity configurations, and (d) low-lying negative-parity ones. Blue circles indicate oblate ($\gamma = 60^\circ$) configurations. The calculated configurations are defined in Table I.

level is then assigned to the terminating state of the $[3(sd);2]$ core-excited configuration, involving a positive-parity 1p-1h excitation.

TABLE IV. A summary of oblate, $\gamma = 60^\circ$, states assigned to ^{157}Ho. The spin-parity values of the configurations, for which an assignment is proposed with confidence, are written in bold face. Where the spin values correspond to the maximum spin I_{max} of the configuration. The excitation energy and configuration is indicated.

I^π	Energy (keV)	Config.	Spin	Band
75/2$^-$	11 190	[3;2]	$I_{max} - 6$	2b
81/2$^+$	13 068	[3;3]	$I_{max} - 6$	4a
87/2$^-$	14 508	[3;2]	I_{max}	2b
91/2$^+$	15 578	[3;3]	I_{max}	4b
91/2$^-$	15 876	[4;3]	$I_{max} - 6$	2b
93/2$^+$	16 290	[3;3]	I_{max}	4a
95/2$^-$	17 333	[3(*sd*);2]	I_{max}	2b
97/2$^+$	17 547	[4;2]	I_{max}	4a

Finally, band 7 exhibits different character to the other sequences in ^{157}Ho. It continues smoothly to very high spins despite becoming highly nonyrast in the terminating spin region, see Fig. 18(b).

A summary of all the candidate noncollective oblate states assigned to ^{157}Ho is given in Table IV, with their energies, spins, parities, and shorthand configuration labels; the full single-particle configurations are listed in Table I.

C. Doubly odd ^{158}Ho

One sequence in ^{158}Ho has been significantly extended in this work. Previously, two strongly coupled bands were established at low spin [28–30]. Band 1 is yrast and is based on a negative-parity $\pi h_{11/2} \otimes \nu i_{13/2}$ configuration, while band 2 is a signature-degenerate band based on the positive-parity $\pi g_{7/2} \otimes \nu i_{13/2}$ one. Here, the proton resides in the high-Ω $[404]7/2^+$ Nilsson orbital. Strongly coupled bands with similar properties have been established in ^{158}Er [2], ^{157}Ho [8], in addition to a band in ^{156}Ho [22].

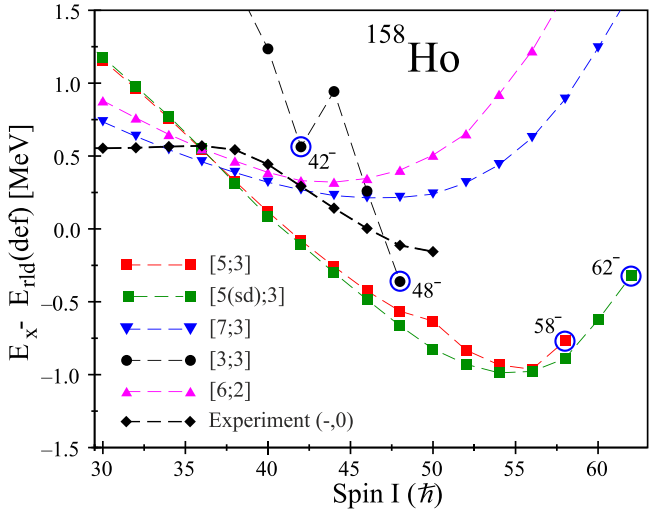


FIG. 22. Experimental excitation energies of the even-spin members of band 1 in ^{158}Ho plotted relative to a deformed rotating liquid-drop reference. Calculated CNS configurations are also provided.

Experimental alignment plots for bands 1 and 2 are shown in Fig. 17(c), while the excitation energies, relative to a deformed rotating liquid-drop reference, are given in Fig. 18(c). The even-spin ($\alpha = 0$) branch of band 1 has been extended to higher spin and becomes particularly favored in energy above $\approx 35\hbar$. Its high-spin behavior is compared with calculated CNS energies in Fig. 22.

For neutron number $N = 91$, terminating states can be formed with configurations containing two or three $\nu i_{13/2}$ neutrons, see Table I; those with three such neutrons result in negative-parity states. Figure 22 indicates that [5;3] and [5(sd);3] configurations become low in energy (yrast) beyond $35\hbar$. These configurations involve particle-hole excitations across $Z = 64$; terminating states are found at 58^- and 62^- for the 2p-2h [5;3] and 3p-3h [5(sd);3] configurations, respectively (see Table I and Fig. 22). In addition, the [3;3] configuration yields a valence-space termination at $I^\pi = 48^-$, which is close to yrast.

D. ^{155}Ho revisited

Results for $N = 88$ ^{155}Ho, obtained from these data, have been published in Ref. [7]. Noncollective states were established at $I^\pi = 79/2^-$, $87/2^-$, and $89/2^+$. These levels are associated with [3;2], [3(sd);2], and [4;2] configurations, respectively, see Table I. Essentially the [3;2] valence-space termination and its positive- ($+4\hbar$) and negative-parity ($+5\hbar$) core-excited terminations have been observed. The CNS calculations also suggest energetically favored terminations of the [3;1] ($I^\pi = 71/2^+, 73/2^+$) and [4;1] ($83/2^-$) configurations. These states are included in Table I and there are clear candidates for them in the ^{155}Ho level scheme of Ref. [7].

VI. TERMINATION IN ERBIUM

The proposed band-terminating states in erbium isotopes are reviewed here with respect to their expected configurations and I_{max} values.

A. Valence-space termination

After the original discovery of three valence-space terminations in ^{158}Er at $I^\pi = 46^+$, 48^-, and 49^- [45], corresponding states have been established in other erbium isotopes. The maximum-spin values, I_{max}, for expected configurations in the $^{154–159}$Er isotopes are listed in Table II. These are analogous to the Ho ones in Table I. Erbium has an additional proton relative to holmium, which often occupies the fourth $h_{11/2}$ proton orbital. The $(h_{11/2})^4$ configuration can generate $I^\pi = 16^+$ when fully aligned. Table II identifies the known terminating states in these nuclei, which are all built on [4; x] configurations. Across the isotopes, x, the number of $i_{13/2}$ neutrons, progresses from 1 to 4. In ^{159}Er, terminating states of the [4;3] and [4;4] valence-space configurations are identified at $I^\pi = (101/2^+)$ and $(105/2^-)$, respectively [6], as seen in Fig. 12, where positive- and negative-parity states are present at similar energies. For the heavier erbium isotopes, the corresponding theoretical terminating levels are higher in spin and beyond the experimentally attained spins. For instance, the [4;3] configuration in ^{160}Er has I_{max} values at $I^\pi = 51^-$ and 52^-, while the [4;4] configuration terminates at 54^+ [46].

B. Core-excited termination

Recently, a new terminating state at $I^\pi = 50^-$ was proposed in ^{158}Er [2], which corresponds to the maximum spin of the core-excited [5;2] configuration of Table II. This level directly feeds the valence-space terminations of the [4;3] configuration at 48^- and 49^-. For erbium, the positive-parity ($\pi d_{5/2}/g_{7/2} \rightarrow s_{1/2}/d_{3/2}$) and negative-parity ($\pi d_{5/2}/g_{7/2} \rightarrow h_{11/2}$) 1p-1h proton excitations both generate an additional four units of spin before termination, and so should generate terminating states of the same spin, but opposite parity. This is in contrast with the holmium isotopes, where the negative-parity excitation can produce one more unit of spin, i.e., $5\hbar$, in comparison to the positive-parity excitation, which only produces $4\hbar$.

In Ref. [9], several high-energy transitions were established in ^{157}Er feeding the $87/2^-$, $89/2^-$, and $93/2^+$ terminating states. It was possible to establish that some of these were of dipole character following a high-fold angular-correlation analysis. The $87/2^-$, $89/2^-$, and $93/2^+$ states represent the valence-space terminations of the [4;2] and [4;3] configurations, respectively, see Table II. However, core-excited terminations at $95/2^-$ ([4(sd);2]) and $95/2^+$ ([5;2]), are expected as well. Both could decay via dipole $E1$ and $M1$ transitions, respectively, into the $93/2^+$ valence-space termination. Effectively, these core excitations then represent the positive- and negative-parity 1p-1h excitations of the [4;2] configuration.

VII. ENERGY SYSTEMATICS

In this section, experimental and theoretical (CNS) energy differences between noncollective oblate states are discussed. Often, the states are related to each other by the simple exchange of a neutron, or proton. This gives an insight into the single-particle spectrum at the extremes of angular momentum.

TABLE V. Summary of the deformation (ε_2) and energy differences (ΔE) between the associated I_{max} and ($I_{max} - 6$) oblate states from experiment and theory (CNS). The high-j $h_{11/2}$ proton and $i_{13/2}$ neutron configurations, $[p;n]$, are given. The relevant band for Ho nuclei is indicated.

Nucleus	Band	$I_{max} \rightarrow (I_{max} - 6)$	$[p;n]$	ε_2 (I_{max})	ε_2 ($I_{max} - 6$)	ΔE_{expt} (keV)	ΔE_{CNS} (keV)
		ν exchange $h_{9/2}$ ($m_j = 5/2$) to $f_{7/2}$ ($m_j = -7/2$)					
^{156}Ho	6	$38^- \rightarrow 32^-$	[3;1]	0.119	0.131	3047	2677
^{156}Ho	9a	$42^+ \rightarrow 36^+$	[3;2]	0.135	0.149	3103	2832
^{157}Ho	2b	$87/2^- \rightarrow 75/2^-$	[3;2]	0.140	0.151	3319	2870
^{157}Ho	4a	$93/2^+ \rightarrow 81/2^+$	[3;3]	0.143	0.154	3223	2929
^{157}Er		$81/2^+ \rightarrow 69/2^+$	[4;1]	0.115	0.132	2831	2695
^{157}Er		$89/2^- \rightarrow 77/2^-$	[3;3]	0.133	0.145	3050	2843
^{158}Er		$46^+ \rightarrow 40^+$	[4;2]	0.136	0.148	3281	2873
^{158}Er		$49^- \rightarrow 43^-$	[4;3]	0.139	0.151	3126	2927
^{159}Er		$101/2^+ \rightarrow 89/2^+$	[4;3]	0.142	0.154	3348	2959
		ν exchange $f_{7/2}$ ($m_j = 5/2$) to $f_{7/2}$ ($m_j = -7/2$)					
^{156}Ho	6	$44^- \rightarrow 38^-$	[3;3]	0.137	0.158	2668	2057
^{156}Er		$42^+ \rightarrow 36^+$	[4;2]	0.128	0.144	2386	2007
^{157}Er		$93/2^+ \rightarrow 81/2^+$	[4;3]	0.135	0.151	2758	2039

A. ($I_{max} - 6$) states

The maximally aligned I_{max} states are known to have associated levels at lower spin, where a pair of valence particles form an antialigned pair, i.e., the nucleons remain paired and are energetically favored (yrast) compared with neighboring states. This mechanism was originally established in ^{158}Er, where a theoretical oblate 40^+ state ($I_{max} - 6$) can be formed from the same basic single-particle configuration as in the maximally aligned 46^+ state (I_{max}), but with a rearrangement of $\nu h_{9/2}$ and $f_{7/2}$ substates [47], see Table II.

This particle exchange involves moving a neutron from the $h_{9/2}$ ($m_j = 5/2$) substate to the $f_{7/2}$ ($m_j = -7/2$) one, forming an antialigned $f_{7/2}$ pair with a total spin change of $6\hbar$. This exchange is illustrated in Fig. 16(b), where the aligned and antialigned neutron configurations for $N = 90$ generate spins of $33\hbar$ and $27\hbar$, respectively, which indeed differ by $6\hbar$. In ^{158}Er, this exchange is also possible for negative parity, and observed from the maximally aligned 49^- state to the ($I_{max} - 6$) one at 43^- [2,48]. Equivalent antialigned ($I_{max} - 6$) oblate states have been observed in ^{157}Er [5,9], ^{159}Er [6,49], and ^{157}Ho [8], while the present work has established further examples in ^{156}Ho and ^{157}Ho. In the ^{156}Ho, the $(42^+) \rightarrow (36^+)$ (Fig. 1), and $(38^-) \rightarrow (32^-)$ (Fig. 2). In ^{157}Ho, they occur for $(87/2^-) \rightarrow (75/2^-)$ and $(93/2^+) \rightarrow (81/2^+)$ (Fig. 7).

Table V summarizes the energy and deformation (ε_2) differences between the associated I_{max} and ($I_{max} - 6$) states, comparing experiment and CNS theory. It is interesting to note that the deformation (ε_2) of the ($I_{max} - 6$) state is consistently higher than that of the I_{max} one. This is understood from the fact that an orbital with a higher value of m_j ($m_j = -7/2$) is filled, which is an orbital corresponding to rotation around the equator of the nucleus.

A summary of the I_{max} and ($I_{max} - 6$) states is presented in Fig. 23. Figures 23(a) and 23(b) provide the experimental and calculated (CNS) energy differences as a function of neutron number, respectively. The theoretical energy-difference predictions are systematically lower than the experimental results ranging from ≈150 to 450 keV, Fig. 23(c). This relatively small difference is impressive for these highly excited nuclear states that occur ≈10 MeV above the nuclear ground state. The individual differences between experiment and theory ($\Delta E_{expt} - \Delta E_{CNS}$) are plotted in Fig. 23(c), along with the associated high-j $h_{11/2}$ proton and $i_{13/2}$ neutron configurations, $[p;n]$. Two systematic trends can be observed. First, for an equal number of $h_{11/2}$ protons the higher number of $i_{13/2}$ neutrons is always lower; that is, closer to experiment. Second, for the same number of $i_{13/2}$ neutrons, the $(h_{11/2})^4$ proton configurations lie below the $(h_{11/2})^3$ ones, again closer to the experimental values. These systematic observations offer important insights into potential refinements of the theoretical high-j proton and neutron single-particle energies.

Figure 23(d) provides the calculated quadrupole deformation ε_2 of the I_{max} state, as a function of the neutron number; it indicates a correlation between deformation and neutron number for these favored oblate states. Indeed, with decreasing deformation, the energy splitting between the single-particle Nilsson orbitals at oblate deformation is reduced, consistent with the experimental observations of Fig. 23(a).

Additional I_{max} to ($I_{max} - 6$) states are also observed, which involve a different neutron exchange: a neutron moves from $f_{7/2}$ ($m_j = 5/2$) to the $f_{7/2}$ ($m_j = -7/2$) state. This is observed in ^{156}Ho from 44^- to 38^- in band 6. The energy difference for this transition (2668 keV) is consistent with the other two examples in ^{156}Er (2386 keV) (42^+ to 36^+ [4]) and ^{157}Er (2758 keV) ($93/2^+$ to $81/2^+$ [9]).

Another interesting comparison between the favored states is given in Table VI, which summarizes the deformation (ε_2) and energy differences between oblate states of opposite parity and a spin change of $3\hbar$ from experiment and theory (CNS). This involves the ν exchange $i_{13/2}$ ($m_j = 9/2$) to the $f_{7/2}$ ($m_j = 3/2$) level. Once again there is significant consistency between the experimental values, which as noted above, are systematically a few hundred keV higher than the theoretical CNS values. It is, however, worth noting that the

TABLE VI. Summary of the deformation (ε_2) and energy differences (ΔE) between oblate states of opposite parity and a spin change of $3\hbar$ from experiment and theory (CNS). Exchanges between $I_{\max}$ and $(I_{\max}-6)$ states are indicated. The high-j $h_{11/2}$ proton and $i_{13/2}$ neutron configurations, $[p;n]$, are given. The relevant bands for Ho nuclei are indicated.

Nucleus	Bands	$I \rightarrow (I-3)$	$[p;n]$	$\varepsilon_2\,(I)$	$\varepsilon_2\,(I-3)$	ΔE_{expt} (keV)	ΔE_{CNS} (keV)
		ν exchange $i_{13/2}$ ($m_j = 9/2$) to $f_{7/2}$ ($m_j = 3/2$)					
		$I_{\max} \rightarrow I_{\max}$					
^{156}Ho	6 → 9b	$44^- \rightarrow 41^+$	[3;3] → [3;2]	0.137	0.130	1749	1462
^{157}Ho	4a → 2b	$93/2^+ \rightarrow 87/2^-$	[3;3] → [3;2]	0.135	0.140	1782	1467
^{158}Er		$49^- \rightarrow 46^+$	[4;3] → [4;2]	0.139	0.136	1749	1462
		$(I_{\max}-6) \rightarrow (I_{\max}-6)$					
^{157}Ho	4a → 2b	$81/2^+ \rightarrow 75/2^-$	[3;3] → [3;2]	0.154	0.151	1872	1404
^{158}Er		$43^- \rightarrow 40^+$	[4;3] → [4;2]	0.151	0.148	1901	1408

biggest experimental energy differences (i.e., $\Delta E_{\text{expt}} = 1872$ and 1901 keV) are associated with the $(I_{\max}-6)$ states.

B. Experimental 1p-1h excitation energies

Evidence has been found for both valence-space and core-excited termination in a series of holmium isotopes. In ^{156,157}Ho, both positive- and negative-parity 1p-1h excitations have been identified on top of [3;1], [3;2], and [3;3] valence-space terminations. The excitations involve both ($\pi d_{5/2}/g_{7/2} \rightarrow s_{1/2}/d_{3/2}$) and ($\pi d_{5/2}/g_{7/2} \rightarrow h_{11/2}$) 1p-1h proton excitations across $Z = 64$, respectively. These core-excitations relative to the valence-space configurations are summarized in Table VII, which provides their relative excitation energies from experiment and theory, together with their predicted quadrupole deformation. Another example is included in the table for ^{158}Er [2]. The table indicates that creating a 1p-1h core excitation leads to a predicted slight decrease in the nuclear quadrupole deformation (ε_2). However, this shape change is not nearly as large as the one observed when comparing the $(I_{\max}-6)$ state to the $I_{\max}$ one.

VIII. COLLECTIVITY AT HIGH SPIN

In contrast with the many irregular "terminating" bands observed and discussed in detail above, there are several sequences which exhibit regular "collective" behavior at the highest spins ($\geqslant$40). Their characteristics are discussed below.

A. ^{157}Ho band 7

Band 7 in ^{157}Ho is based on an $I^\pi = 9/2^-$ state that lies 84 keV above the ground state; the odd proton has been assigned to the [541]1/2$^-$ Nilsson orbital, originating from the $h_{9/2}$ subshell [8] A long sequence of collective stretched-$E2$ transitions has been established built on this state [8], while the present work has extended it by eight transitions ($16\hbar$) to $(105/2^-)$. Although it is briefly yrast around spin $12\hbar$, see Fig. 18, it is well over 1 MeV above yrast at spin $\approx 50\hbar$, yet it persists with a smooth behavior with respect to frequency (N.B. band 1 in ^{156}Ho shows similar characteristics). Both neutron $i_{13/2}$ and proton $h_{11/2}$ alignments are expected in band 7 and it thus forms a stable collective structure to high spin bypassing the lower-lying terminating states. Its single-particle configuration must have an $I_{\max}$ value of at least $105/2\hbar$ ($52.5\hbar$) or even higher, which suggests that multiple particle-hole excitations are involved.

Mean lifetimes of levels from $37/2^-$ to $53/2^-$ in band 7 have been measured by Gascon *et al.* [26], together with those of band 2 over a similar spin range. It was found that band 7 ($h_{9/2}$) has a larger quadrupole moment than band 2 ($h_{11/2}$) and is thus more deformed.

One consequence of the larger quadrupole deformation of band 7 is that the first backbend of $i_{13/2}$ neutrons is delayed. This can be seen in Fig. 17(b), where the alignment frequency is delayed from 0.25 to 0.35 MeV/$\hbar$, and a more gradual upbend is observed rather than a sharp backbend.

Another interesting observation by Gascon *et al.* [26] involved a clear difference in the lifetimes of the feeding of high-spin states in band 2 and band 7 in ^{157}Ho. In band 2,

TABLE VII. Summary of the deformation (ε_2) and energy difference (ΔE) for the 1p-1h proton core-excited terminations in ^{156,157}Ho from experiment and theory (CNS). Results for ^{158}Er [2] are also included. The relevant bands for Ho nuclei are indicated.

Nucleus	Bands	$I_i \rightarrow I_f$	Config. change	ε_2 change	ΔE_{expt}(keV)	ΔE_{CNS}(keV)
^{156}Ho	6	$38^- \rightarrow 42^-$	[3; 1] → [3(sd); 1]	0.119 → 0.117	2105	2829
^{156}Ho	9b	$41^+ \rightarrow 45^+$	[3; 2] → [3(sd); 2]	0.130 → 0.128	2979	2894
^{156}Ho	9a	$42^+ \rightarrow 46^+$	[3; 2] → [3(sd); 2]	0.135 → 0.131	2493	2942
^{157}Ho	2b	$87/2^- \rightarrow 95/2^-$	[3; 2] → [3(sd); 2]	0.140 → 0.133	2825	2930
^{156}Ho	6 → 9b	$38^- \rightarrow 43^+$	[3;1] → [4;1]	0.119 → 0.117	2479	2602
^{157}Ho	2b → 4a	$87/2^- \rightarrow 97/2^+$	[3;2] → [4;2]	0.140 → 0.139	3039	2704
^{158}Er		$46^+ \rightarrow 50^-$	[4;2] → [5;2]	0.136 → 0.129	3065	2883

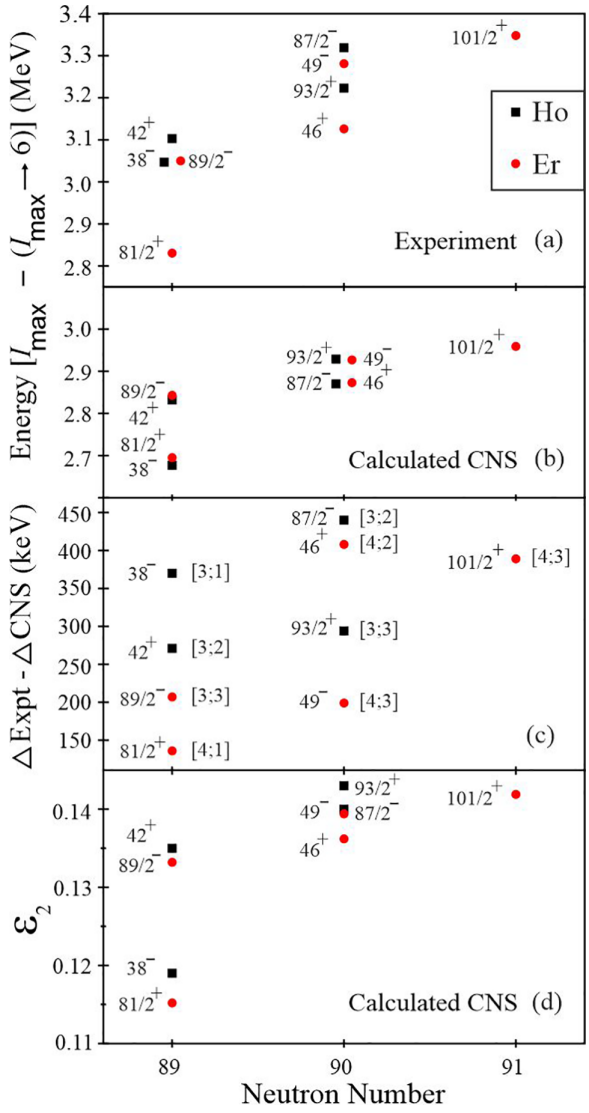


FIG. 23. (a) Experimental energy differences between I_{max} and $(I_{max} - 6)$ states observed in ^{156,157}Ho and $^{157-159}$Er, and (b) the calculated (CNS) energy difference. The particle exchange is a neutron moving from the $h_{9/2}$ ($m_j = 5/2$) to the $f_{7/2}$ ($m_j = -7/2$) state. The data are summarized in Table V, and details of the I_{max} configurations are given in Tables I and II. The experimental energies are taken from [4] (^{156}Er), [9] (^{157}Er), [2] (^{158}Er), [6] (^{159}Er) and this work (^{156,157}Ho). (c) Difference between the experimental and calculated (CNS) energies from the I_{max} to $(I_{max} - 6)$ levels. The configuration of the I_{max} level is displayed. (d) Deformation ε_2 of the I_{max} states from the CNS calculations; each state is labeled by I^{π}.

it was stated that "they all have a rather intense stopped component," which indicates slow feeding from long-lived states (i.e., consistent with the band-termination interpretation), whereas in band 7, significant "fully shifted components" were observed, consistent with fast-feeding lifetimes.

B. Triaxial strongly deformed bands

Long sequences of regularly spaced gamma rays have been established in neighboring nuclei to $N \approx 90$ Ho nuclei that bypass the band-termination regime, and appear to extend beyond $60\hbar$, marking a reprise of collectivity. These nuclei include ^{157,158}Er [11] and ^{159,160}Er [46].

It was proposed [11] that these bands correspond to triaxial strongly deformed (TSD) structures, based on the predictions of early cranking calculations of Bengtsson and Ragnarsson [50] and Dudek and Nazarewicz [51]. The transition quadrupole moments of the observed ultrahigh-spin sequences in ^{157,158}Er were measured, confirming that they were all associated with strongly deformed shapes [12,27], see also Ref. [52]. These experimental measurements helped to trigger further theoretical studies, for example, Refs. [53–56] with the high-spin TSD bands interpreted as corresponding to triaxial shapes with quadrupole deformation in the range of $\varepsilon_2 = 0.35$–0.45, with triaxiality of $\gamma = 20°$–$30°$, thus leading to high quadrupole-moment values.

In the present work, as displayed in Fig. 9, three new candidate TSD bands have been assigned to ^{157}Ho, see also Ref. [25]. Figure 24 plots the dynamic moment of inertia ($\mathcal{J}^{(2)}$) of TSD bands in ^{157}Ho and ^{157,158}Er together with band 7 in ^{157}Ho. The peak in the moment of inertia of band 7 at $\omega = 0.35$ MeV/$\hbar$ corresponds to the $i_{13/2}$ neutron alignment (though this occurs with the gradual underlying $h_{11/2}$ proton alignment). It is noteworthy that, at high rotational frequency, the moment of inertia of band 7 is similar to those of the TSD bands; all exhibit relatively high $\mathcal{J}^{(2)}$ values, but with a decreasing trend.

The relative energies of the transitions in TSD2 and TSD3 in ^{157}Ho, as evident in their spectra and $\mathcal{J}^{(2)}$ moments of inertia, suggest that they are signature-partner bands. It is also interesting to note that the transition energies in TSD2 in ^{157}Ho are very close (within 1 to 2 keV for all but the 1256-keV transition) to those in TSD1 ^{157}Er. This similarity means that their $\mathcal{J}^{(2)}$ values follow each other closely, see Fig. 24(b). A similar correspondence with TSD1 in ^{157}Er was noted in Ref. [57] in a TSD sequence in ^{161}Tm. This phenomenon of "identical" bands suggest a similar underlying structure.

The optimal way for the finite nucleus to generate more angular momentum than the high-spin terminating states and advance into the ultrahigh-spin region beyond $60\hbar$ is to form additional neutron particle-hole excitations across the $N = 82$ shell gap, thus increasing the valence space and increasing the potential I_{max} value. Such excitations involve promoting a neutron from the topmost $h_{11/2}$ orbital ($[505]11/2^-$) below $N = 82$ into low-Ω $i_{13/2}$ and $f_{7/2}/h_{9/2}$ orbitals above the gap. CNS calculations suggest that the experimental TSD bands involve the promotion of neutrons into deformation-driving $N_{osc} = 6$ $i_{11/2}$ and $g_{9/2}$ orbitals, in addition to $N_{osc} = 7$ $j_{15/2}$ ones [2]. In the case of $Z = 67$ ^{157}Ho, with one proton less than erbium, analogous configurations involving both proton and neutron particle-hole excitations, would be expected to drive similar TSD shapes. As an example, the configuration for the strongest TSD band in ^{158}Er is conjectured to be $\pi[(g_{7/2}/d_{5/2})^{-4}(h_{11/2})^6(h_{9/2})^1(i_{13/2})^1] \otimes \nu[(h_{11/2})^{-2}(N_{osc} = 4)^{-2}(h_{9/2}f_{7/2})^8(i_{13/2})^4]$ [11], where the dominant components relative to a ^{146}Gd core are indicated. Therefore, this configuration with one extra hole in the $(\pi d_{5/2}/g_{7/2})$ orbitals would be expected in ^{157}Ho. Excited

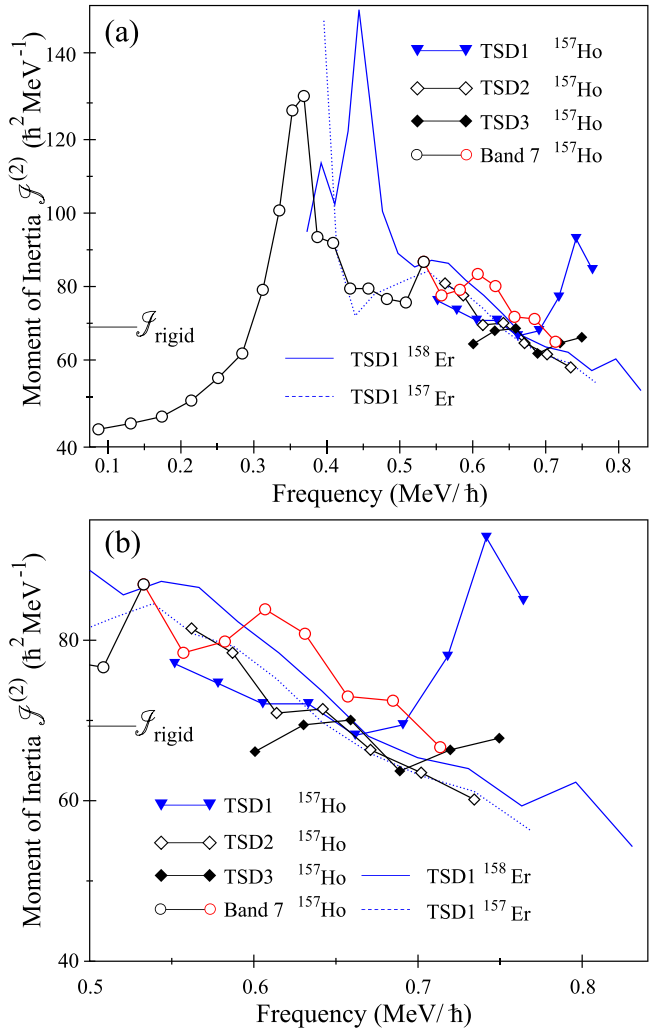


FIG. 24. (a) The dynamic moment of inertia $\mathcal{J}^{(2)}$ as a function of rotational frequency for the three TSD bands tentatively assigned to ^{157}Ho, band 7 in ^{157}Ho, and the strongest sequences (labeled TSD1) in ^{158}Er and ^{157}Er [11]. New states in band 7 correspond to the red symbols. (b) Expanded plot for high frequency. The rigid-body moment of inertia for mass 157 and a deformation of $\beta_2 = 0.3$ is indicated.

TSD configurations can then be formed by moving the eighth $(h_{9/2}/f_{7/2})$ neutron into the fifth $i_{13/2}$ neutron orbital [2].

However, many questions remain regarding the detailed nature of the TSD structures in these nuclei; for instance, what are their excitation energies and how do they feed into the lower spin states, and what are their specific deformations, spins, and parities? In addition, the theoretical investigation of Ref. [58] challenges previous interpretations of the related TSD structures in the Lu isotopes. Clearly, further experimental and theoretical studies are needed.

IX. SUMMARY AND CONCLUSIONS

The level structures of the rare-earth $^{156–158}$Ho isotopes have been substantially extended through high-fold γ-ray coincidence analysis, unveiling approximately two hundred new transitions in these nuclei. Many rotational bands have been extended to higher spin and several new structures have been established. Intrinsic configurations have been proposed through comparisons with cranked Nilsson-Strutinsky calculations. In addition, specific noncollective-oblate states have been identified based on single-particle configurations where the valence particles (and holes) are maximally aligned, thus generating the total nuclear angular momentum. These states are clearly manifested in doubly odd ^{156}Ho, where they are particularly low-lying in energy (yrast). In the heavier isotopes, ^{157,158}Ho, such states compete with the surrounding collective ones for yrast status.

An additional feature of the maximally aligned oblate states in the Ho and Er nuclei, is the fact that they are often accompanied by other aligned states six units lower in spin, where one neutron is antialigned, i.e., rotating in the opposite direction. The consistent experimental energy differences between these related levels, including the proposed change in ^{159}Er, both within a single nucleus and also in neighboring nuclei, along with detailed theoretical comparisons, provides strong evidence that the suggested spin-parity assignments are reliable. This is particularly the case for doubly odd ^{156}Ho, where a definitive connection to the ground state is not established.

The oblate band-terminating states represent nuclear levels where the angular momentum is generated by pure single-particle configurations; single-particle and collective motion is completely decoupled. They may be viewed as "standard" marker points for any theoretical high-spin model and provide important insights into potential refinements of the proton and neutron single-particle energies at oblate deformation.

To progress to even higher spin, the nucleus requires additional particle-hole excitations of both protons and neutrons in order to increase the possible $I_{\max}$ values. These excitations might lead to further noncollective states at even higher-spin values than observed. However, they could also induce a return of collectivity and allow the nucleus to rotate into the ultrahigh-spin regime, beyond $60\hbar$, giving rise to the observation of triaxial strongly deformed structures; indeed, three such bands have been assigned to ^{157}Ho. The deployment of the next-generation 4π gamma-ray tracking spectrometers, i.e., GRETA [59] and AGATA [60] will enable a significant advance in nuclear-structure physics. Their capacity for high-statistics, high-fold data is essential to fully address the many unresolved issues of nuclear shape evolution up to ultrahigh spin.

ACKNOWLEDGMENTS

The authors thank the operations staff of Gammasphere both at LBNL and ANL and gratefully acknowledge the efforts of John Greene and Paul Morrall for their target preparations. This work has been supported in part by the United Kingdom Science and Technology Facilities Council under Grants No. ST/P004598/1, No. ST/V001027/1, and No. PP/F000677/1, by the U.S. National Science Foundation under Grants No. PHY-0756474 (FSU), No. PHY-2208137 (USNA), and No. PHY-0754674 and No. PHY-2310059 (UND), by the U.S. Department of Energy, Office of Nuclear

Physics under Contracts No. DE-AC02–06CH11357 (ANL), No. DE-AC02–05CH11231 (LBNL), and No. DE-AC05–00OR22725 (ORNL), and Grants No. DE-FG02–94ER40834 (UMD), No. DE-FG02–97ER41041 (UNC), No. DE-FG02–97ER41033 (TUNL), and No. DE-FG02–96ER40983 (UTK), and by the State of Florida. This research used resources of Argonne National Laboratory's ATLAS facility, which is a DOE Office of Science User Facility.

The views expressed in this article are those of the authors and do not reflect the official policy or position of the U.S. Naval Academy, Department of the Navy, the Department of Defense, or the U.S. Government.

DATA AVAILABILITY

The data that support the findings of this article are not publicly available upon publication because it is not technically feasible and/or the cost of preparing, depositing, and hosting the data would be prohibitive within the terms of this research project. The data are available from the authors upon reasonable request.

APPENDIX A: EXPERIMENTAL DATA FOR ^{156}Ho

Experimental properties of the γ rays assigned to ^{156}Ho are listed in Tables VIII–XIV

TABLE VIII. Excitation energies E_x, transition energies E_γ, relative intensities, angular-intensity ratios R, and spin-parity assignments for ^{156}Ho band 1. The γ-ray energies are estimated to be accurate to $\approx \pm 0.2$ keV, with low-intensity transitions ($I_\gamma < 2$) $\approx \pm 0.5$ keV. The excitation energies relative to the 4^- ground states are not known hence all values have an additional unknown energy offset (y keV). The relative intensities are normalized to the 210.3-keV ($12^- \rightarrow 11^-$) transition. Errors on the relative intensities are estimated to be <5% for transitions of intensity $\geqslant$5, and up to $\approx$20% for weaker transitions. The angular intensity ratios, R, were normalized to 1.0 for known stretched quadrupole ($E2$) transitions, and this then gives a value of $\approx$0.65 for a pure stretched dipole transition.

E_x (keV)	E_γ (keV)	Relative intensity	R	$I^\pi_{\text{initial}} \rightarrow I^\pi_{\text{final}}$
0.0				(8^-)
90.5	90.5	19.6		$(9^-) \rightarrow (8^-)$
184.9	94.4	26.0	0.62(5)	$(10^-) \rightarrow (9^-)$
319.3	228.8	5.9		$(11^-) \rightarrow (9^-)$
319.3	134.6	54.4	0.63(5)	$(11^-) \rightarrow (10^-)$
529.6	210.3	≡100		$(12^-) \rightarrow (11^-)$
659.0	129.5	48.4	0.65(5)	$(13^-) \rightarrow (12^-)$
659.0	339.7	50.6	0.93(7)	$(13^-) \rightarrow (11^-)$
923.0	264.1	46.0	0.68(8)	$(14^-) \rightarrow (13^-)$
923.0	393.4	2.9	0.96(5)	$(14^-) \rightarrow (12^-)$
1135.4	212.3	27.3		$(15^-) \rightarrow (14^-)$
1135.4	476.4	55.3	0.9(7)	$(15^-) \rightarrow (13^-)$
1434.5	299.2	30.4	0.74(6)	$(16^-) \rightarrow (15^-)$
1434.5	511.5	28.6	0.97(5)	$(16^-) \rightarrow (14^-)$
1718.3	283.4	14.9	0.66(5)	$(17^-) \rightarrow (16^-)$
1718.3	582.9	43.6	1.08(5)	$(17^-) \rightarrow (15^-)$
2044.3	326.4	16.8	0.63(5)	$(18^-) \rightarrow (17^-)$
2044.3	609.8	34.8	0.96(5)	$(18^-) \rightarrow (16^-)$
2389.1	344.1	8.0	0.63(5)	$(19^-) \rightarrow (18^-)$
2389.1	670.8	28.5	1.05(10)	$(19^-) \rightarrow (17^-)$
2736.6	348.0	10.4	0.66(7)	$(20^-) \rightarrow (19^-)$
2736.6	692.3	26.7	1.05(6)	$(20^-) \rightarrow (18^-)$
3132.5	395.0	5.7		$(21^-) \rightarrow (20^-)$
3132.5	743.4	14.8	0.83(6)	$(21^-) \rightarrow (19^-)$
3494.1	362.2	4.7	0.64(5)	$(22^-) \rightarrow (21^-)$
3494.1	757.5	16.9	1.05(6)	$(22^-) \rightarrow (20^-)$
3928.5	433.4	1.3		$(23^-) \rightarrow (22^-)$
3928.5	796.0	5.7	1.09(6)	$(23^-) \rightarrow (21^-)$
4295.0	367.1	2.6		$(24^-) \rightarrow (23^-)$
4295.0	800.9	5.2	0.95(5)	$(24^-) \rightarrow (22^-)$
4747.7	452.0	3.0		$(25^-) \rightarrow (24^-)$
4747.7	819.2	4.7	1.30(10)	$(25^-) \rightarrow (23^-)$
5119.6	372.4	2.8		$(26^-) \rightarrow (25^-)$
5119.6	824.6	5.5	1.11(9)	$(26^-) \rightarrow (24^-)$
5583.1	462.6	2.1		$(27^-) \rightarrow (26^-)$
5583.1	835.4	5.8		$(27^-) \rightarrow (25^-)$
5975.1	393.1	1.6		$(28^-) \rightarrow (27^-)$
5975.1	855.5	5.1	1.02(6)	$(28^-) \rightarrow (26^-)$
6460.1	484.5	2.0		$(29^-) \rightarrow (28^-)$
6460.1	877.0	3.5	1.05(6)	$(29^-) \rightarrow (27^-)$
6880.8	905.8	1.2		$(30^-) \rightarrow (28^-)$
7395.4	935.3	3.1	1.04(6)	$(31^-) \rightarrow (29^-)$
7848.9	968.0	3.2	0.97(6)	$(32^-) \rightarrow (30^-)$
8400.3	1004.9	3.1		$(33^-) \rightarrow (31^-)$
8883.0	1034.1	1.7		$(34^-) \rightarrow (32^-)$
9475.5	1075.2	1.7		$(35^-) \rightarrow (33^-)$
9984.4	1101.4	1.4		$(36^-) \rightarrow (34^-)$
10 623.0	1147.5	0.8		$(37^-) \rightarrow (35^-)$
11 150.6	1166.2	0.3		$(38^-) \rightarrow (36^-)$
11 836.2	1213.2	0.7		$(39^-) \rightarrow (37^-)$
12 374.5	1223.9	0.5		$(40^-) \rightarrow (30^-)$
13 651.9	1277.4	0.6		$(42^-) \rightarrow (40^-)$
14 970.7	1318.8	0.2		$(44^-) \rightarrow (42^-)$

TABLE IX. Excitation energies E_x, transition energies E_γ, relative intensities, angular intensity ratios R, and spin-parity assignments for ^{156}Ho band 2. See Table VIII for more details.

E_x (keV)	E_γ (keV)	Relative intensity	R	$I^\pi_{\text{initial}} \rightarrow I^\pi_{\text{final}}$
2386.6	951.1	4.8	0.59(7)	$(17^+) \rightarrow (16^-)$
2683.1	964.8	9.3		$(18^+) \rightarrow (17^-)$
2905.7	222.5	1.5	0.72(7)	$(19^+) \rightarrow (18^+)$
2905.7	520.1	3.3		$(19^+) \rightarrow (17^+)$
2905.7	860.5	12.6	0.55(6)	$(19^+) \rightarrow (18^-)$
3194.7	289.2	6.5	0.53(5)	$(20^+) \rightarrow (19^+)$
3194.7	511.6	[a]	1.00(5)	$(20^+) \rightarrow (18^+)$

TABLE IX. (*Continued.*)

E_x (keV)	E_γ (keV)	Relative intensity	R	$I^\pi_{\text{initial}} \to I^\pi_{\text{final}}$
3194.7	806.0	8.1	0.6(5)	$(20^+) \to (19^-)$
3446.8	251.7	10.7		$(21^+) \to (20^+)$
3446.8	541.1	9.6	1.08(6)	$(21^+) \to (19^+)$
3446.8	709.6	6.8	0.64(6)	$(21^+) \to (20^-)$
3762.0	315.6	10.8	0.56(5)	$(22^+) \to (21^+)$
3762.0	567.3	11.9	1.03(5)	$(22^+) \to (20^+)$
3762.0	630.2	3.0	0.86(5)	$(22^+) \to (21^-)$
4055.7	293.0	10.7	0.54(5)	$(23^+) \to (22^+)$
4055.7	560.2	9.9		$(23^+) \to (22^-)$
4055.7	608.9	16.3	1.00(5)	$(23^+) \to (21^+)$
4411.0	355.8	8.1	0.61(5)	$(24^+) \to (23^+)$
4411.0	649.0	12.2	0.92(5)	$(24^+) \to (22^+)$
4748.0	336.1	8.0		$(25^+) \to (24^+)$
4748.0	692.3	20.3	1.06(5)	$(25^+) \to (23^+)$
5136.8	389.3	3.9	0.58(5)	$(26^+) \to (25^+)$
5136.8	725.8	13.6	1.02(5)	$(26^+) \to (24^+)$
5522.9	385.3	0.3	0.62(8)	$(27^+) \to (26^+)$
5522.9	774.9	20.1	1.13(5)	$(27^+) \to (25^+)$
5936.1	413.9	5.0		$(28^+) \to (27^+)$
5936.1	799.3	14.5	1.06(6)	$(28^+) \to (26^+)$
6389.9	453.3	3.9		$(29^+) \to (28^+)$
6389.9	867.0	18.8	1.02(6)	$(29^+) \to (27^+)$
6813.9	425.1	2.7		$(30^+) \to (29^+)$
6813.9	877.8	18.8	1.02(6)	$(30^+) \to (28^+)$
7323.6	509.0	[a]		$(31^+) \to (30^+)$
7323.6	933.7	14.4	0.96(7)	$(31^+) \to (29^+)$
7740.0	417.4	1.6		$(32^+) \to (31^+)$
7740.0	926.1	14.2	0.85(7)	$(32^+) \to (30^+)$
8287.3	963.7	8.5	0.99(6)	$(33^+) \to (31^+)$
8676.0	936.0	11.2	1.27(12)	$(34^+) \to (32^+)$
9285.3	998.0	4.1		$(35^+) \to (33^+)$
9622.0	946.0	5.4	1.01(10)	$(36^+) \to (34^+)$
10 241.6	956.3	2.2		$(37^+) \to (35^+)$
10 400.1	1114.8	1.0		$(37^+) \to (35^+)$
10 636.5	1014.5	1.1		$(38^+) \to (36^+)$
11 238.6	997.0	0.7		$(39^+) \to (37^+)$
11 632.5	996.0	0.7		$(40^+) \to (38^+)$
	1177.4	1.3		$(40^+) \to (38^+)$
12 730.8	1098.3	1.7	1.06(10)	$(42^+) \to (40^+)$
	1309.7	1.8	1.08(26)	$(42^+) \to (40^+)$
13 860.1	1129.3	2.4	0.93(15)	$(44^+) \to (42^+)$
	1488.8	3.8	0.86(10)	$(44^+) \to (42^+)$
15 040.5	1180.4	1.0	0.83(10)	$(46^+) \to (44^+)$

[a]doublet.

TABLE X. Excitation energies E_x, transition energies E_γ, relative intensities, angular intensity ratios R, and spin-parity assignments for ^{156}Ho band 3. See Table VIII for more details.

E_x (keV)	E_γ (keV)	Relative intensity	R	$I^\pi_{\text{initial}} \to I^\pi_{\text{final}}$
660.5	382.3			$(11^-) \to (9^-)$
660.5	474.9	4.9		$(11^-) \to (10^-)$
848.1	187.6	1.3	0.61(7)	$(12^-) \to (11^-)$
848.1	529.0	5.2		$(12^-) \to (11^-)$
1042.8	195.0	4.1	0.60(9)	$(13^-) \to (12^-)$
1042.8	382.3	4.4	1.11(7)	$(13^-) \to (11^-)$
1042.8	512.9	4.3		$(13^-) \to (12^-)$
1042.8	722.6	2.0		$(13^-) \to (11^-)$
1266.2	222.9	2.8		$(14^-) \to (13^-)$
1266.2	418.1	5.6	0.87(6)	$(14^-) \to (12^-)$
1266.2	607.2	4.0	0.67(7)	$(14^-) \to (13^-)$
1266.2	736.5	1.1		$(14^-) \to (12^-)$
1503.9	237.7	4.6	0.62(6)	$(15^-) \to (14^-)$
1503.9	461.1	8.7	0.88(5)	$(15^-) \to (13^-)$
1503.9	580.1	3.5		$(15^-) \to (14^-)$
1503.9	845.7	2.6		$(15^-) \to (13^-)$
1767.4	263.7	5.4	0.80(5)	$(16^-) \to (15^-)$
1767.4	501.2	8.7		$(16^-) \to (14^-)$
1767.4	631.3	2.1		$(16^-) \to (15^-)$
1767.4	845.7	2.6		$(16^-) \to (14^-)$
2035.6	267.8	1.9	0.84(7)	$(17^-) \to (16^-)$
2035.6	531.7	12.1	0.99(6)	$(17^-) \to (15^-)$
2035.6	601.2	3.3		$(17^-) \to (16^-)$
2035.6	899.8	1.3		$(17^-) \to (15^-)$
2334.7	299.1	5.6	0.66(5)	$(18^-) \to (17^-)$
2334.7	567.3	10.1	0.99(5)	$(18^-) \to (16^-)$
2334.7	900.4	0.5		$(18^-) \to (16^-)$
2637.3	302.4	5.1	0.69(9)	$(19^-) \to (18^-)$
2637.3	601.7	5.1	0.98(6)	$(19^-) \to (17^-)$
2637.3	920.1	3.3	0.98(6)	$(19^-) \to (17^-)$
2966.0	329.0	6.0	0.66(11)	$(20^-) \to (19^-)$
2966.0	631.3	10.6	1.13(8)	$(20^-) \to (18^-)$
3312.5	346.2	6.0	0.67(11)	$(21^-) \to (20^-)$
3312.5	675.2	11.6	1.0(6)	$(21^-) \to (19^-)$
3312.5	924.7	3.8		$(21^-) \to (19^-)$
3664.4	351.7	4.2		$(22^-) \to (21^-)$
3664.4	698.4	7.0	0.94(8)	$(22^-) \to (20^-)$
4064.7	400.2	1.9	0.66(5)	$(23^-) \to (22^-)$
4064.7	752.2	9.4	1.09(7)	$(23^-) \to (21^-)$
4436.2	371.4	4.0	0.56(8)	$(24^-) \to (23^-)$
4436.2	771.8	6.3		$(24^-) \to (22^-)$
4920.4	855.7	4.3	1.23(12)	$(25^-) \to (23^-)$
5297.4	376.8	3.1		$(26^-) \to (25^-)$
5297.4	861.2	6.2	1.14(7)	$(26^-) \to (24^-)$
5849.6	929.2	6.0	0.91(7)	$(27^-) \to (25^-)$
6209.2	359.5	2.3		$(28^-) \to (27^-)$
6209.2	911.8	7.0	1.14(14)	$(28^-) \to (26^-)$
6807.4	957.8	[a]		$(29^-) \to (27^-)$
7154.1	944.9	4.6		$(30^-) \to (28^-)$
7653.2	845.8	4.1		$(31^-) \to (29^-)$
8081.7	927.6	[a]		$(32^-) \to (20^-)$
8544.6	891.4	3.4		$(33^-) \to (31^-)$
8948.3	866.6	4.2		$(34^-) \to (32^-)$
9452.3	909.2	1.1		$(35^-) \to (33^-)$
9875.9	927.6	[a]		$(36^-) \to (24^-)$
10 411.6	957.8	[a]		$(37^-) \to (35^-)$
10 833.8	957.9	1.3		$(38^-) \to (26^-)$
11 350.2	938.6	0.6		$(39^-) \to (37^-)$

[a]doublet.

TABLE XI. Excitation energies E_x, transition energies E_γ, relative intensities, angular intensity ratios R, and spin-parity assignments for ^{156}Ho band 5. See Table VIII for more details.

E_x (keV)	E_γ (keV)	Relative intensity	R	$I^\pi_{\text{initial}} \to I^\pi_{\text{final}}$
3660.8	924.2	3.8		$(21^-) \to (20^-)$
3751.5	1015.2	[a]		$(21^-) \to (20^-)$
4082.7	950.9	2.5	0.61(7)	$(22^-) \to (21^-)$
4082.7	1346.4	0.4		$(22^-) \to (20^-)$
4399.6	738.8	0.3	1.05(11)	$(23^-) \to (21^-)$
4399.6	903.1	0.3		$(23^-) \to (22^-)$
4422.3	339.6	1.8	0.77(5)	$(23^-) \to (22^-)$
4422.3	670.8	3.0		$(23^-) \to (21^-)$
4422.3	761.5	3.5	0.87(6)	$(23^-) \to (21^-)$
4422.3	1291.0	0.3		$(23^-) \to (21^-)$
4758.7	336.0	0.1	0.65(6)	$(24^-) \to (23^-)$
4758.7	676.0	2.9	1.05(6)	$(24^-) \to (22^-)$
4758.7	1264.7	0.5		$(24^-) \to (22^-)$
5117.3	359.6	1.9		$(25^-) \to (24^-)$
5117.3	695.0	5.5		$(25^-) \to (23^-)$
5117.3	720.1	1.8		$(25^-) \to (23^-)$
5488.0	369.9	1.6		$(26^-) \to (25^-)$
5488.0	729.3	6.7		$(26^-) \to (24^-)$
5870.5	382.6	5.8		$(27^-) \to (26^-)$
5870.5	753.2	6.8	0.99(7)	$(27^-) \to (25^-)$
6256.6	385.4	1.6		$(28^-) \to (27^-)$
6256.6	768.6	7.1	0.88(7)	$(28^-) \to (26^-)$
6661.6	405.2	0.7		$(29^-) \to (28^-)$
6661.6	791.1	6.6	1.03(6)	$(29^-) \to (27^-)$
7059.9	397.9	1.0		$(30^-) \to (29^-)$
7059.9	803.3	5.3	1.04(6)	$(30^-) \to (28^-)$
7059.9	851.3	3.0		$(30^-) \to (28^-)$
7492.5	432.3	0.9		$(31^-) \to (30^-)$
7492.5	830.9	6.9		$(31^-) \to (29^-)$
7908.4	416.2	0.3		$(32^-) \to (31^-)$
7908.4	845.3	2.8		$(32^-) \to (30^-)$
7908.4	848.5	4.8		$(32^-) \to (30^-)$
8371.9	464.0	3.3		$(33^-) \to (32^-)$
8371.9	879.4	4.8	0.97(6)	$(33^-) \to (31^-)$
8814.2	442.2	3.5		$(34^-) \to (33^-)$
8814.2	905.8	4.5		$(34^-) \to (32^-)$
9307.4	493.8	0.3		$(35^-) \to (34^-)$
9307.4	935.5	4.9	0.93(6)	$(35^-) \to (33^-)$
9784.0	476.1	1.2		$(36^-) \to (35^-)$
9784.0	969.8	2.9	1.16(7)	$(36^-) \to (34^-)$
10 295.5	988.1	4.5	1.03(7)	$(37^-) \to (35^-)$
10 790.5	1006.5	2.8		$(38^-) \to (36^-)$
11 209.5	914.0	3.7	1.05(8)	$(39^-) \to (37^-)$
11 310.8	1015.2	[a]		$(39^-) \to (37^-)$
11 382.6	1083.2	1.3		$\to (37^-)$
11 771.3	980.8	0.5		$\to (38^-)$
11 835.3	1044.8	0.6		$(40^-) \to (38^-)$
12 004.1	1213.6	0.5		$\to (38^-)$
12 168.1	958.6	0.9	0.99(7)	$(41^-) \to (39^-)$
12 168.1	857.1	0.8		$(41^-) \to (39^-)$
12 248.2	1038.7	1.0		$\to (39^-)$
12 525.7	1143.1	0.1		
12 645.4	874.1	0.4		
13 198.1	1030.0	2.5		$(43^-) \to (41^-)$
13 350.5	1102.3	0.4		

[a]doublet.

TABLE XII. Excitation energies E_x, transition energies E_γ, relative intensities, angular intensity ratios R, and spin-parity assignments for ^{156}Ho band 6. See Table VIII for more details.

E_x (keV)	E_γ (keV)	Relative intensity	R	$I^\pi_{\text{initial}} \to I^\pi_{\text{final}}$
7064.6	807.0	4.2		$(30^-) \to (28^-)$
7064.6	855.4	4.3	1.23(7)	$(30^-) \to (28^-)$
7689.3	535.0	0.5		$(32^-) \to (30^-)$
7689.3	624.7	4.3	1.17(10)	$(32^-) \to (30^-)$
7689.3	629.4	5.4	0.80(8)	$(32^-) \to (30^-)$
8740.2	1050.9	4.7	0.94(8)	$(34^-) \to (32^-)$
9702.0	961.8	3.8	0.94(11)	$(36^-) \to (34^-)$
10 619.0	834.8	2.7		$(38^-) \to (36^-)$
10 619.0	916.8	2.7		$(38^-) \to (36^-)$
10 736.5	1034.5	1.1		$(38^-) \to (36^-)$
11 619.2	1000.4	2.7	1.16(13)	$(40^-) \to (38^-)$
11 647.2	910.7	[a]		$(40^-) \to (38^-)$
12 646.9	1027.7	0.6		$(42^-) \to (40^-)$
12 841.6	1222.4	0.2		$(42^-) \to (40^-)$
13 286.9	640.0	0.6		$(44^-) \to (42^-)$

[a]doublet.

TABLE XIII. Excitation energies E_x, transition energies E_γ, relative intensities, angular-intensity ratios R, and spin-parity assignments for ^{156}Ho band 9a. See Table VIII for more details.

E_x (keV)	E_γ (keV)	Relative intensity	R	$I^\pi_{\text{initial}} \to I^\pi_{\text{final}}$
7185.6	(1249.5)			$(30^+) \to (28^+)$
7908.4	585.9	1.3		$(32^+) \to (31^+)$
7908.4	722.8	5.1		$(32^+) \to (30^+)$
7908.4	1094.5	4.0	1.27(10)	$(32^+) \to (30^+)$
8419.6	511.2	10.0	0.90(5)	$(34^+) \to (32^+)$
8419.6	679.6	4.1		$(34^+) \to (32^+)$
9267.9	134.8	[a]		$(36^+) \to (35^+)$
9267.9	591.4	5.0		$(36^+) \to (34^+)$
9267.9	848.3	6.1	1.17(7)	$(36^+) \to (34^+)$
10 455.4	833.2	3.0		$(38^+) \to (36^+)$
10 454.4	1187.5	6.8	1.05(7)	$(38^+) \to (36^+)$
11 421.6	966.2	4.0	1.02(7)	$(40^+) \to (38^+)$
12 371.1	900.0	0.5		$(42^+) \to (41^+)$
12 371.1	949.5	3.3	0.97(9)	$(42^+) \to (40^+)$
14 864.6	1004.5	2.8	0.82(10)	$(46^+) \to (44^+)$

[a]doublet.

TABLE XIV. Excitation energies E_x, transition energies E_γ, relative intensities, angular-intensity ratios R, and spin-parity assignments for ^{156}Ho band 9b. See Table VIII for more details.

E_x (keV)	E_γ (keV)	Relative intensity	R	$I^\pi_{\text{initial}} \rightarrow I^\pi_{\text{final}}$
9133.1	711.8	3.0	0.93(11)	$(35^+) \rightarrow (34^+)$
9133.1	845.8	4.5		$(35^+) \rightarrow (33^+)$
9912.9	627.5	0.5		$(37^+) \rightarrow (35^+)$
9912.9	643.6	5.5	0.38(5)	$(37^+) \rightarrow (36^+)$
9912.9	779.8	4.5		$(37^+) \rightarrow (35^+)$
10 805.3	892.4	3.9		$(39^+) \rightarrow (37^+)$
10 805.3	349.9	2.9		$(39^+) \rightarrow (38^+)$
11 470.9	665.6	3.9		$(41^+) \rightarrow (39^+)$
12 181.7	1376.4	3.2		$(41^+) \rightarrow (39^+)$
12 351.0	880.1	0.7		$(41^-) \rightarrow (41^+)$
12 867.9	1397.0	0.8		$\rightarrow (41^+)$
12 971.9	1501.0	1.0		$\rightarrow (41^+)$
13 023.9	1553.0	0.6		$\rightarrow (41^+)$
13 215.6	1035.0	1.3		$(43^+) \rightarrow (41^+)$
13 215.6	1744.7	1.9		$(43^+) \rightarrow (41^+)$
13 329.9	1859.0	1.4		$\rightarrow (41^+)$
14 289.5	1072.8	1.8		$(45^+) \rightarrow (43^+)$
14 450.4	1233.7	1.6		$(45^+) \rightarrow (43^+)$
15 540.6	1252.2	0.5		$(47^+) \rightarrow (45^+)$

APPENDIX B: EXPERIMENTAL DATA FOR ^{157}Ho

Experimental properties of the γ rays assigned to ^{157}Ho are listed in Tables XV–XX.

TABLE XV. Excitation energies E_x, transition energies E_γ, relative intensities, and spin-parity assignments for ^{157}Ho band 2a states starting from the $53/2^-$ level. Intensities are relative to the 424-keV, $17/2^+ \rightarrow 13/2^+$ yrast transition having a value of 100. The γ-ray energies are estimated to be accurate to $\approx \pm 0.2$ keV, with low-intensity transitions ($I_\gamma < 2$) $\approx \pm 0.5$ keV.

E_x (keV)	E_γ (keV)	Relative intensity	$I^\pi_{\text{initial}} \rightarrow I^\pi_{\text{final}}$
6179.3			$53/2^-$
7073.6	470.0	2.2	$57/2^- \rightarrow 55/2^-$
7073.6	894.3	13.5	$57/2^- \rightarrow 53/2^-$
8044.6	532.7	1.0	$61/2^- \rightarrow 59/2^-$
8044.6	971.0	12.2	$61/2^- \rightarrow 57/2^-$
9080.5	609.9	0.6	$65/2^- \rightarrow 63/2^-$
9080.5	1035.9	10.3	$65/2^- \rightarrow 61/2^-$
10 150.3	702.6	1.3	$69/2^- \rightarrow 67/2^-$
10 150.3	1069.8	6.4	$69/2^- \rightarrow 65/2^-$
11 210.5	814.0	0.6	$(73/2^-) \rightarrow 71/2^-$
11 210.5	1060.2	4.2	$(73/2^-) \rightarrow 69/2^-$
12 319.5	1109.0	1.3	$(77/2^-) \rightarrow (73/2^-)$
13 394.2	1074.7	1.3	$(81/2^-) \rightarrow (77/2^-)$
14 502.1	1107.9	0.6	$(85/2^-) \rightarrow (81/2^-)$

TABLE XVI. Excitation energies E_x, transition energies E_γ, relative intensities, and spin-parity assignments, for ^{157}Ho band 2b. See Table XV for more details.

E_x (keV)	E_γ (keV)	Relative intensity	$I^\pi_{\text{initial}} \rightarrow I^\pi_{\text{final}}$
6603.5	424.3	3.2	$55/2^- \rightarrow 53/2^-$
7511.9	438.3	2.2	$59/2^- \rightarrow 57/2^-$
7511.9	908.4	15.4	$59/2^- \rightarrow 55/2^-$
8470.5	426.0	1.3	$63/2^- \rightarrow 61/2^-$
8470.5	958.6	14.7	$63/2^- \rightarrow 59/2^-$
9447.8	367.5	1.6	$67/2^- \rightarrow 65/2^-$
9447.8	977.4	14.1	$67/2^- \rightarrow 63/2^-$
10 396.7	246.0	1.0	$71/2^- \rightarrow 69/2^-$
10 396.7	948.8	14.1	$71/2^- \rightarrow 67/2^-$
11 412.5	1015.8	6.4	$75/2^- \rightarrow 71/2^-$
12 566.4	1153.9	3.5	$79/2^- \rightarrow 75/2^-$
13 587.3	1020.9	2.4	$(83/2^-) \rightarrow 79/2^-$
13 587.3	1279.8	1.9	$(83/2^-) \rightarrow 79/2^-$
11 189.5	792.8	6.4	$75/2^- \rightarrow 71/2^-$
12 306.7	894.6	4.8	$79/2^- \rightarrow 75/2^-$
12 306.7	1117.2	7.7	$79/2^- \rightarrow 75/2^-$
13 369.6	1063.2	7.7	$83/2^- \rightarrow 79/2^-$
14 508.1	1138.2	5.1	$87/2^- \rightarrow 83/2^-$
15 876.2	1368.1	5.1	$(91/2^-) \rightarrow 87/2^-$
17 045.9	1169.7	1.9	$(95/2^-) \rightarrow (91/2^-)$
17 193.3	1317.3	2.6	$(95/2^-) \rightarrow (91/2^-)$
17 333.2	1457.0	1.7	$(95/2^-) \rightarrow (91/2^-)$
18 095.4	1049.5	1.3	$(99/2^-) \rightarrow (95/2^-)$

TABLE XVII. Excitation energies E_x, transition energies E_γ, relative intensities, and spin-parity assignments, for ^{157}Ho band 4a. See Table XV for more details.

E_x (keV)	E_γ (keV)	Relative intensity	$I^\pi_{\text{initial}} \rightarrow I^\pi_{\text{final}}$
7231.4	416.8	1.6	$57/2^+ \rightarrow 55/2^+$
8097.5	442.8	0.6	$61/2^+ \rightarrow 59/2^+$
8097.5	866.1	12.8	$61/2^+ \rightarrow 57/2^+$
9015.6	469.5	1.0	$65/2^+ \rightarrow 63/2^+$
9015.6	918.8	11.5	$65/2^+ \rightarrow 61/2^+$
9984.7	494.7	1.3	$69/2^+ \rightarrow 67/2^+$
9984.7	969.0	9.6	$69/2^+ \rightarrow 65/2^+$
11 002.2	514.6	0.5	$73/2^+ \rightarrow 71/2^+$
11 002.0	1017.3	9.3	$73/2^+ \rightarrow 69/2^+$
12 055.6	518.4	0.5	$77/2^+ \rightarrow 75/2^+$
12 055.6	1053.6	6.4	$77/2^+ \rightarrow 73/2^+$
13 067.5	1011.9	3.8	$(81/2^+) \rightarrow 77/2^+$
14 119.5	1052.0	5.1	$(85/2^+) \rightarrow (81/2^+)$
15 198.4	1078.9	3.8	$(89/2^+) \rightarrow (85/2^+)$
16 290.2	1091.8	3.2	$(93/2^+) \rightarrow (89/2^+)$
17 546.9	1256.7	2.2	$(97/2^+) \rightarrow (93/2^+)$
18 893.3	1346.4	1.9	$(101/2^+) \rightarrow (97/2^+)$
20 217.4	1324.1	1.3	$(105/2^+) \rightarrow (101/2^+)$
21 748.1	1530.7	0.8	$(109/2^+) \rightarrow (105/2^+)$

TABLE XVIII. Excitation energies E_x, transition energies E_γ, relative intensities, and spin-parity assignments, for ^{157}Ho band 4b, see Table XV for more details.

E_x (keV)	E_γ (keV)	Relative intensity	$I^\pi_{\text{initial}} \rightarrow I^\pi_{\text{final}}$
6814.9			$55/2^+$
7655.0	423.3	1.9	$59/2^+ \rightarrow 57/2^+$
7655.0	840.1	10.9	$59/2^+ \rightarrow 55/2^+$
8546.4	448.6	1.3	$63/2^+ \rightarrow 61/2^+$
8546.4	891.4	10.3	$63/2^+ \rightarrow 59/2^+$
9490.2	474.3	0.9	$67/2^+ \rightarrow 65/2^+$
9490.1	943.8	10.9	$67/2^+ \rightarrow 63/2^+$
10 487.5	502.7	1.9	$71/2^+ \rightarrow 69/2^+$
10 487.5	997.3	11.2	$71/2^+ \rightarrow 67/2^+$
11 537.3	535.2	1.3	$75/2^+ \rightarrow 73/2^+$
11 537.3	1049.8		$75/2^+ \rightarrow 71/2^+$
12 587.1	531.4	0.6	$(79/2^+) \rightarrow 77/2^+$
12 587.1	1049.8		$(79/2^+) \rightarrow 75/2^+$
12 635.9	1098.6	8.3	$(79/2^+) \rightarrow 75/2^+$
13 599.5	1012.4	3.8	$(83/2^+) \rightarrow (79/2^+)$
13 674.4	1038.5	3.8	$(83/2^+) \rightarrow (79/2^+)$
13 817.4	1181.5	5.1	$(83/2^+) \rightarrow (79/2^+)$
14 647.9	1049.4		$(87/2^+) \rightarrow (83/2^+)$
14 822.3	1147.9	1.9	$(87/2^+) \rightarrow (83/2^+)$
15 032.3	1214.9	2.6	$(87/2^+) \rightarrow (83/2^+)$
15 578.3	929.4	1.9	$(91/2^+) \rightarrow (87/2^+)$

TABLE XIX. Excitation energies E_x, transition energies E_γ, relative intensities, and spin-parity assignments, for ^{157}Ho band 7, see Table XV for more details.

E_x (keV)	E_γ (keV)	Relative intensity	$I^\pi_{\text{initial}} \rightarrow I^\pi_{\text{final}}$
6782.1			$53/2^-$
7621.2	839.1	1.3	$(57/2^-) \rightarrow 53/2^-$
8510.2	889.0	1.2	$(61/2^-) \rightarrow (57/2^-)$
9449.1	938.9	1.1	$(65/2^-) \rightarrow (61/2^-)$
10 439.6	990.5	1.0	$(69/2^-) \rightarrow (65/2^-)$
11 482.3	1042.7	0.8	$(73/2^-) \rightarrow (69/2^-)$
12 571.0	1088.7	0.5	$(77/2^-) \rightarrow (73/2^-)$
13 710.7	1139.7	0.4	$(81/2^-) \rightarrow (77/2^-)$
14 900.5	1189.8	0.3	$(85/2^-) \rightarrow (81/2^-)$
16 138.0	1237.5	0.2	$(89/2^-) \rightarrow (85/2^-)$
17 425.0	1287.0	0.1	$(93/2^-) \rightarrow (89/2^-)$
18 766.8	1341.8	0.1	$(97/2^-) \rightarrow (93/2^-)$
20 163.8	1397.0	0.1	$(101/2^-) \rightarrow (97/2^-)$
21 620.8	1457.0	0.1	$(105/2^-) \rightarrow (101/2^-)$

TABLE XX. Transition energies of the TSD bands assigned to ^{157}Ho.

TSD1 E_γ (keV)	TSD2 E_γ (keV)	TSD3 E_γ (keV)
1077.6	1099.5	1171.2
1129.5	1148.6	1231.7
1183.1	1199.6	1289.3
1238.6	1256.0	1346.4
1294.1	1312.0	1409.2
1352.8	1372.3	1469.5
1410.4	1435.3	1528.5
1461.7	1501.8	
1504.8		
1551.9		

APPENDIX C: EXPERIMENTAL DATA FOR ^{158}Ho

Experimental properties of the γ rays assigned to ^{158}Ho are listed in Table XXI.

TABLE XXI. Excitation energies E_x, transition energies E_γ, relative intensities, and spin-parity assignments for states starting from the 19^- level in ^{158}Ho band 1. The band labeling, lowest excitation energy, and spin-parity assignments are based on Ref. [29] and accepted in Ref. [28]. The γ-ray energies are estimated to be accurate to $\approx \pm 0.2$ keV, with low-intensity transitions ($I_\gamma < 2$) $\approx \pm 0.5$ keV. The relative intensities are normalized to the 159-keV ($12^- \rightarrow 11^-$) transition [29]. Errors on the relative intensities are estimated to be <5% for transitions of intensity $\geqslant$5, and up to $\approx$20% for weaker transitions.

E_x (keV)	E_γ (keV)	Relative intensity	$I^\pi_{\text{initial}} \rightarrow I^\pi_{\text{final}}$
2404.1			19^-
2710.6	306.7	4.5	$20^- \rightarrow 19^-$
3085.4	374.7	3.3	$21^- \rightarrow 20^-$
3085.4	681.3	9.6	$21^- \rightarrow 19^-$
3405.0	320.8	4.1	$22^- \rightarrow 21^-$
3405.0	694.4	8.5	$22^- \rightarrow 20^-$
3813.2	407.7	2.5	$23^- \rightarrow 22^-$

TABLE XXI. (*Continued.*)

E_x (keV)	E_γ (keV)	Relative intensity	$I^\pi_{\text{initial}} \rightarrow I^\pi_{\text{final}}$
3813.2	727.8	7.2	$23^- \rightarrow 21^-$
4143.3	330.2	1.1	$24^- \rightarrow 23^-$
4143.3	738.2	7.7	$24^- \rightarrow 22^-$
4573.9	429.9	0.8	$(25^-) \rightarrow 24^-$
4573.9	760.7	4.4	$(25^-) \rightarrow 23^-$
4916.2	343.3		$(26^-) \rightarrow (25^-)$
4916.2	772.9	5.3	$(26^-) \rightarrow 24^-$
5370.3	453.5		$(27^-) \rightarrow (26^-)$
5370.3	796.4	3.2	$(27^-) \rightarrow (25^-)$
5732.1	362.5		$(28^-) \rightarrow (27^-)$
5732.1	815.9	3.7	$(28^-) \rightarrow (26^-)$
6218.8	486.0		$(29^-) \rightarrow (28^-)$
6218.8	848.6	2.5	$(29^-) \rightarrow (27^-)$
6601.7	384.3		$(30^-) \rightarrow (29^-)$
6601.7	869.6	3.1	$(30^-) \rightarrow (28^-)$
7131.5	528.7		$(31^-) \rightarrow (30^-)$
7131.5	912.6	2.2	$(31^-) \rightarrow (29^-)$
7531.9	930.3	2.0	$(32^-) \rightarrow (30^-)$
8114.8	983.3	1.5	$(33^-) \rightarrow (31^-)$
8521.7	989.7	1.8	$(34^-) \rightarrow (32^-)$
9167.8	1053.0[a]		$(35^-) \rightarrow (33^-)$
9562.1	1040.3		$(36^-) \rightarrow (34^-)$
10 285.8	1118.0[a]		$(37^-) \rightarrow (35^-)$
10 623.2	1061.1	1.6	$(38^-) \rightarrow (36^-)$
11 663.5	1040.3		$(40^-) \rightarrow (38^-)$
12 703.7	1040.3		$(42^-) \rightarrow (40^-)$
13 795.7	1092.0	1.1	$(44^-) \rightarrow (42^-)$
14 948.9	1153.2	0.6	$(46^-) \rightarrow (44^-)$
16 173.4	1224.5	0.4	$(48^-) \rightarrow (46^-)$
17 519.3	1345.9		$(50^-) \rightarrow (48^-)$

[a]Transitions reported in Refs. [28,31] are included for completeness.

[1] M. A. Riley, J. Simpson, and E. S. Paul, High resolution gamma-ray spectroscopy and the fascinating angular momentum realm of the atomic nucleus, Phys. Scr. **91**, 123002 (2016).

[2] J. Simpson, M. A. Riley, A. Pipidis, E. S. Paul, X. Wang, P. J. Nolan, J. F. Sharpey-Schafer, A. Aguilar, D. E. Appelbe, A. D. Ayangeakaa, *et al.*, Evolution of structure and shapes in ^{158}Er to ultrahigh spin, Phys. Rev. C **107**, 054305 (2023).

[3] I. Ragnarsson, A. Kardan, B. G. Carlsson, E. S. Paul, C. M. Petrache, M. A. Riley, J. F. Sharpey-Schafer, and J. Simpson, Band terminations and maximum spin values with up to 18 aligned particles (and holes) in the $Z, N = 50$ to 82 shells, Phys. Rev. C **110**, 034313 (2024).

[4] E. S. Paul, S. V. Rigby, M. A. Riley, J. Simpson, D. E. Appelbe, D. B. Campbell, P. T. W. Choy, R. M. Clark, M. Cromaz, A. O. Evans, *et al.*, Loss of collectivity in the transitional ^{156}Er nucleus at high spin, Phys. Rev. C **79**044324 (2009).

[5] S. J. Gale, J. Simpson, M. A. Riley, J. F. Sharpey-Schafer, E. S. Paul, M. A. Bentley, A. M. Bruce, R. Chapman, R. M. Clark, S. Clarke, *et al.*, Band termination spectroscopy in ^{157}Er J. Phys. G: Nucl. Part. Phys. **21**, 193 (1995).

[6] M. Mustafa, J. Ollier, J. Simpson, M. A. Riley, E. S. Paul, X. Wang, A. Aguilar, M. P. Carpenter, I. G. Darby, D. J. Hartley, *et al.*, Diverse collective excitations in ^{159}Er up to high spin, Phys. Rev. C **84**, 054320 (2011).

[7] J. M. Rees, E. S. Paul, J. Simpson, M. A. Riley, A. D. Ayangeakaa, M. P. Carpenter, C. J. Chiara, U. Garg, P. Hampson, D. J. Hartley, *et al.*, High-spin terminating states in the $N = 88$ ^{155}Ho and ^{156}Er isotones, Phys. Rev. C **91**, 054301 (2015).

[8] D. C. Radford, H. R. Andrews, G. C. Ball, D. Horn, D. Ward, F. Banville, S. Flibotte, S. Monaro, S. Pilotte, P. Taras, *et al.*, Multiple band structure and band termination in ^{157}Ho towards complete high-spin spectroscopy, Nucl. Phys. A **545**, 665 (1992).

[9] A. O. Evans, E. S. Paul, J. Simpson, M. A. Riley, D. E. Appelbe, D. B. Campbell, P. T. W. Choy, R. M. Clark, M. Cromaz, P. Fallon, *et al.*, High-spin structure beyond band termination in ^{157}Er, Phys. Rev. Lett. **92**, 252502 (2004).

[10] A. O. Evans, E. S. Paul, J. Simpson, M. A. Riley, D. E. Appelbe, D. B. Campbell, P. T. W. Choy, R. M. Clark, M. Cromaz, P. Fallon, *et al.*, High-spin structure in ^{157}Er up

to and above band termination, Phys. Rev. C **73**, 064303 (2006).
[11] E. S. Paul, P. J. Twin, A. O. Evans, A. Pipidis, M. A. Riley, J. Simpson, D. E. Appelbe, D. B. Campbell, P. T. W. Choy, R. M. Clark, *et al.*, Return of collective rotation in ^{157}Er and ^{158}Er at ultrahigh spin, Phys. Rev. Lett. **98**, 012501 (2007).
[12] X. Wang, M. A. Riley, J. Simpson, E. S. Paul, J. Ollier, R. V. F. Janssens, A. D. Ayangeakaa, H. C. Boston, M. P. Carpenter, C. J. Chiara, *et al.*, Quadrupole moments of collective structures up to spin $\sim 65\hbar$ in ^{157}Er and ^{158}Er: A challenge for understanding triaxiality in nuclei, Phys. Lett. B **702**, 127 (2011).
[13] I.-Y. Lee, The GAMMASPHERE, Nucl. Phys. A **520**, c641 (1990).
[14] R. Janssens and F. Stephens, New physics opportunities at Gammasphere, Nucl. Phys. News **6**, 9 (1996).
[15] D. C. Radford, ESCL8R and LEVIT8R: Software for interactive graphical analysis of HPGe coincidence data sets, Nucl. Instrum. Methods Phys. Res., Sect. A **361**, 297 (1995).
[16] D. C. Radford, M. Cromaz, and C. J. Beyer, in *AIP Conference Proceedings* (AIP, Gatlinburg, 1999).
[17] D. C. Radford, Background subtraction from in-beam HPGe coincidence data sets, Nucl. Instrum. Methods Phys. Res., Sect. A **361**, 306 (1995).
[18] B. Crowell, M. P. Carpenter, R. G. Henry, R. V. F. Janssens, T. L. Khoo, T. Lauritsen, and D. Nisius, Background subtraction for high-fold gamma-ray coincidence data, Nucl. Instrum. Methods Phys. Res., Sect. A **355**, 575 (1995).
[19] K. S. Krane, R. M. Steffen, and R. M. Wheeler, Directional correlations of gamma radiations emitted from nuclear states oriented by nuclear reactions or cryogenic methods, At. Data Nucl. Data Tables **11**, 351 (1973).
[20] L. P. Ekström and A. Nordlund, Gamma-gamma correlations with detector arrays, Nucl. Instrum. Methods Phys. Res., Sect. A **313**, 421 (1992).
[21] P. J. T. Hampson, High-spin spectroscopic studies of ^{156}Ho: shape changes and band termination, Ph.D. thesis, The University of Liverpool, 2014.
[22] D. M. Cullen, C.-H. Yu, D. Cline, M. Simon, D. C. Radford, M. A. Riley, and J. Simpson, High-spin states and the first signs of band termination in ^{156}Ho, Phys. Rev. C **57**, 2170 (1998).
[23] R. Neugart, E. Arnold, W. Borchers, W. Neu, G. Ulm, and K. Wendt, in *AIP Conference Proceedings* (AIP, 1987), Vol. 164, pp. 126–135.
[24] C. Reich, Nuclear Data Sheets for A = 156, Nucl. Data Sheets **113**, 2537 (2012).
[25] J. S. Baron, Exotic nuclear deformation and the evolution of nuclear structure with angular momentum and excitation energy in ^{157}Ho, ^{166}Er, and ^{169,170}Yb, Ph.D. thesis, Florida State University, 2018, https://repository.lib.fsu.edu/islandora/object/fsu.
[26] J. Gascon, C. H. Yu, G. B. Hagemann, M. C. Carpenter, J. M. Espino, Y. Iwata, T. Komatsubara, J. Nyberg, S. Ogaza, G. Sletten, *et al.*, Configuration-dependent transition rates in ^{157}Ho, Nucl. Phys. A **513**, 344 (1990).
[27] X. Wang, M. A. Riley, J. Simpson, E. S. Paul, R. V. F. Janssens, A. D. Ayangeakaa, H. C. Boston, M. P. Carpenter, C. J. Chiara, U. Garg, *et al.*, Collective structures up to spin $\sim 65\hbar$ in the $N = 90$ isotones ^{158}Er and ^{157}Ho, J. Phys.: Conf. Ser. **381**, 012065 (2012).
[28] N. Nica, Nuclear data sheets for $a = 158$, Nucl. Data Sheets **141**, 1 (2017).
[29] J. Lu, Y. Liu, X. Wu, Y. Ma, G. Zhao, H. Sun, J. Huo, S. Wen, G. Li, and C. Yang, High-spin states in doubly odd ^{158}Ho, Phys. Rev. C **59**, 3461 (1999).
[30] Y. Liu, Y. Ma, H. Yang, and S. Zhou, Systematic features of signature inversion of $(h_{11/2})_p(i_{13/2})_n$ bands in doubly odd nuclei around $A \sim 160$, Phys. Rev. C **52**, 2514 (1995).
[31] C. H. Yu, D. M. Cullen, D. Cline, M. Simon, D. C. Radford, I. Y. Lee, and A. O. Macchiavelli, *Gammasphere Physics-Proceedings Of The Workshop*, edited by M. A. Deleplanque, O. Augusto, Macchiavelli, and I. Y. Lee (World Scientific, 1996), pp. 254–265.
[32] L. Fortunato, Solutions of the Bohr Hamiltonian, a compendium, Eur. Phys. J. A **26**, 1 (2005).
[33] G. Andersson, S. Larsson, G. Leander, P. Möller, S. Nilsson, I. Ragnarsson, S. Åberg, R. Bengtsson, J. Dudek, B. Nerlo-Pomorska, *et al.*, Nuclear shell structure at very high angular momentum, Nucl. Phys. A **268**, 205 (1976).
[34] A. Afanasjev, D. Fossan, G. Lane, and I. Ragnarsson, Termination of rotational bands: Disappearance of quantum many-body collectivity, Phys. Rep. **322**, 1 (1999).
[35] B. G. Carlsson and I. Ragnarsson, Calculating the nuclear mass in the very high angular momentum regime, Phys. Rev. C **74**, 011302(R) (2006).
[36] T. Bengtsson and I. Ragnarsson, Rotational bands and particle-hole excitations at very high spin, Nucl. Phys. A **436**, 14 (1985).
[37] S. G. Nilsson and I. Ragnarsson, *Shapes and Shells in Nuclear Structure* (Cambridge University Press, 1995).
[38] C. Schück, M. A. Deleplanque, R. M. Diamond, F. S. Stephens, and J. Dudek, High-spin states in ^{154}Er and parallel proton- and neutron-core breaking, Nucl. Phys. A **496**, 385 (1989).
[39] N. Nica, G. Duchêne, V. E. Iacob, J. Dudek, F. A. Beck, T. Byrski, D. Curien, G. de France, B. Haas, B. Kharraja, *et al.*, High-spin states in ^{155}Er, Phys. Rev. C **64**, 034313 (2001).
[40] R. Bengtsson and S. Frauendorf, Quasiparticle spectra near the yrast line, Nucl. Phys. A **327**, 139 (1979).
[41] S. M. Harris, Higher order corrections to the cranking model, Phys. Rev. **138**, B509 (1965).
[42] J. Simpson, D. V. Elenkov, P. D. Forsyth, D. Howe, B. M. Nyako, M. A. Riley, J. F. Sharpey-Schafer, B. Herskind, A. Holm, and P. O. Tjom, The strong interaction strength of the first proton alignment in ^{157}Ho, J. Phys. G: Nucl. Phys. **12**, L67 (1986).
[43] M. A. Riley, J. Simpson, J. F. Sharpey-Schafer, J. R. Cresswell, H. W. Cranmer-Gordon, P. D. Forsyth, D. Howe, A. H. Nelson, P. J. Nolan, P. J. Smith, *et al.*, Near yrast discrete line gamma-ray spectroscopy in ^{156}Dy up to spin $40\hbar$, Nucl. Phys. A **486**, 456 (1988).
[44] W. C. Ma, R. V. F. Janssens, T. L. Khoo, I. Ragnarsson, M. A. Riley, M. P. Carpenter, J. R. Terry, J. P. Zhang, I. Ahmad, P. Bhattacharyya, *et al.*, Competition between terminating and collective structures above spin $40\hbar$ in ^{154}Dy, Phys. Rev. C **65**, 034312 (2002).
[45] J. Simpson, M. A. Riley, S. J. Gale, J. F. Sharpey-Schafer, M. A. Bentley, A. M. Bruce, R. Chapman, R. M. Clark, S. Clarke, J. Copnell, *et al.*, Single particle excitations and properties of multiple band terminations near spin $50\hbar$ in ^{158}Er, Phys. Lett. B **327**, 187 (1994).
[46] J. Ollier, J. Simpson, M. A. Riley, E. S. Paul, X. Wang, A. Aguilar, M. P. Carpenter, I. G. Darby, D. J. Hartley, R. V. F.

Janssens, *et al.*, Structure changes in ^{160}Er from low to ultrahigh spin, Phys. Rev. C **83**, 044309 (2011).

[47] I. Ragnarsson, Z. Xing, T. Bengtsson, and M. A. Riley, Properties of terminating bands in nuclei, Phys. Scr. **34**, 651 (1986).

[48] J. Simpson, M. A. Riley, J. R. Cresswell, P. D. Forsyth, D. Howe, B. M. Nyakó, J. F. Sharpey-Schafer, J. Bacelar, J. D. Garrett, G. B. Hagemann, *et al.*, Observation of a prolate-to-oblate shape change near spin 40$\hbar$ in ^{158}Er, Phys. Rev. Lett. **53**, 648 (1984).

[49] F. G. Kondev, M. A. Riley, J. Simpson, R. V. F. Janssens, A. V. Afanasjev, I. Ragnarsson, T. B. Brown, D. J. Hartley, M. P. Carpenter, P. Fallon, *et al.*, Exploring the $I = 50$-$60\hbar$ domain: Collective and terminating structures in ^{156}Dy, ^{159}Er and ^{160}Er, J. Phys. G **25**, 897 (1999).

[50] T. Bengtsson and I. Ragnarsson, Shape changes, band crossings and band terminations in the very high spin region of $A = 150$-160 nuclei, Phys. Scr. **T5**, 165 (1983).

[51] J. Dudek and W. Nazarewicz, Shape evolution in the transitional gadolinium, dysprosium, erbium, and ytterbium nuclei, Phys. Rev. C **31**, 298 (1985).

[52] J. P. Revill, E. S. Paul, X. Wang, M. A. Riley, J. Simpson, R. V. F. Janssens, J. Ollier, A. J. Boston, M. P. Carpenter, C. J. Chiara, *et al.*, Quadrupole moments of coexisting collective shapes at high spin in ^{154}Er, Phys. Rev. C **88**, 031304(R) (2013).

[53] Y. Shi, J. Dobaczewski, S. Frauendorf, W. Nazarewicz, J. C. Pei, F. R. Xu, and N. Nikolov, Self-consistent tilted-axis-cranking study of triaxial strongly deformed bands in ^{158}Er at ultrahigh spin, Phys. Rev. Lett. **108**, 092501 (2012).

[54] Y. Shi, C. L. Zhang, J. Dobaczewski, and W. Nazarewicz, Kerman-Onishi conditions in self-consistent tilted-axis-cranking mean-field calculations, Phys. Rev. C **88**, 034311 (2013).

[55] A. Kardan, I. Ragnarsson, H. Miri-Hakimabad, and L. Rafat-Motevali, Interpretation of the large-deformation high-spin bands in select $A = 158$-168 nuclei, Phys. Rev. C **86**, 014309 (2012).

[56] A. V. Afanasjev, Y. Shi, and W. Nazarewicz, Description of ^{158}Er at ultrahigh spin in nuclear density functional theory, Phys. Rev. C **86**, 031304(R) (2012).

[57] C. Teal, K. Lagergren, A. Aguilar, D. J. Hartley, M. A. Riley, J. Simpson, M. P. Carpenter, U. Garg, R. V. F. Janssens, D. T. Joss, *et al.*, Triaxial strongly deformed bands in ^{160,161}Tm, Phys. Rev. C **78**, 017305 (2008).

[58] I. Ragnarsson, How deformed are the TSD bands in odd Lu isotopes? Phys. Scr. **92**, 124004 (2017).

[59] I. Y. Lee, M. A. Deleplanque, and K. Vetter, Developments in large gamma-ray detector arrays, Rep. Prog. Phys. **66**, 1095 (2003).

[60] W. Korten, A. Atac, D. Beaumel, P. Bednarczyk, M. A. Bentley, G. Benzoni, A. Boston, A. Bracco, J. Cederkäll, B. Cederwall, *et al.*, Physics opportunities with the advanced gamma tracking array: AGATA, Eur. Phys. J. A **56**, 137 (2020).